STUDY OF THE ELASTIC BEHAVIOR OF SYNTHETIC LIGHTWEIGHT AGGREGATES (SLAs)

A dissertation submitted by

Na Jin

in partial fulfillment of the requirements for the degree of

Doctor of Philosophy

in

Civil and Environmental Engineering

TUFTS UNIVERSITY

May 2016

Advisor: Professor Christopher W. Swan

ABSTRACT

Synthetic lightweight aggregates (SLAs), composed of coal fly ash and recycled plastics, represent a resilient construction material that could be a key aspect to future sustainable development. This research focuses on a prediction of the elastic modulus of SLA, assumed as a homogenous and isotropic composite of particulates of high carbon fly ash (HCFA) and a matrix of plastics (HDPE, LDPE, PS and mixture of plastics), with the emphasis on SLAs made of HCFA and PS. The elastic moduli of SLA with variable fly ash volume fractions are predicted based on finite element analyses (FEA) performed using the computer programs ABAQUS and PLAXIS. The effect of interface friction (roughness) between phases and other computation parameters; e.g., loading strain, stiffness of component, element type and boundary conditions, are included in these analyses. Analytical models and laboratory tests provide a baseline for comparison. Overall, results indicate ABAQUS generates elastic moduli closer to those predicted by well-established analytical models than moduli predicted from PLAXIS, especially for SLAs with lower fly ash content. In addition, an increase in roughness, loading strain indicated increase of SLAs stiffness, especially as fly ash content increases. The elastic moduli obtained from unconfined compression generally showed less elastic moduli than those obtained from analytical and ABAQUS 3D predictions. This may be caused by possible existence of pre-failure surface in specimen and the directly interaction between HCFA particles. Recommendations for the future work include laboratory measurements of SLAs moduli and FEM modeling that considers various sizes and random distribution of HCFA particles in SLAs.

ACKNOWLEDGEMENTS

First and foremost I would deeply express my appreciation and thanks to my advisor, professor Christopher W. Swan, for his guidance, encouragement, and tremendous help. He is always supportive in each stage of my study, research, and lives throughout these years. I would also like to thank professor Qiaobing, Xu and his advisee Kyle A. Alberti for their generous help for seeking the laboratory resources to carry out part of the laboratory tests. Without their help, this research could not be fully completed in designated time frame. I am also sincerely thankful to professor Anil Saigal, professor Robert C. Viesca, and professor Qiaobing Xu for being my committee members and providing me with valuable advices and suggestions.

I would give my special thanks to my parents for their sacrifices and their selfless dedication to the family. My great gratitude also goes to my husband for being supportive and understanding all the time. I would also like to thank my two daughters for brightening my life and bringing the family with endless happiness.

TABLE OF CONTENTS

LIST OF FIGURES

LIST OF TABLES

INTRODUCTION

1. 1 Background

With rapid consumption of carbon-based energy resources, and their impact on the global environment, the need to develop sustainable uses of the byproducts of their use has drawn attention in the infrastructure field. For decades, researchers have been worked to develop innovative composite materials with unique characteristics such as lightness, durability and high recyclability. Synthetic lightweight aggregate (SLA) represents such a material; composed of high carbon fly ash (HCFA) – generated as a coal burning by-product – and various types of recyclable plastics, including polystyrene (PS), high density polyethylene (HDPE), low density polyethylene (LDPE), or even a mixture of different plastics (MP). As a construction material, SLA has the potential for use as a substitute of traditional lightweight and normal weight aggregates in concrete and geotechnical fill.

SLA properties, including bulk specific gravity, absorption capacity, moisture content, and porosity has been the subject of previous studies (e.g., Swan 2009). Additional studies had explored the compressibility, compressive strength, and stress-strain behavior of SLAs (Elsayed 2006; Holmstrom and Swan 1999; Gaudreau 2002; Swan and Sacks 2005). However, these studies were carried out on test specimens of SLAs in their granular state. No analysis had been performed on a single, solid SLA particle alone – a condition essential to more fully elucidate the behavior of SLA when used as a granular material. Towards generating, and testing and analyzing solid SLA specimens, this research began with a theoretical analysis, at the micro-

scale, of the elastic moduli of a solid SLA composed of fly ash and various types of recycled plastics. Various fly ash-to-plastic ratios were considered in this analysis.

One of the important parameters to evaluate the performance of this new material is Young's modulus, which indicates the stiffness of the material. In addition, as SLA can be used as aggregates in concrete, its Young's modulus helps to predict the modulus of concrete when the modulus of the mortar is also known. Although some laboratory tests have been conducted to study the Young's modulus of this type of composite material theoretical study have been very limited. An alternative to understand the stiffness of the material is to physically create and test trial mixtures; which, given to range of SLA formulations would be time and energy intensive. Theoretical methods could dramatically simplify the process and lead to quicker predictions of modulus and a faster optimization of a SLA's formulation. Therefore, this study focuses on the evaluation of Young's modulus of various types of SLA using both analytical method and finite element method (FEM). However, theoretical analyses alone would not be sufficient in characterizing the elastic modulus of SLAs; therefore, laboratory tests were carried out to check the applicability of the FEM modeling.

1. 2 Objective

One of the research goals was to explore and compare various methods (analytical, FEM modeling) used to predict the elastic moduli of solid SLAs. Based on these comparisons, an appropriate model was chosen and modified to simulate the stress-strain behavior of SLAs with laboratory test results on specific SLAs-HCFA/PS adopted to validate and modify the FEM model, so that it could simulate the SLAs-HCFA/PS specimen more specifically. The stress-strain curves from FEM modeling and laboratory tests were compared to evaluate the

applicability of the FEM model. It is expected the results of this study will help elucidate the behavior of SLAs, especially in understanding the elastic behavior of solid SLAs, which will assist in justifying its use in practice.

1. 3 Organization

The theoretical computation in this research includes two parts. Part (I) is general elastic moduli computations of SLAs, composed of HCFA and PS (SLAs-HCFA/PS) or MP (SLAs-HCFA/MP), based on the assumed values of material properties (E, ν) of the plastics and HCFA and the various volume fractions of the plastics and HCFA. Part (II) is elastic moduli computations of specific SLAs-HCFA/PS that have designed HCFA to PS mass ratios of 50:50 and 65:35, using physical tests that a) confirm the SLAs compositions and the densities of PS and HCFA, and b) compression testing to determine elastic modulus of PS (alone) and the SLAs. In addition, this work was compared to FEM computations of SLAs' elastic moduli based on assumed elastic modulus of HCFA and assumed Poisson's ratio.

The organization of this thesis is:

- Chapter 2 – literature review on SLAs and its components (fly ash and recycled plastics); previous studies on SLAs and other types of composite material that emphasized studies on elastic moduli of SLAs determined by various methods including analytical equations, FEM modeling, and laboratory tests;
- Chapter 3 – the methodology of theoretical computation, including analytical method, FEM modeling, and material properties employed in the computation.
- Chapter 4 – laboratory tests, including specific gravity and LOI tests on HCFA, PS, and SLAs for obtaining the actual compositions of SLAs; confined

compression test on granulated SLAs for preparing solid SLAs specimen; unconfined compression test on solid SLAs specimen for evaluating the stress strain behavior of SLAs; and scanning electro microscope (SEM) test for observing SLAs in microscopic level.

- Chapter 5 – theoretical computation results and discussions of Part (I) of the research effort described above;
- Chapter 6 – laboratory test results, theoretical computation results of Part (II), and the comparison of results acquired from these different methods.
- Chapter 7 – summary and conclusions from the research effort along with recommendations for future studies.

LITERATURE REVIEW

2. 1 Introduction

The chapter reviews previous work and studies on composite materials. It mainly includes three parts: (1) an introduction of environmental-friendly composite materials with emphasis on Synthetic Lightweight Aggregates (SLAs) that are made from high carbon fly ash (HCFA) and recycled plastics; (2) review of previous studies on SLAs, focusing on the modulus studies of both granulated SLAs and solid SLAs; (3) analytical and numerical methods that have been used for calculating the elastic modulus of particle-reinforced composite material.

2. 2 Environmental-friendly Composite Material Made with Recycled Products

Building materials have been considered an important factor in the LEED (Leadership in Energy and Environmental Design) standard when evaluating their sustainability. Materials characterized as energy saving, durability, low maintenance and healthy indoor environment can be considered as 'green' material. One type of well-developed green material is a composite material, which is composed with reinforcement material such as glass fibers, natural fibers, and carbon fibers, and particulate material such as sand, talc and other fillers, color chips, and recycled glass (ASHLAND 2011).

One type of composite materials that has been studied for decades is made of recycled material such as coal combustion byproduct (Slag, FGD, fly ash), recovered plastics, and shredded rubbers. Hassett et al. (1995) reported the study on the application of cenospheres, hollow spherical ash particles as "functional filler" in recycled plastics. Three types of ashes

included slag, fly ash and three grades of cenospheres and two types of polymeric materials including polyester and acrylic were used. The composite material had volume of fly ash up to 80%. The study concluded with positive potential application of cenosphere ash as a filler in recycled plastics to produce strong and lightweight aggregates. Li, et al. (1998) made a composite material from fly ash and post-consumer polyethylene terephthalate (PET). The fly ash content ranged from 0% to 50% by weight. During the manufacture process, shredded PET and fly ash were mixed together in a container, which was heated by an electric burner. After thoroughly mixing, the PET and fly ash mixture were poured into pre-heated cylindrical molds and cooled down. In laboratory, the compressive strength test, absorption test, linear shrinkage in molding process, X-ray diffraction (XRD) analysis, and SEM test were carried out on this composite material. The manufacture process and laboratory tests on the composite material showed that the fly ash served not only as a reinforcement, but also heat conductor, decomposition inhibitor and lubricating agent, which benefited the melting and mixing process of the product. According to the experimental results, Li et al. (1998) also proposed its potential usage as an alternative of lightweight aggregate.

Researchers had also discussed the amount of fly ash content used in the composite materials. Alkan et al. (1995) composed a new building material with two typical coal fly ashes and waste polyethylene (PE) bags. The fly ash content ranged from 10% to 50% by weight was used. The measurement on tensile strength of the materials showed that the composite fly ash – polyethylene mixture containing 20% fly ash had a tensile strength value at 20% of that of polyethylene alone. White (2000) conducted composite material made with high-lime (ASTM class C) fly ash and recycled polyethylene terephthalate (PET), and studied its mechanical and microstructure properties. White (2000) derived theoretical equations that correlate the elastic

modulus with compressive strength and fly ash content. According to White (2000), the composite materials were manufactured with various fly ash contents from zero up to 70%. However, it is time-consuming to obtain homogenous mixture when the fly ash dry weight was more than 50%. The compressive strength increased when fly ash content was increasing from 0% to 65%, while decreased when fly ash content kept increasing from 65% to 70%, probably because of the lack of thorough fly ash mixing. Similarly, Li et al. (1998) also reported the difficulty of getting completely homogenous composite material when mixing low-lime class F fly ash with recycled PET. However White (2000) found the high-lime class C fly ash particles could be completely homogenized, well-bonded and coated with recycled PET. The appropriate proportions of reinforcement particle and plastic matrix had also been studied by Ku et al. (2010), who performed tensile test on composites made from vinyl ester resin and reinforcement particle of cenospheres (ceramic hollow sphere or SLGs) derived from fly ash. Ku et al. (2010) found 33 percent the optimum contentof SLG by weight in vinyl ester resin, based on obtaining appropriate yield strength, tensile strength, Young's modulus, and Poisson's ratio of the composite. The 33 percent SLG mixture was also favorable and convenient to use as the generated composite was easy to cast. From a mechanical properties point of view, this proportion was an appropriate value because when the weight of fly ash was higher, the yield and tensile strength of the composite material dramatically decreased; and the Poisson's ratio increased rapidly.

Instead of using only fly ash and plastics, other recycled material have also been used to compose innovative materials. Sobhan and Mashnad (2000) presented a pavement base course material, which was a mixture of mixed recycled concrete aggregate, cement, ASTM Class C fly ash, and recycled high-density polyethylene (HDPE) stripes from post-consumer water and milk

containers. The tests on compressive strength, split tensile strength, and flexural strength showed that the mixture could be used as a substitute of traditional material for the construction and rehabilitation of highway pavements. Guleria and Dutta (2011) reported studies on the unconfined compressive strength of various mixtures of fly ash, lime, gypsum and tire chips. The effect of tire chip content, curing period, curing method, and treatment were examined. The unconfined compressive strength increased with the decrease in tire chip content, and the increment of compressive strength varied for different curing methods, in which the water-filled container generated the most amount of increment in compressive strength, followed by burlap and desiccator. The strength of the mixture was also significantly improved when treating with sodium hydroxide and carbon tetrachloride. Most importantly, the composite material meets the requirement of durability and was recommended for use in road sub-base with light traffic. Duta et al. (2011) presented a study on composite materials made from rubber, polyethylene terephthalate (PET), high-density polyethenelene (HDPE) and low amount of ASTM Class F fly ash (0.25%). With improved compression resistance, non-wetting behavior, and dense surface structure, the mixture was recommended for use in pavement slabs or anti-shock carpets for parks. White (2012) proposed the plunger-casting manufacturing method of making composite tubular pipes by using post-consumer recycled PET beverage bottle materials and one or more filler materials such as rock crusher fines, lime sludge or waste coal combustion by-product.

The study in this research focuses on various composite mix designs of high carbon fly ash (HCFA) and different types of recovered plastic at different weight ratios. As presented by Kashi et al. (2001), HCFA was mixed with recyclable plastics, including polystyrene (PS), high density polyethylene (HDPE), low density polyethylene (LDPE), or a mixture of these plastics and other thermoplastics at various high temperature ($200^{o}C \sim 300^{o}C$), and the compound was

extruded using twin-screw compounding extruder, creating flat strips about 50-mm wide and 9.5-mm thick. After cooling, it was granulated to desired size as coarse aggregates. The advantage of this high-recycled material is their utilization as substitute of natural lightweight and normal weight aggregates in various building components (Kashi et. al 2002). It can also be used as green roof and pervious pavement material (Swan 2009).

2. 3 Composite Material – Synthetic Light Weight Aggregates (SLAs)

ASTM D3878-15 defines composite material as "*a substance consisting of two or more materials, insoluble in one another, which are combined to form a useful engineering material possessing certain properties not possessed by the constituents*." The constituents in SLAs are HCFA and one type of recycled plastic or mixture of various types of recycled plastics. One of the properties that SLAs possess is sustainability compared to its constituents. In addition, as an environmental-friendly material, it has higher strength than plastics because being reinforced by HCFA. However, to understand the mechanical properties of SLAs, we need to understand the properties of its components first.

2. 3. 1 SLAs Component – High Carbon Fly Ash (HCFA)

According to the ASTM C618-12a "*Standard specification for coal fly ash and raw or calcined natural pozzolan for use in concrete*", fly ash is "the finely divided residue that results from the combustion of ground or powdered coal and that is transported by flue gasses." The fly ash used in concrete is categorized as Class N, Class F, and Class C fly ash. The Class N fly ash usually requires calcination to induce satisfactory properties; Class F fly ash has pozzolanic properties; Class C fly ash has both pozzolanic and cementitious properties. For each type of fly ash, the Loss of Ignition (LOI), which is a indication of unburned carbon content is required to be less than 10% (10% for Class N fly ash; 6% for Class F and Class C fly ash). ASTM C618 or

AASHTO M 295 also requires only low carbon fly ash (less than 6%) could be used in concrete to ensure the workability of concrete and durability in freezing temperature (Kashi, et al. 2001, Wen 2008). On the other hand, in the U.S. low-NOx burner and catalytic reduction system generates fly ash with high carbon content (more than 10%), in order to meet the Clean Air standards of 1990 that required low NOx emission into the atmosphere. Hence the recycling of HCFA was initiated, aiming to develop its beneficial usage and to eliminate the energy resource consumption and environmental impact.

2.3.1.1 Utilizations of Fly Ash

According to the 2013 Coal Combustion Product (CCP) Production & Use Survey Report, over 50 millions of tons of fly ash were produced in the U.S., 43.7% of this fly ash was recycled, as shown in Fig. 2.1, which also shows the generation and percentage of fly ash usage over a nearly 50 year span. Although overall the utilization of fly ash had been kept increasing over decades, the percentage of fly ash usage dropped sharply from 2007 to 2011, which might be caused by the "*regulatory uncertainty surrounding the rulemaking EPA commenced in the wake of a December 2008 failure of a coal ash disposal facility in Tennessee*" (American Coal Ash Association (ACAA), 2014). Ash users keep endeavoring to drive USEPA to finalize the regulations on coal ash and recently the USEPA has issued a rule on the management of coal combustion residuals (CCRs) with a focus on the beneficial reuse and disposal on coal fly ash (USEPA, 2015).

Fig. 2.2 illustrates the various utilizations of fly ash in 2013 in the United States. As shown, more than half of the recycled fly ash has been used in concrete-related product, followed by the structural fill/embankments (13%), blended cement/feed for clinker (10%), waste stabilization (9%), mining application (8%) and others. One of the reasons that the majority of

fly ash was utilized in concrete might be because of the existence of standard regulation provided by ASTM international or ASSHTO, which specifies the application of Class F and Class C fly ash in concrete, taking advantage of their pozzolanic and cementitious characteristic.

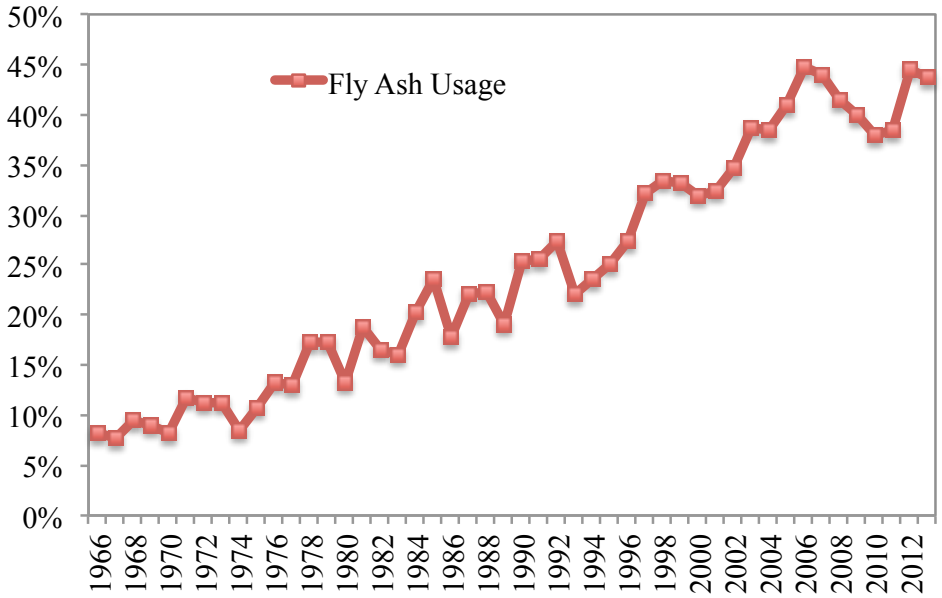

Fig. 2.1 ACAA Fly Ash Production & Use Comparisons 1966-2013 (Adapted from American Coal Ash Association (ACAA) 2013)

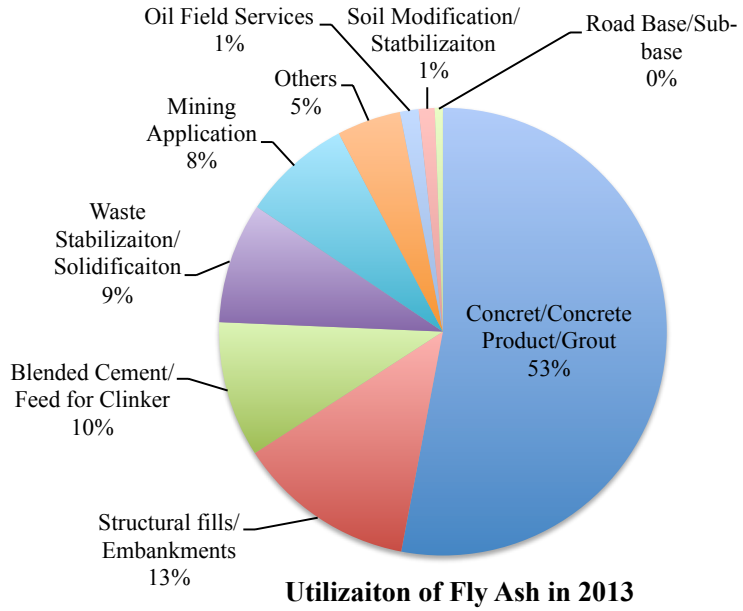

Fig. 2.2 Utilization of Fly Ash in 2013 (Adapted from American Coal Ash Association (ACAA) 2013)

As stated before, Class F and Class C fly ash are both low carbon fly ash, which both has LOI less than 6%. On the other hand, researchers have also kept working on high carbon fly ash (HCFA) to explore its application in industry in order to eliminate its disposal in landfills. Bhatty et al. (2002) performed two commercial-scale demonstration of HCFA in cement manufacture as an alternative of raw materials such as shale and soil without preprocessing, which decrease the energy cost and improved compressive strength of the cement. Naik et al. (2006) studied the mixture of controlled low-strength material (CLSM) mixtures contain various proportions of high-carbon fly ash (HCFA), and concluded that HCFA can be used in manufacturing-conductive CLSM and concrete for conducting electrical charge from lightening to the ground more safely. Ma and Wang (2007) presented study adding 0% to 20% of pulverized coal and fly ash into formamide and urea-plasticized thermoplastic starch (FUPTPS) and glycerol-plasticized thermoplastic starch (GPTPS), respectively. Both cases showed improved tensile strength, Young's modulus, and water resistance feature of the polymer. Wen et al. (2011) performed studies on stabilizing recycled asphalt pavement as a base course material under real world conditions in Minnesota, and concluded that HCFA stabilized recycled pavement material (RPM) was both economic and environmental beneficial base materials compared to the unstabilized RPM and crushed aggregate. Similarly, The SLAs discussed in this research contains only HCFA and recycled plastics, and the amount of HCFA used in the SLAs can reach up to 80% by weight. The recycling of tremendous amount of HCFA will unquestionably generate long term environment and economic benefits.

2.3.1.2 Mechanical Property of Fly Ash

Previous studies have concluded that fly ash consists of fine, powdery particles that are predominantly spherical in shape, either solid or hollow, and mostly glassy (amorphous) in

nature, having similar physical characteristic as soil silts. The solid fly ash particles are classified as precipitator; while the hollow fly ash particles are classified as cenosphere. Matsunaga et al. (2002) studied the morphology, composition and crystallinity of both types of fly ash particles of different sizes, using the techniques of scanning electron microscopy (SEM), energy-dispersive X-ray microanalysis (EDX) system, and X-ray diffraction (XRD). The SEM micrograph and EDX result for different type and sizes of FA are shown in Fig. 2.3 and Fig. 2.4. As shown, both types of the fly ash particles have spherical shape, although the cenosphere particles exhibit a more spherical shape compared to the precipitator particles. The Young's moduli of different types and sizes of FA particles were also estimated based on the crystallinity and volume fraction of each component of FA particles, as summarized in Table 2.1. As shown, the precipitator particles have a Young's modulus that is up to ten times higher than that of the cenosphere particles.

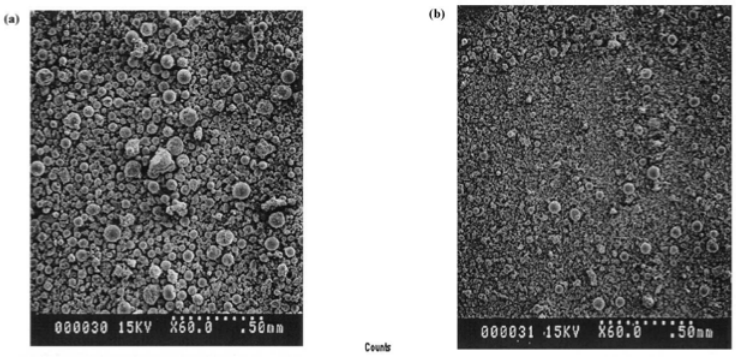

Fig. 2.3 (a) SEM micrograph and EDX result of 75–106 mm precipitator fly ash. (b) SEM micrograph and EDX result of 20–53 μm precipitator fly ash (Matsunaga et al. (2002)).

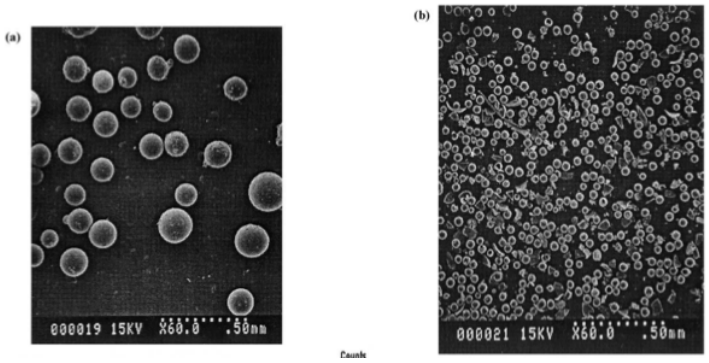

Fig. 2.4 (a) SEM micrograph and EDX result of 106–150 µm cenosphere fly ash. (b) SEM micrograph and EDX result of 20–45 µm cenosphere fly ash (Matsunaga et al. (2002)).

Table 0.1 Size and Young's Moduli of Fly Ash Particles (Adapted from Matsunaga et al. (2002)).

Type	Percipitator		Cenosphere
Size Range (µm)	150-250	5-10	20-150
Young's Modulus E (GPa)	126	98	13-17

However, Fig. 2.3 and Fig. 2.4 shows the morphologies of fly ash particles only. For HCFA, not only fly ash, but also unburned carbon exists. Hwang et al. (2002) took the images of unburned carbon in fly ash on SEM as shown in Fig. 2.5 (a). It shows that the unburned carbon is a particle with a porous structure that is embedded in the fly ash mixture.. Similarly, the SEM micrographs of fly ash and unburned particles from Ahn, et al. (1999) as shown in Fig. 2.5 (b) also illustrates the combination of fly ash particle and unburned carbon.

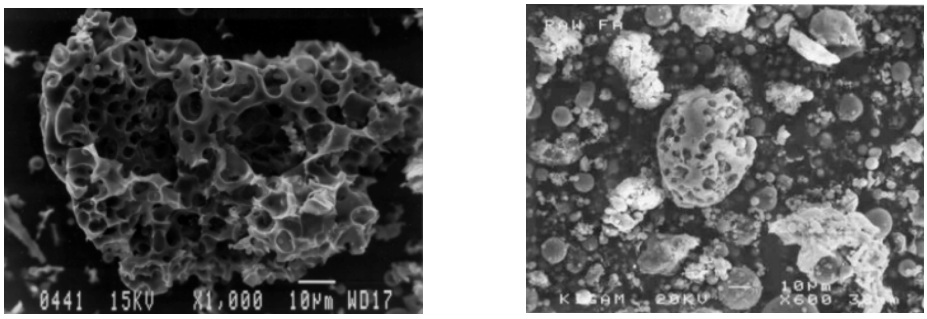

(a) (b)

Fig. 2.5 SEM Micrograph of (a) Unburned Carbon in Fly Ash (Huwang et. al (2002)); and (b) Unburned Carbon and Fly Ash micrograph (Ahn, et. al (1999)).

2. 3. 2 SLAs Component – Recycled Plastics

Plastic recycling helps to reduce greenhouse gas emission and toxic chemical production by reducing the fossil fuels used in producing raw plastics. Plastic recycling also saves natural source because the virgin plastics are made of non-renewable resources, and reduces the volume of plastics in landfill (Clean Up@ 2009).

2.3.2.1 Plastic Categories

Typically, in conversation, "plastic" and "polymer" are used interchangeably. However, in literatal terms, "plastic is made up of mostly polymer, but also contains such things as colorant and many other additives" (Cantor and Watts 2011). Polymers can be categorized in two ways: (1) Thermoplastic or thermoset material, depending on whether the crosslink existence or not, as shown in Fig. 2.6; (2) Semi-crystalline or amorphous state, which is varied by the presence or absence of ordered regions of crystals, as shown in Fig. 2.7 (Cantor and Watts 2011). Thermoplastic is widely used in industry because it is easier to be processed, and cost much less than thermoset. But thermosets have higher strength and heat resistance, and is generally used when this characteristic is required. A semi-crystalline polymer has ordered regions known as crystals. The polymer chains align into layers in some sections and remain disordered elsewhere, while amorphous polymers are those that do not contain any crystalline regions. Both semi-crystalline polymers and amorphous polymers constitute about half of the major polymers used today. But all polymers are in an amorphous state when melted (Cantor and Watts 2011). Recycled plastics generally are thermoplastic polymers that can be in an amorphous or semi-crystalline state. Among recycled plastics used in SLAs, PS is amorphous thermoplastic; HDPE, LDPE, and PP is semi-crystalline thermoplastic in room temperature; while PET is also semi-crystalline but can be quenched to form amorphous PET (APET) (Cantor and Watts 2011).

Thermoplastic:
- independent polymer chains
- will flow with heat

Thermoset:
- chemically crosslinked chains
- will not flow with heat

Fig. 2.6 Thermoplastic vs. thermoset (Cantor and Watts 2011)

Amorphous:
- disordered
- individual chains do not pack

Semi-crystalline:
- some chain sections pack into ordered regions (crystals)
- some sections remain amorphous

Fig. 2.7 Amorphous vs. Semi-crystalline (Cantor and Watts 2011)

2.3.2.2 Plastic Recycling

In 1988, the Society of the Plastic Industry (SPI) introduced the Resin Identification Code (RIC) system to help with the plastic recycling. In 2008 SPI began work with ASTM international for developing a globally-recognized code system. ASTM International issued the ASTM D7611 – *Standard Practice for Coding Plastic Manufactured Articles for Resin Identification* in 2010, and revisions in 2013 (SPI 2015). Basically, the recycled plastic resins are identified as seven types as listed in Table 2. 2.

As mentioned before, most recycled plastic generally are thermoplastic that can be recycled by melting and reusing. Thermoplastic can also be used as filler by being ground up.

Example of thermoplastics are PET, SPI code No. 1 and commonly used in soda bottles, that can be recycled into fibers, strappings, and reinforcement for concrete; and HDPE, No. 2 and used for milk bottles and other containers, that can be recycle into flower pots, pipes, toys, trash cans, soft-drink-bottles carriers, pails, and drums.

Table 2.2 SPI Resin Coding System and Examples (Adapted from ASTM D7611)

Resin Identification Number	Resin	Resin Identification Code – Option A	Resin Identification Code – Option B	Examples (Stevens1999)
1	Poly (ethylene terephthalate)			2-liter soda bottles, some condiment containers
2	High density polyethylene			Milk jugs, laundry detergent containers
3	Poly (vinyl chloride)			Some drinking water, vegetable oil containers
4	Low density polyethylene			Flexible film bags, flexible lids, plastic bags
5	Polypropylene			Jar lids, container closures, battery cases, box liners, some bottles
6	Polystyrene			Fast food foam boxes, foam cups, meat trays, computer housing
7	Other resins			Multiple resin materials, some squeezable containers

Recycled plastics have been utilized as construction materials for decades. In 1989, a newly developed plastic concrete was first used in the General Electric “Living Environments”

concept house in Pittsfield, Massachusetts. In the project, concrete was mixed with virgin and recycled polybutylene terephthalate (PBT), which is predominantly used mainly for electrical parts, automotive exterior parts, and small appliances. The concrete had 38% higher 28-day compressive strength and 50% less weight than a regular concrete. In addition, the plastic concrete showed good freeze-thaw durability and has colorful features (Nasvik, 1991). Currently, recycled plastics are mainly used in concrete and asphalt as an addition or substitution of aggregates. Thiagarajar College (Nigam and Akolkan, 2009) used recycled plastic as a coat for aggregates in pavement; Glisevic (2012) presented a project developing expanded granules and densified flakes, which are made from the sorting of recycled plastic. The expanded granules could be used as aggregates for light structural and nonstructural concrete while the densified flakes could be used as aggregate for mortar and raw material for expanded granules. Kumar and Prakash (2012) studied the utilization of HDPE powder as a substitute for part of cement and sand. The HDPE powder was added into the coarse aggregates and heated at a temperature of 750°C ~ 850°C. After being thoroughly mixed, the mixture was then cooled and mixed with cement, fine aggregate and water to prepare concrete mix. An optimum substitution amount of 5% was determined as it doubled the compressive strength over that of plain cement concrete. Ho, et al., (2006) studied the properties of asphalt modified with polyethylene materials. The combinations of three low molecular weight polyethylene (PE) wax materials and three recycled LDPE materials were used as asphalt modifier. The PE and LDPE materials were mixed into asphalt with a low shear mixer for 1h at 160°C and high shear mixer for 1h at 185°C, respectively. Different types of recycled LDPE were used as the asphalt modifier, taking up to various percentages (0.5% to 4%) of the base asphalt. The different mixes were tested to examine the shear stress, failure strain, and critical temperature, which are important parameters

to determine pavement performance. The results indicated the LDPE with lower molecular weight and wider molecular weight was more suitable for use as an asphalt modifier.

Alternatively, instead of being used in concrete directly, recycled plastics have been combined with other materials to create fine or coarse aggregates that then could be used as aggregates in concrete. Choi, et al., (2009) presents the utilization of a synthetic fine aggregate that was made by recycled waste polyethylene terephthalate (PET) bottles. The waste PET bottles were cut into 5~15mm and mixed with river sand powder that had diameter less than 0.15mm in a rotating mixer at temperature of 250°C. After being discharged and cooled from the mixer, the aggregate was screened to remove particles less than 0.15mm in size. This screened material represented the synthetic fine aggregate, and was used as fine aggregate in concrete. The research evaluated various percentages (0%, 25%, 75%, and 100%) of substitution of fine aggregate by the synthetic aggregate. The results showed that the synthetic aggregate had the advantage of increasing the flowability (workability), decreasing the weight of concrete. However, the 28-day compressive strength was decreased by 6%, 16% and 30% on average when 25%, 50%, and 75% of fine aggregate were replaced by the synthetic aggregate, respectively. But the synthetic aggregate has higher strength over density ratio compared to the traditional lightweight aggregates. Similarly, the recycled plastics/river sand powder composite was used to make coarse aggregate. The SLAs material that is studied in this research can also be used as fine and/or coarse aggregates to produce lightweight concrete.

Instead of using only one resin of recycled plastics, some researcher use a mixture of plastics to develop synthetic coarse aggregate. For example, Elzafraney et al. (2005) developed the granulated mixed plastic (HDPE, PVC, PP) that can be used as coarse aggregate of concrete. The adoption of this type of concrete helps to save thermal energies because it reduces the

cooling and heating loss of the building. Comparably, one type of SLA developed by Kashi et al. (2002) used plastics mixture of plastics from resin #1 to #6 (with exclusion of #3 (PVC)), which mimicked the typical recycled plastics waste stream collected from residential recycling programs that is then processed by Material Recycling Facilities (MRFs). The #1 (PET) and #2 (HDPE) plastics each represented 30% of the overall recycled plastic's composition. Previous study showed that the SLAs aggregate had low absorption and concretes exhibited relatively ductile properties.

The utilization of recycled plastic in construction materials not only benefits the plastic recycling, but also enhances the performance or characteristics of the materials. For example, use of the polymer-coated aggregate in concrete provides: (1) less exposed (surface) voids and, thus, water absorption, increasing the quality of the aggregate; (2) reduced porosity, improving the soundness of the aggregate; and (3) higher hydrophobicity (i.e., enhanced 'waterproof' property) preventing the occurrence of stripping (Wansbrough and Yuen 2002). For pavements, use of recycled plastic as an asphalt modifier can improve the performance and decrease the thickness of pavement (Kumar 2012).

2.3.2.3 Difficulty and Cost of Plastic Recycling

One problem with plastic recycling is its difficult to sort plastic waste, especially for smaller plastic parts. In addition, the cost of raw material is also low, leaving little to no profit advantage for manufacturers to recycle the plastics. Mainly because of these reasons, only around 9% of plastics are recovered for recycling, according to the U. S. Environmental Protection Agency (2013).

The cost of using recycled aggregates varies depending on the type of the recycled plastic, the purpose, and the product. As discussed, when small amounts of recycled plastic is

used as a modifier and substitute of part of cement; the cost is reduced. When the PBT was used to reach higher compressive strength of concrete, it was more expensive; while when a typical mix of recycled plastic was used such as SLAs-HCFA/MP, it is believed to reduce the sorting cost. Generally, the equipment, supplies, and energy requirements need to be considered to compare the overall recycling costs. In addition, the transportation cost and post construction cost should also be included. Since the recycled plastics are lighter, it reduces the cost of transportation (Strong 2005). The lightweight nature of plastics will help reduce the loads on bearing elements such as beam, column, and foundations, generating less stress, and consequently reducing costs. Moreover, when using recycled plastic as a modifier, the pavement is more durable leading to less maintenance cost. Finally, the re-utilization of plastic reduces the cost of disposal of plastic, saving landfills, and reducing environment pollution. Hence it is environmental-cost friendly in the long term.

2. 4 Previous Studies on SLAs Mechanical Properties

Elsayed (2006) summarized the history of SLAs research program. The first generation of SLAs was made from low carbon fly ash (LCFA) and HDPE, followed by the mixture of either LCFA or high carbon fly ash (HCFA) and other types of recycled plastics at various mass ratios. The physical properties of granulated SLAs, including bulk specific gravity, absorption capacity, moisture content, and porosity has been the subject of previous studies as well (e.g., Swan 2009). Its mechanical properties such as compressibility, compressive strength, and stress-strain behavior have also been explored (Holmstrom and Swan 1999; Gaudreau 2002; Swan and Sacks 2005; Elsayed 2006).

The study from Holmstrom and Swan (1999) had SLAs with specific gravities in the range of 1.1 to 1.9; increasing with increased fly ash content. Weingam (2003), who studied the

bulk specific gravity of HCFA-with-MP-based SLAs, the bulk gravity increases not only with the fly ash content but also with time as more water absorption occurred, and the increase is sharper for SLAs with higher fly ash content. In addition, he found that the absorption slightly increased as the percent of HCFA in the SLA increased (Weingam 2003).

Shah (2000) (cited by Elsayed 2006) investigated the effect of HCFA on SLAs made from HDFE, LDPE, PS, and MP, and concluded that the stiffness of SLAs increase with the increasing amount of HCFA. The stiffest (most brittle) SLAs are those made from PS; while the softest (most ductile) SLAs are those made from LDPE.

SLA stress-strain behavior and modulus were studied by conducting consolidation test (Holmstrom and Swan 1999, Cook 2000 cited by Elsayed 2006, Swan & Sacks 2004, Elsayed 2006), and triaxial compression tests (Holmstrom and Swan 1999, Cook 2000 cited by Elsayed 2006, Gaudreau 2002, Elsayed 2006). The composite of LCFA and HDPE exhibits consolidation behavior that is similar as natural soil (Homstrom and Swan 1999). Constrained modulus and modulus of elasticity of SLAs made of HCFA and various types of plastics had also been studied from 1-D and confined compression tests (Gaudreau (2002), Elsayed (2006)).

2. 4. 1 Modulus of Granulated SLAs

Elsayed (2006) conducted strain-control and stress-control 1-D compression test on sand, pure PS, and SLAs composed of HCFA (80% by weight) and various plastics (HDPE, LDPE, PS, and MP). All samples has initial relatively density of 70% and experienced strain rate of 0.2, 1, and 5 % per min respectively. Experiment results show that the constrained modulus of SLAs and pure PS increased with the increment of effective vertical stress, and in linear correlation at each loading speed. These results agreed with those obtained by Swan and Sacks (2004), who performed 1-D compression tests on SLAs of PS, LDPE, HDPE, and MP. The constrained

modulus of SLAs at different strain rate and stress level is provided in Table 2.3. Generally, the constrained modulus increased with the increase of loading speed, but to varying degrees. As shown, the loading speed affected HDPE material most, followed by the LDPE, MP and PS.

Table 2.3 Constrained modulus results for SLAs samples at stress of 175, 300, and 700kPa from constant rate of strain tests (Elsayed (2006)).

Stress Level	175 kPa			300 kPa			700 kPa		
	Constrained Modulus, D (MPa)			Constrained Modulus, D (MPa)			Constrained Modulus, D (MPa)		
Material	$\dot{\varepsilon}$ 5%/min	$\dot{\varepsilon}$ 1%/min	$\dot{\varepsilon}$ 0.2%/min	$\dot{\varepsilon}$ 5%/min	$\dot{\varepsilon}$ 1%/min	$\dot{\varepsilon}$ 0.2%/min	$\dot{\varepsilon}$ 5%/min	$\dot{\varepsilon}$ 1%/min	$\dot{\varepsilon}$ 0.2%/min
HDPE	-	4.5	4.0	14	8.0	4.9	15	8.0	6.7
PS	6.0	4.5	4.4	9.5	8.5	7	9.6	8.8	10.1
MP	5.0	4.0	2.5	7.2	6.5	3.5	7.5	6.2	4.9
LDPE	5.8	4.0	2.0	7.2	4.0	2.9	7.5	4.0	4.5

Elsayed (2006) also performed volume-control traixial tests for aggregates (sand, EC, pure PS, SLAs) with the same initial relative density of D_r = 70% and confining pressure of 214kPa in both drained and undrained condition; and stress-control triaxial test for SLAs at different initial relative density (D_r = 0.1% - 30% for loose, Dr = 38% - 84% for dense) with various confining pressures in undrained condition. The results showed that the modulus of elasticity increased with the increment of effective confining stress, and the correlation could be modeled with a linear function with moderate values of coefficient of regression as shown in Fig. 2.8. In addition, most SLAs had modulus of elasticity that was less than 0.08GPa when the effective confining stress is less than 800kPa. The triaxial test results also had good agreement with those from consolidated isotropic drained compression (CIDC) tests on SLAs of HDPE,

LDPE, PS, and MP confining pressure of 200kPa, 400kPa, and 800kPa carried out by Gaudreau (2002).

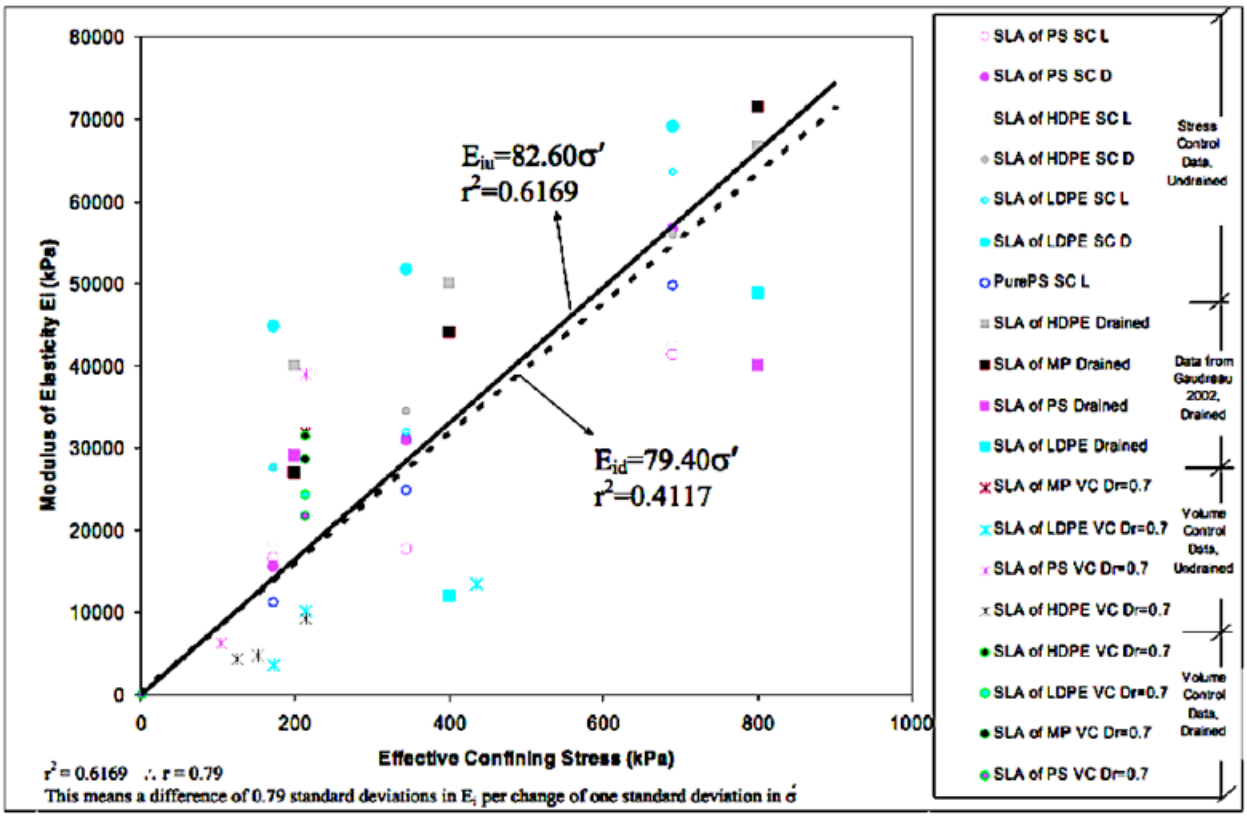

Fig. 2.8 Modulus of elasticity vs. effective confining stress for SLAs from drained and undrained tests, using stress and volume control techniques (Elsayed (2006)).

As shown in Fig. 2.8, the value of elastic moduli of granulated SLAs were influenced by the components (i.e., recycled plastic type), relative density, and effective confining stress. Fig. 2.8 also showed that for the cases at confining stress greater than 200kPa, SLAs-HCFA/PS had lower elastic modulus than the pure PS did when the relative density and effective confining stress were the same. This is counter-intuitive as one would expect that the addition of HCFA particles in PS would generate stiffer material than PS because HCFA has relatively higher stiffness. To understand this contradictory phenomenon, the parameters that affect the stiffness

of the specimen should be specified and investigated. Since the specimen was made from a granulated SLA particle instead of a monolithic or 'solid' particle, both the mechanical properties of individual particles and the interaction between particles should be considered in determining the behavior of SLAs specimen. Even when a SLAs-HCFA/PS 'solid' is stiffer than pure PS 'solid', the SLAs 'solid' created from compressing individual SLA particles may show less stiffness, depending on the interaction behavior between the particles. In fact, studies on the fly ash content effect on friction of glass fiber reinforced polymer composites have concluded that the addition of fly ash decreases the coefficient of friction of the glass vinylester composites significantly (Chauhan 2010). In conclusion, it can be stated that the mechanical properties of SLAs are determined not only by the properties of each phase but also the interaction between the phases as well.

2. 4. 2 Elastic Modulus of Solid SLAs

As can be seen, previous studies on the modulus of SLAs were carried out on the specimen that was complied with granulated SLAs particle. Comparatively, solid SLA itself should be studied because its properties are fundamental characteristics and are critical to determine the behavior of the structure when SLAs was used as construction materials such as in concrete and pavement system.

Weingam (2003) predicted the elastic moduli of SLA aggregates made of mixed plastic (MP) and HCFA. In that study, SLA aggregates were used in casting Portland cement-based concrete. The research used an equation based on the Bach and Nepper-Christinasen model, which show the correlation between the elastic modulus of SLAs aggregate, mortar, and concrete, and aggregates volume fraction. The elastic moduli of concrete and mortar were first calculated from experimental tests. The aggregates moduli were then deduced using the equation.

The elastic moduli of SLAs-HCFA/MP were summarized as in Fig. 2.9. Where 30%, 15% is the coarse aggregate volume fraction in concrete. As shown, the elastic moduli SLAs that has various amount of HCFA were very close. The SLAs-HCFA/MP that contains actual fly ash of 43%~53% and 70%~73% has elastic modulus in a range of 300~370ksi(2.07~2.55GPa) and 300~470ksi (2.07~3.24GPa) respectively.

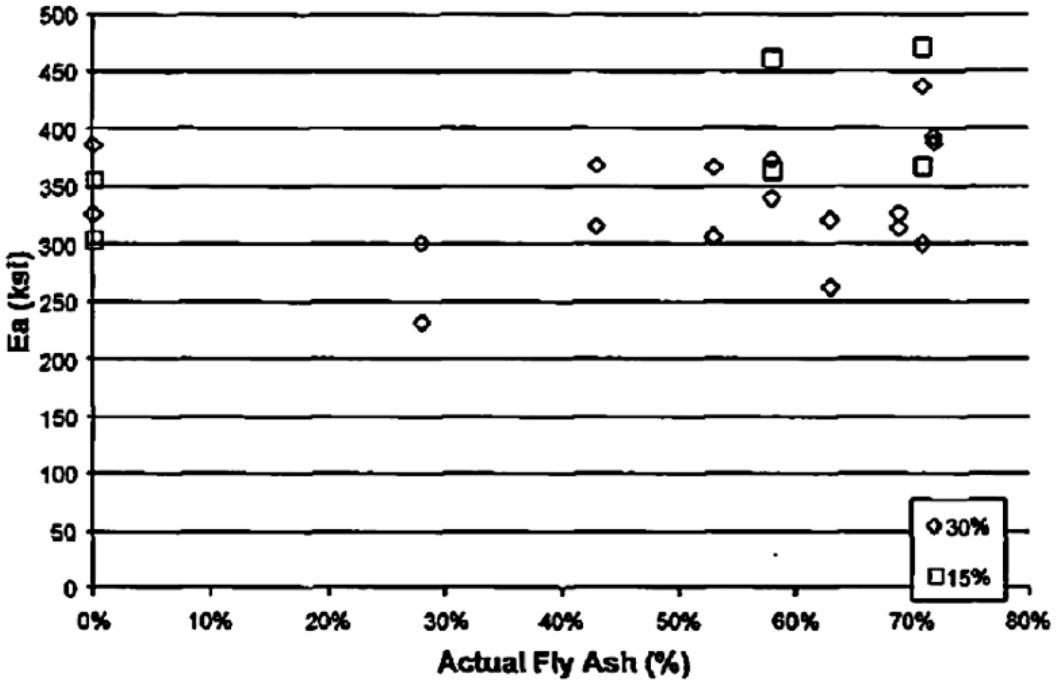

Fig. 2.9 Modulus of Elasticity of Aggregates vs. Fly Ash Content (Weingam (2003))

2. 5 Elastic Modulus Studies on Composite Materials

Since SLA is a two-phase composite material made of spherical shaped HCFA reinforcement and recycled plastics matrix, its elastic modulus can be predicted using general methods for particle reinforced composite materials. The elastic modulus of composite material can usually be predicted using both analytical and fine element methods (FEM).

2. 5. 1 Analytical Method

The elastic properties of the composite materials have been theoretically studied since the early 1950s (Kerner, 1956; Counto, 1964; Hashin and Shtrikman, 1963; Ishai and Cohen, 1967). Watt et al. (1976) summarized that the evaluation of the elastic properties of composite materials may be realized using theoretical methods, such as statistical method, scattering theory, and bounding methods. The statistical method studies the macroscopic elastic properties of composite materials using a complete statistical analysis, which writes all random quantities as functions with several orders. The correlation functions of all orders, including combinations of material properties, are required to be acknowledged in detail. Although it is the most complete method, the tedious process and its uncertainties limited its practical application (Watt et al. 1976). The scattering theory method utilizes the quantum mechanical scattering theory in solid mechanics, and defines the stiffness tensor as a sum of spatially constant and varying terms. However, approximation has to be taken to get solutions except for very simple problems. Hence the drawback of this method arises due to the problem of correlating specific mathematical approximations to physical properties of materials.

Compared to these two methods, bounding methods are broadly used in practical applications with limitation to isotropic composites. The Hashin-Shtrikman bounds are broadly used and have been proven to be consistent with results of several experimental studies (Watt et al. 1976). Watt et al. summarized that in the Hashin and Shtrikman bounding method, a reference body with stiffness C_0, Stress τ' and Strain E is introduced to replace an isotropic composite body with stiffness C(x), stress τ, and strain E(x). Equations $\tau'(x) = (C- C_0)E(x)$ was introduced so that the internal stress field $\tau'(x)$ doesn't change the strain E(x). The selection of τ' in the reference body then were involved in the bounding process. Hahsin and Shtrikman (1963) then

apply variational principles to the bounding of the moduli and obtain the upper and lower bounds of bulk and shear modulus for n-phase composite material. The equations that correlate bulk modulus, shear modulus, particle volume fraction, and Poisson's ratio for two-phase composite material will be introduced in Chapter 3, and will be adopted in this research.

Other analytical methods include Mura's expression (Chawla and Shen (2001)), Kerner's equation (1956), and Counto's equation (1964); all predict the elastic modulus of particulate reinforce composite materials such as SLAs. Each will also be discussed further in Chapter 3. Although the expressions of these methods are various, their application is limited to a homogenous composite material that is a coherent mixture of several isotropic elastic materials.

2. 5. 2 Finite Element Method (FEM) – Unit Cell Model

The description of the mechanical behavior can be divided into four levels, "nano- (atomistic level), micro- (dislocations and unit voids and inclusions), meso- (larger part of a microstructure of material, i.e. combinations of many inclusions, layers, gradients) and macrolevel (specimen)" (Mishnaevsky & Schmauder, 2001). Another way to predict the elastic moduli of composite material is the Finite Element Method (FEM), which is one of the mesomechanical simulation methods based on continuum mechanics, containing constitutive equations and conservation laws (Mishnaevsky & Schmauder, 2001). Two modeling methods – unit cell model and real structure simulation are appropriate for the real complex microstructure of a multi-phase material. The unit cell model is the method (used in this research) is limited to a composite material that has periodical structure composed by reinforcement and matrix; while real structure simulation could be realized by capturing the real microstructure of material and using Digital-Image-Based (DIB) modeling to generate FE mesh for further computation.

A unit cell model was initially developed for fiber-reinforced material that has a round fiber surrounded by a matrix layer, and that has strict periodical distribution of equally sized fibers (Dong & Schmauder, 1995 cited by Mishnaevsky & Schmauder, 2001). It was further used in 3D and particulate-reinforce materials with extended particle shapes of "unit cylinder", "truncated cylinder", "double-cone", and "sphere" (Chawla and Shen 2001). Generally, the isotropic homogenous particulate composite material has periodically distributed reinforcement, and can be taken as being formed by repeated unit cell of reinforcement and matrix.

Although the unit cell was applicable and efficient for the material that has some periodicity/regularity in the structure, and the regularity is deterministic of the material properties, it has been widely used in alloy material, which has random structure in three dimensions (Mishnaevsky & Schmauder, 2001). Shen et al. (1994) adopted axisymmetric and plan strain cell model and studied the effect of different reinforcement particle shape (unit cylinder, truncated cylinder, double-cone, and sphere) on a two-phase composite material made from aluminum alloy matrix and SiC particles. In numerical modeling analysis, the composite unit cell subjected to tensile loading and free to contract laterally. Perfect bonding between matrix and particle was assumed. The numerical simulation results showed that the Young's modulus increased in the order of double-cone (lowest) to sphere to truncated cylinder to unit cylinder (highest). This is reasonable because the transverse strain constraining around the particle helps in enhancing the stiffness.

Fang and Chuwei (1997) used unit cell model in conjunction with continuum plasticity theory to evaluate the elastoplastic stress-strain behavior during tensile deformation of a composite material made from aluminum alloy matrix and alumina reinforcement. Various uniform arrays (cubic edge array, hexagonal array, rectangular array and cubic diagonal array)

and particle shapes (spherical, cylindrical, oblate, cubic and rectangular parallelepiped) were considered. Finite element simulation was performed based on a 3D cell model of periodic particulate distribution, introducing the elastic and compliance tensors in the structure as periodic functions of the position. In the simulation, the reinforcement particle was assumed elastic and perfectly bonded to the matrix. Stress-strain curves under uniaxial tensile loading condition were represented for composites with various volume fraction, aspect ratio of non-circular particles, non-circular particle orientation, particle packing and cell array, and particle shape. The results showed that the reinforcement was more effective along the direction with higher aspect ratio. In fact, the effect of cell array, non-circular particles alignment, and particle shape is actually the reflection of the effect of aspect ratio as well.

Li and Wongsto (2004) fully investigated particle-reinforce composite in a range of typical packing systems (simple cubic packing, body centered cubic packing, face centered cubic packing, and close packed hexagonal packing as shown in Fig. 2.10 using the unit cell model, containing spherical particle with both regular and irregular geometries in 3D coordination system. Both particle and the matrix were assumed to be linear elastic and perfectly bonded to each other. FEM analysis was performed using ABAQUS to predict the effective Young's modulus in orthogonal directions E and E', shear modulus and Poisson's ratio of composite material that had been tested in previous research. The Young's modulus (E and E') was both compared with experiment results. It showed that the average of E and E' obtained from simple cubic packing had the best agreement value with the experimental results.

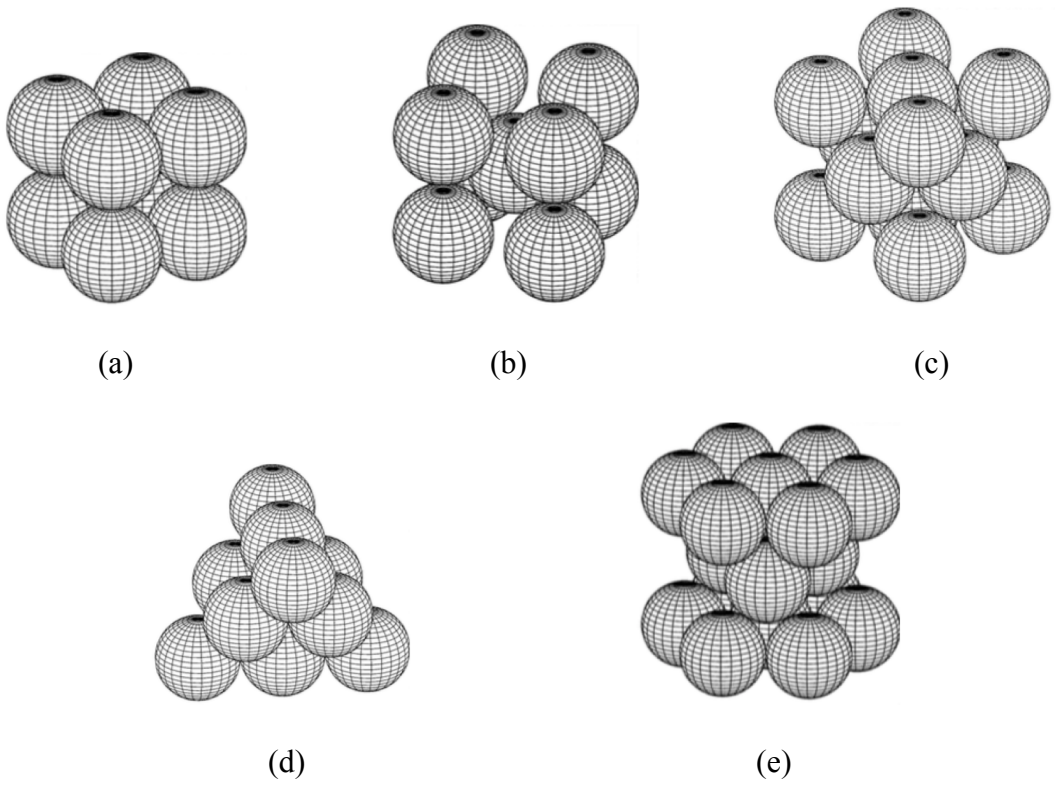

Fig. 2.10 (a) A simple cubic packing; (b) A body centered cubic packing; (c) A face centered cubic packing; (d) a different persepctive of a face centered cubic packing; (e) a close packed hexagonal packing. (Li and Wongsto (2004)).

Gaudig et al. (2003) employed a self-consistent one-particle 3D unit cell model to compute the Young's modulus and Poisson's ratio of ferritic cast-iron. Instead of using conventional unit cell modeling that is made up of ellipsoid of graphite surrounded by α Fe–2.5% Si matrix, "the cube shaped unit cell is made up of an inner rotational ellipsoid of graphite surrounded by α Fe–2.5%Si matrix in a concentric outer ellipsoid of the same aspect ratio as the inner graphite ellipsoid. The remainder of the unit cell is filled up by the cast-iron compound, the elastic behavior of which is determined self-consistently" (Gaudig et al. 2003). Uniaxial tension loading was applied and elastic properties were analyzed using finite element method. By comparing the results from the self-consistent model with those obtained from conventional unit

cell model, Gaudig et al. (2003) discussed the advantages of using the self-consistent model in predicting the elastic properties of cast-iron as a function of the graphite particle shape.

As noted, most alloy studies discussed above employed unit cell model with the assumption of perfect bound between reinforcement and matrix, and uniaxial tension loading condition in FEM solution. In this research, SLAs are assumed as isotropic homogeneous material composed by periodically distributed fly ash particles in sphere shape and plastic matrix. Therefore, unit cell method could be used for numerical modeling analysis. Additionally, various bounding effect between HCFA and recycled plastics will be considered. In contrast to these studies, uniaxial compression loading will be used in FEM analysis.

2. 5. 3 Experimental Studies on Composite Material Made of FA and Recycled Plastics

Overall, both analytical and FEM modeling methods are available for predicting the elastic modulus of composite material, and will both be used for SLAs in this research. On the other hand, laboratory testing is another process that can be used to study the modulus of SLAs. Laboratory tests have been performed on composite materials similar to SLAs to study the stress strain behavior.

An informative study was performed by Ku et al. (2010), who performed tensile test on composites specimen made from vinyl ester resin and fly ash as discussed before. The specimen was casted as rectangular prism pillars with cross section of 14.46mm x 4.32mm. Fig. 2.11 (Ku et al. 2010) illustrates that the method of calculating the Young's modulus is to take regression of the data from the most linear part on the stress strain curve. Fig. 2.12 shows the Young's Modulus and Poisson's ratio of the material containing various fly ash contents. As shown, the Young's modulus increased when fly ash content increased from 30% to 35%, and the Poisson's ratio increased rapidly when fly ash content was more than 33%. It should be noted that these

studies only considered the amount of fly ash content changing in a small range (5%), and at low fly ash content (< 35%).

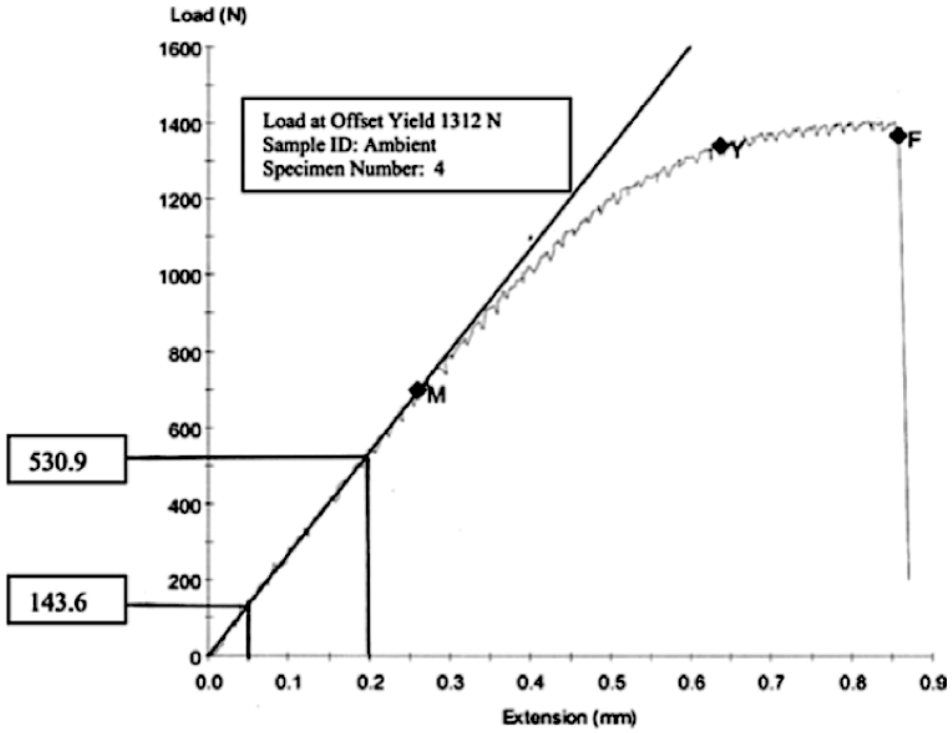

Fig. 2.11 Illustration of Calculating Young's Modulus (Ku et al. 2010).

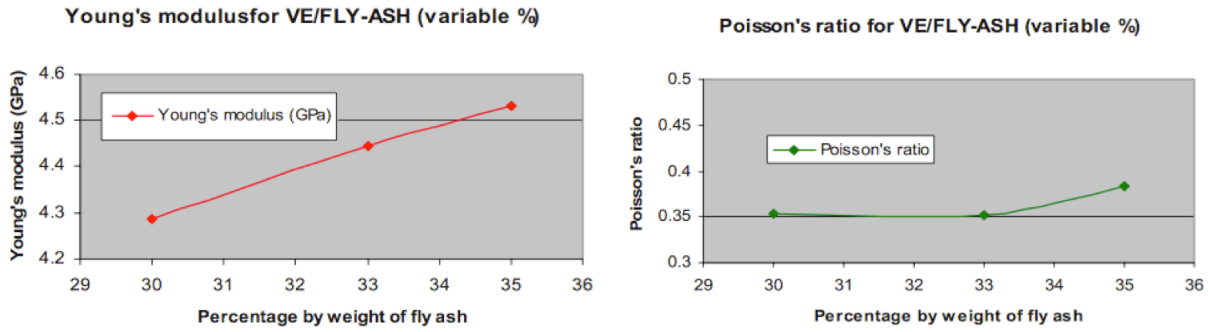

Fig. 2.12 Young's Modulus and Poisson's Ratio for VE/FLY-ASH at Various Fly Ash Content (Ku et al. 2010).

Another laboratory reference was presented by White (2000), who obtained the compressive stress-strain curves of a composite material made with ASTM class C fly ash and

recycled polyethylene terephthalate (RPET) as shown in Fig. 2.13. The stress-strain curves were recorded using a material testing system at loading rate of 5mm/min. The elastic modulus was 1.29GPa, 1.50GPa, and 2.25GPa for composite with 0%, 37.5%, and 70% of fly ash. As illustrated, composite specimens containing 37.5% and 70% fly ash had stress strain curves that exhibited a stiffing response at lower strains. But with continued straining, the curve shows nearly linear stress-strain behavior until strain reached up to 2.5% and strain-softening begins. These curves will be used to compare with those obtained from experimental tests on SLAs in this research.

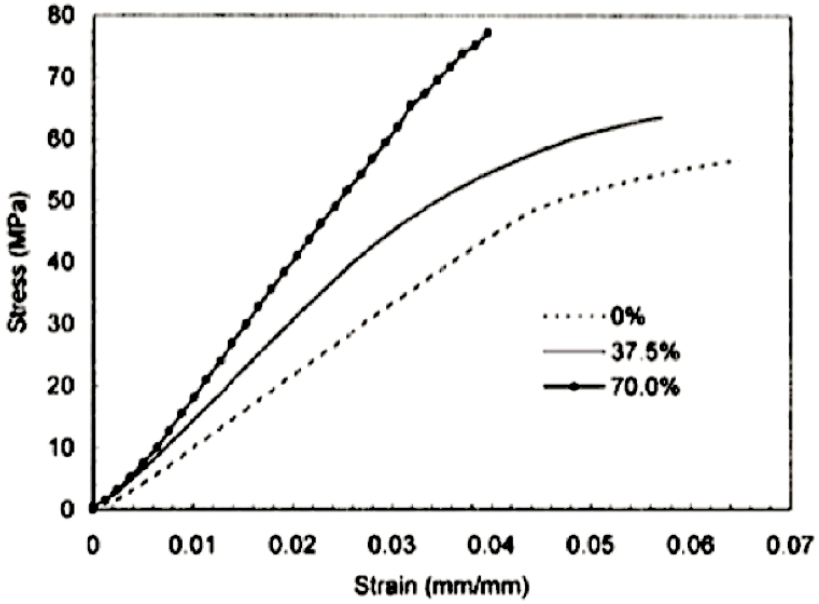

Fig. 2.13 Effect of Fly Ash Concentration on Stress/Strain Response of Composite Material (White 2000).

THEORETICAL COMPUTATION

3. 1 Introduction

This chapter reviews the analytical computation methods and FEM systems used in this research. FEM modeling, specifically, PLAXIS axisymmetric, ABAQUS Axisymmetric, and ABAQUS 3D systems, was used to predict the elastic modulus of SLAs-HCFA/PS SLAs at various volume fractions (0.083, 0.341, 0.627 for axisymmetric coordination system; and 0.065, 0.268, and 0.493 for ABAQUS 3D coordination system). Results will be compared and discussed in Chapter 5. In addition, the elastic modulus of SLAs-HCFA/MP was also computed and compared using a variety of analytical methods. One of the purposes of the theoretical computations was to compare these results to the different FEM systems used for predicting the elastic moduli of SLAs, which are assumed as isotropic and homogenous material. Another goal was to use the data obtained from these comparison, to choose the most appropriate model for predicting the elastic modulus of SLAs-HCFA/PS(65:35) and SLAs-HCFA/PS(50:50) more specifically.

3. 2 Analytical Computation

In this research, analytical methods posited by Hashin-Shtrikman bounds, Mura expression, Kerner equation, and Counto equation were used to predict the elastic moduli of SLAs at volume fraction from 0.1 to 0.9 with increment of 0.1. Hahsin and Shtrikman (1961, 1963) applied variational principles to provide an upper and lower boundary of the moduli obtained from analysis results. The method is applicable for n-phase composite materials.

Specifically in this research, for a two-phase composite material, the upper and lower bounds of bulk moduli and shear moduli are written as in Eqs. 3.1- 3.4. (Chawla and Shen 2001), where the K is the bulk moduli; μ is the shear modulus; f is the volume fraction of reinforcing particles. The "upper", "lower", "M", and "R" refer to the upper bound estimates, lower bound estimates, matrix and reinforcement, respectively. Once the K and μ has been calculated, the Young's modulus of the material E can be calculated using Eq. 3.5.

$$\boldsymbol{K^{upper} = K_R + (1-f)\left[\frac{1}{K_M - K_R} + \frac{3f}{3K_R + 4\mu_R}\right]^{-1}} \quad \textbf{(3.1)}$$

$$\boldsymbol{K^{lower} = K_M + f\left[\frac{1}{K_R - K_M} + \frac{3(1-f)}{3K_M + 4\mu_M}\right]^{-1}} \quad \textbf{(3.2)}$$

$$\boldsymbol{\mu^{upper} = \mu_R + (1-f)\left[\frac{1}{\mu_M - \mu_R} + \frac{6f(K_R + 2\mu_R)}{5\mu_R(3K_R + 4\mu_R)}\right]^{-1}} \quad \textbf{(3.3)}$$

$$\boldsymbol{\mu^{lower} = \mu_M + f\left[\frac{1}{\mu_R - \mu_M} + \frac{6(1-f)(K_M + 2\mu_M)}{5\mu_M(3K_M + 4\mu_M)}\right]^{-1}} \quad \textbf{(3.4)}$$

$$E = \frac{9K}{1 + 3K/\mu} \quad \textbf{(3.5)}$$

Chawla and Shen (2001) rewrote the Mura expression, as shown in Eq. 3.6 and Eq. 3.7, for material with spherical reinforcement particle, where the ν_M is the Poisson's ratio of the matrix. The elastic modulus is also calculated using Eq. 3.5.

$$\mu = \mu_M\left[1 + f(\mu_M - \mu_R)/\left\{\mu_M + 2(\mu_R - \mu_M)\frac{4 - 5\nu_M}{15(1-\nu_M)}\right\}\right]^{-1} \quad \textbf{(3.6)}$$

$$K = K_M\left[1 + f(K_M - K_R)/\left\{K_M + \frac{1}{3}(K_R - K_M)\frac{1+\nu_M}{1-\nu_M}\right\}\right]^{-1} \quad \textbf{(3.7)}$$

Fu et. al. (2008) simplified the Kerner's equation (1956) to estimate the Young's modulus of the composite material with spherical shaped particle in matrix and $E_R >> E_M$. The equation is rewritten in Eq. 3.8.

$$E = E_M \left[1+\frac{f}{(1-f)}\frac{15(1-\nu_M)}{(8-10\nu_M)}\right] \quad \textbf{(3.8)}$$

Where, E and E_M are Young's modulus of composite and matrix, respectively.

The model proposed by Counto (1964) assumed perfect bonding between reinforcement and matrix. For a two-phase particulate composite, it was rewritten as Eq. 3.9 (Fu et al. 2008):

$$E = \left[\frac{1-\sqrt{f}}{E_M} + \frac{1}{\frac{1-\sqrt{f}}{\sqrt{f}}E_M + E_R}\right]^{-1} \quad \textbf{(3.9)}$$

Where E_R is Young's modulus of reinforcement particle.

3. 3 FEM Modeling

As discussed in Chapter 2, SLAs are assumed as homogenous, isotropic composite materials formed by uniformly-distributed, repeating unit cells, which are composed of the HCFA reinforcement and recycled plastic matrix. Other factors that determine a unit cell model include the shape of reinforcement particle, particle orientation, cell array and distribution. Starting with a simple principle, cubic edge array was adopted in this research. The reinforcement was assumed to be spherical in shape as most fly ash is in this shape as discussed in Chapter 2. Subsequently, unit cell models were built for the PLAXIS axisymmetric, ABAQUS axisymmetric, and ABAQUS 3D coordination systems. Depending on the system in which the model was built, the plastic resin is either in cubic or cylindrical shape.

3. 3. 1 PLAXIS Axisymmetric Modeling

A unit cell plane was built for the PLAXIS axisymmetric system as shown in Fig. 3.1(a), which shows a spherical fly ash particle entrapped in a cylinder of plastic resins. An interaction surface was established between fly ash and plastic. The loading and boundaries conditions include: (i) uniform pressure on the top surface; (ii) on the surface of Y = 0, the displacement

along Y direction: $U_{YY} = 0$; (iii) on the axisymmetric line of X = 0, the displacement along X direction: $U_{XX} = 0$. For meshing purpose, 6-node element and 15-node element, as shown Fig. 3.1(b), were used in analyses. These configurations were used to study the effect of element type on the computed Young's modulus of SLAs. In addition, the mesh was varied from coarse to very fine, so that the effect of mesh fineness could also be evaluated.

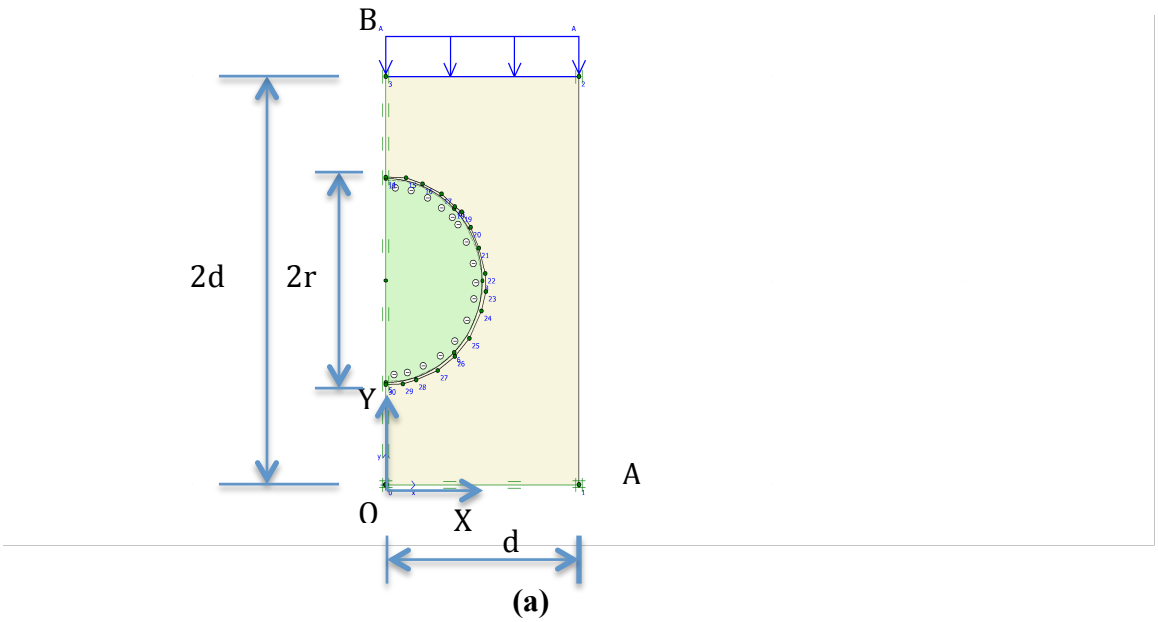

Fig. 3.1 (a) Illustration of PLAXIS Axisymmetric Model, and (b) Illustration of PLAXIS 6-note and 15-node Elements

3. 3. 2 ABAQUS Axisymmetric Modeling

Similarly, the same type of unit cell built in PLAXIS was also built in ABAQUS axisymmetric system, but only with half of the plane, as shown in Fig. 3.2(a). The loading and

boundary conditions are: (i) uniform pressure on the top surface; (ii) on the surface of Y = 0, the displacement along Y direction: UYY = 0; (iii) X = 0 is the axisymmetric line; (d) no rotation occurs on the outer surfaces AC so that uniform displacement will be generated. In these models, the coefficient of friction between the fly ash surface and the PS surfaces is varied with the value of 0.1, 0.3, 0.5, 0.7, and 0.9. This helps to evaluate the effect of friction between the HCFA reinforcement and plastic matrix. In addition, to examine the effect of element type, two types of mesh element, CAX3 (A 3-node linear axisymmetric triangle); and CAX6M (A 6-node modified quadratic axisymmetric triangle); as shown in Fig. 3.2(b) and (c), respectively, were used in the models, but only for the case when the coefficient of friction was set equal to 0.9.

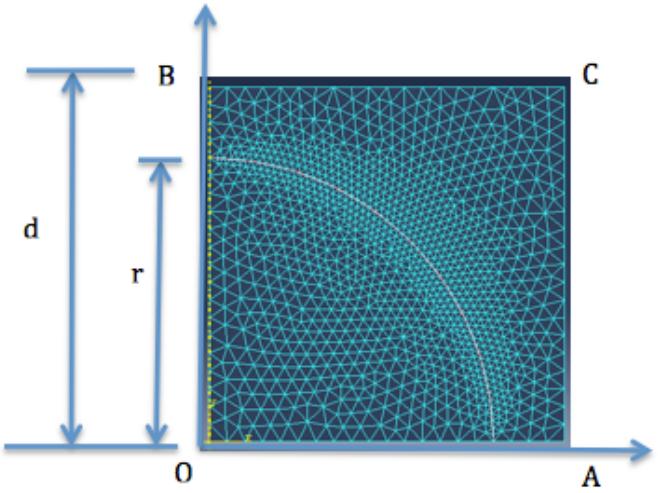

(a)

(b) **(c)**

Fig. 3.2 (a) Illustration of ABAQUS Axisymmetric Model (b) 3-node linear axisymmetric triangle (CAX3); and (c) 6-node modified quadratic axisymmetric triangle (CAX6M)

3. 3. 3 Difference between PLAXIS and ABAQUS Axisymmetric Modeling

Although ABAQUS and PLAXIS software are developed based on the same finite element method, different choice of element type, mesh fineness may cause divergence of results on the same problem. In this section, models built in PLAXIS and ABAQUS axisymmetric system is compared and discussed. First, as shown in Figure 3.1(b) and Figure 3.2(c), the element types of 6-node & 15-node, and 3-node & 6-node elements were used in PLAXIS and ABAQUS models respectively. Both methods use Gauss integration in calculation, in which 3-node triangle provides a first order interpolation for displacements and numerical integration involves one Gauss points, 6-node triangle provides a second order interpolation for displacements and numerical integration involves three Gauss points, and 15-node provides a fourth order interpolation and involves twelve Gauss points. Theoretically, more nodes provide results with more accuracy, but with more computational effort. Moreover since PLAXIS and ABAQUS software both uses displacement-based finite element method, in which the displacement is obtained by interpolating between the nodal displacements using a shape function, fewer nodes may generate over-stiff results because of the restraints on displacement. However, rather than the element type, the interface parameter (coefficient of friction) would more significantly affect the computed results. In PLAXIS models, the interface can be defined from smooth to rough by assigning different strength reduction factors. However, since no strength value was available in this research, no strength reduction was assigned in the model. This indicates rough contact or perfect bound between fly ash and plastic. In contrast, different friction coefficients were used in the ABAQUS models that allowed for variously smoothed interfaces. As a result, the ABAQUS models should generate lower modulus than the PLAXIS models would.

3. 3. 4 ABAQUS 3D Modeling

Slightly differentiating with the previous models, one quarter of a cubic unit cell is used in the ABAQUS 3D models, as shown in Fig. 3.3. The loads and boundaries include: (i) uniform pressure (stress-control model) or uniform displacement (strain-control model) is applied on the top surface; (ii) inner faces, which are X = 0, Y = 0, Z = 0 are symmetric faces and have the boundary conditions of $U_X = UR_Y = UR_Z = 0$, $U_Y = UR_Z = UR_X = 0$, and $U_Z = UR_X = UR_Y = 0$ respectively; where the U_X U_Y U_Z is the displacement along X, Y, Z direction, and UR_X, UR_Y, UR_Z is rotation along X, Y, Z axis, respectively; (iii) the outer surfaces X = d, Y = d, Z = d have no rotation, that is the $UR_Y = UR_Z = 0$, $UR_Z = UR_X = 0$, $UR_X = UR_Y = 0$, respectively. In these models, the coefficient of friction between the HCFA surface and the PS surface is various with the values of 0.1, 0.3, 0.5, 0.7, 0.9, and "rough", which means no movement between contact surfaces. In addition, computational geometries of linear hexahedral element type of C3D8 and quadratic tetrahedral element of type C3D10, as shown in Fig. 3.4, were used during the meshing process to study the effect of different element type on the elastic modulus.

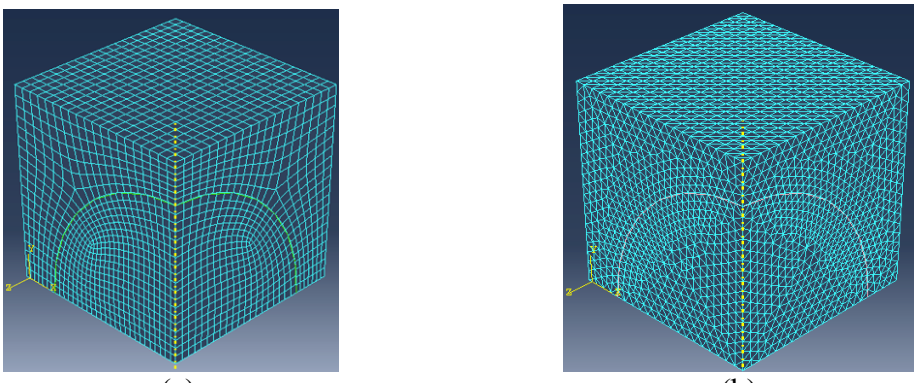

(a) (b)

Fig. 3.3 Illustration of ABAQUS 3D Model: (a) linear hexahedral element type of C3D8 (8-node brick); (b) quadratic tetrahedral element of type C3D10 (10-node tetrahedron)

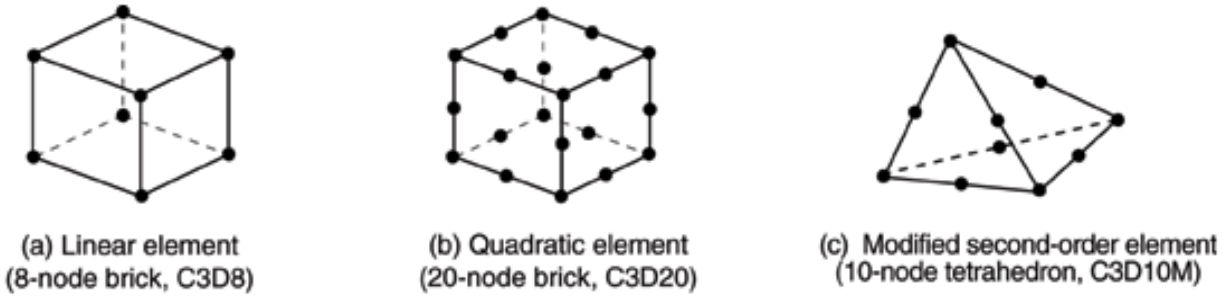

Fig. 3.4 Element Type in ABAQUS 3D (ABAQUS 6.12 User's Manual)

For each model mentioned above, various volume fractions were involved by changing the ratio of the spherical fly ash diameter to the cubic PS edge length (r/d). The ratio is 0.5, 0.8, and 0.98, generating the volume fraction (f) of 0.065, 0.268, and 0.493 for ABAQUS 3D models, and 0.083, 0.341, and 0.627 for unit cell in axisymmetric model. Analyses showed that the axisymmetric models neglect the plastic cubic corner compared to the cubic unit cell. However, since the stiffness of the resin (PS) is much lower than the reinforcement (FA), it is assumed that the cubic corner resin (PS) has insignificant effect on the overall modulus of the composite material.

3. 3. 5 ABAQUS 3D Modeling with Two-layer of Matrix

The ABAQUS 3D model introduced above was used for elastic moduli prediction of SLAs composed by HCFA and one type of recycled plastic. However for the SLAs-HCFA/MP, the formation of plastic layers are more complicated due to different melting points (T_m) of the various type of plastic. The type and recommended melting point of recycled plastic of the plastic mixture is listed in Table 3.1. As shown, PET has a relatively higher melting point compared to the other plastics. Therefore, during the forming process of SLAs, PET may grab HCFA particle and turn to solid first when cooling down, followed by the other plastics, which will form the outer-layer of SLAs. In this scenario, the matrix layer in ABAQUS 3D model is

divided into two layers as shown in Fig. 3.5, in which the inner-layer is PET and the outer-layer is a mixture of HDPE, LDPE, PP, and PS. To consider the uncertainty of the plastic mixing process, this research will compare the elastic modulus in these two scenarios for SLAs-HCFA/MP with r/d ratio of 0.3, 0.5, 0.65, 0.8 and 0.98, corresponding to the volume fractions of 0.014, 0.065, 0.144, 0.268, and 0.493, and R/d ratio of 0.78, 0.82, 0.87, 0.95, 1.05 respectively. Where R is the outer radius of PET. And the On the other hand, it is also possible that the plastics with lower melting points bounded with fly ash particle first and then were enclosed by PET.

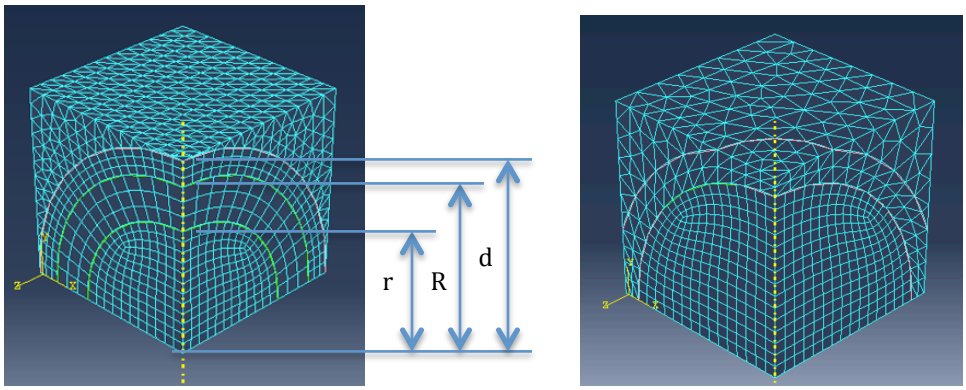

Fig. 3.5 Illustration of ABAQUS 3-D Model with Two-layer of Matrix: (a) r/d = 0.65, R/d = 0.87; (b) r/d = 0.98, R/d = 1.05

Table 3.1 Type and Recommended Melting Temperature of Plastics (Texas Plastic Technologies, 2015)

	PET	HDPE	LDPE	PP	PS
Melting Temperature T_m (^{o}C)	280	205	160	175	175~200

3. 4 Material Properties

As illustrated in analytical method equations, to calculate the elastic modulus of SLAs, the material property such as elastic modulus and Poisson's ratio of fly ash and recycled plastics need to be determined first. This is also the case for FEM modeling.

3. 4. 1 Mechanical Property of FA

As discussed in Chapter 2, Matsuaga et al. (2002) comprehensively studied the physical properties of fly ash and obtained the elastic modulus and density of different type of fly ash at different size range. Matsuaga concluded that the precipitator fly ash has density that is between 2.0~2.5 g/cm^3, while the cenosphere particles has density less than 1.0 g/cm^3. Since previous studies has shown that the fly ash used in SLAs has density that is greater than 1.0 g/cm^3, the fly ash in this research might be precipitator-dominated particles or cenosphere particles with larger thickness. In turn a Young's modulus of 90GPa, which is a value between the elastic moduli of cenosphere and precipitator particles, but close to the precipitator's elastic modulus value was chosen. The Poisson's ratio of 0.21 as assumed by Matsunaga et al. (2002) was taken in this research. By roughly averaging the particle sizes of different type of fly ash, and for simplifying purpose, the particle size of 100 μm in diameter is used in this research. All models were built at this micro level.

3. 4. 2 Mechanical Property of Recycled Plastics

Compared to fly ash, the mechanical properties of recycled plastics are better established and standardized. The value of density, elastic modulus, and Poisson's ratio of different type of

plastic is listed as in Table 3.2 (Matweb, 2013). Table 3.2 also illustrates the composition of Mixed Plastics (MP), which was used to produce the SLAs-HCFA/MP.

Table 3.2 Composition of MP and Properties of Plastics used for Computation Methods Comparison (source, Matweb, 2013)

	PET	HDPE	LDPE	PP	PS
% by mass	30%	35%	10%	10%	15%
ρ (g/cm3)	1.3	0.94	0.91	0.905	1.04
E (GPa)	2.4	0.8	0.3	1.6	3.0
ν	0.43	0.47	0.49	0.43	0.38

As discussed before, two scenarios of plastic resins were used in ABAQUS 3D models for predicting the elastic modulus of SLAs-HCFA/MP. They are differentiated by the formation of plastic matrix during mixing process. The matrix is considered as either one layer, which is the mixture of PET, HDPE, LDPE, PP, and PS; or two layers, which has PET as the inner layer and the mixture of HDPE, LDPE, PP and PS as the outer layer. In either case, the mixture of plastics was also considered as uniform and homogenous material, and the elastic modulus and Poisson's ratio of the mixture was calculated first using the "rule of mixture" as shown in Eq. 3.10 and Eq. 3.11.

$$E = \Sigma E_n f_n \quad \textbf{(3.10)}$$

$$\nu = \Sigma \nu_n f_n \quad \textbf{(3.11)}$$

Where, the E_n, ν_n is the elastic modulus and Poisson's ratio of different type of plastics.

LABORATORY TESTING

4. 1 Introduction

This chapter describes the laboratory tests that have been conducted on pure polystyrene (PS), HCFA, SLAs-HCFA/PS and SLAs-HCFA/MP. The laboratory tests include specific gravity test and Loss of Ignition (LOI) test on all materials; and confined compression test on granulated pure PS and SLAs-HCFA/PS, unconfined compression test on solid PS and SLAs-HCFA/PS, and SEM test on SLAs-HCFA/PS particles. For both type of SLAs, the designed mass ratios of HCFA-to-plastic were 50:50, 65:35, and 80:20. The purpose of specific gravity and LOI test was to obtain the actual proportion of HCFA and plastic in the SLAs, which help to refine the FEM models. The objectives of the confined compression test on granulated SLAs were two-fold; 1) to measure the stress-strain response of granular SLAs subjected to high stresses and 2) produce solid SLAs specimen, which will be used in unconfined compression test for evaluating its Young's modulus through unconfined compression test.

4. 2 Specific Gravity Test

Specific gravity tests were performed on SLAs-HCFA/MP, SLAs-HCFA/PS, pure PS, HCFA and HCFA after calcination. Two gradation ranges of the SLA particles were tested; those passing the No. 4 (4.75mm opening) sieve and retained on the No. 8 (2.36mm opening) sieve; and those passing the No. 8 (2.36mm opening) sieve and retained on the No. 16 (1.18mm opening) sieve. All tests were performed referring to the ASTM 854-10 "*Standard Test Methods*

for Specific Gravity of Soil Solids by Water Pycnometer" and "*Soil Mechanics Laboratory Manual – Edition 8*" (Das, B. M., 2012).

Following the requirements of ASTM 854-10, distilled water (G_s = 1.0 at temperature of 20^{o}C) was used in the specific gravity test of SLAs. However, since pure polystyrene has an estimated specific gravity that is less than 1, kerosene (Gs = 0.8 at temperature of 20^{o}C, Plymouth Pro®) was used as a substitution for distilled water. In addition, since no obvious pozzolanic reaction was observed between the HCFA and distilled water, distilled water was also used for the specific gravity test of HCFA. As shown in Fig. 4.1, each sample was put into a 250ml volumetric flask filled with distilled water or kerosene. The flask was connected to a vacuum for at least 24hrs to remove air bubbles in the mixture. Room temperature was recorded and the density of water was adjusted with a temperature coefficient according to ASTM 854-10. Since no temperature coefficient was available for kerosene, its density was measured at the room temperature and was used to calculate the density of polystyrene that had been tested at the same room temperature.

Fig. 4.1 Illustration of Specific Gravity Test

After obtaining all the measurements, Eq. 4.1 was used to calculate the specific gravity of specimen. For each material, three or four specimens were tested and the results were limited within a 20% difference. The final value was taken as an average of the valid results.

$$\mathbf{G_s} = \frac{\boldsymbol{M_s}}{(\boldsymbol{M_1}+\boldsymbol{M_s})-\boldsymbol{M_2}} \frac{\boldsymbol{\rho_w\ (at\ T_1\ ^oC)}}{\boldsymbol{\rho_w\ (at\ 20\ ^oC)}} \quad \textbf{(4.1)}$$

Where, M_s = the mass of dry specimen;

M_1 = mass of flask filled with water;

M_2 = the mass of flask filled with water and specimen;

4. 3 Loss of Ignition (LOI) Test

Loss of Ignition (LOI) test was performed on HCFA, SLAs-HCFA/PS and SLAs-HCFA/MP with designed HCFA-to-PS mass ratios of 50:50, 65:35, and 80:20. Since LOI test helps to determine the mass loss of test specimen when heated at high temperature, the LOI test on HCFA can determine the amount of carbon residue in fly ash. In correlation with this result, LOI test on SLAs allow the determination of the amount of HCFA and plastic components. Each test had been completed following the ASTM D7348-08 "*Standard Test Methods for "Loss on Ignition (LOI) of Solid Combustion Residues*". Approximately 1g of the specimen that weighed around 1/13 of the porcelain crucible was used in each test. Four or eight specimens were tested for each type of material. A two-step procedure was used to determine the LOI values. The first step is to dry specimen in the furnace at programmed temperature reaching up to 105^{o}C and maintaining for 20hrs. Then the test specimen crucibles were removed from the furnace, covered with lid, and placed in a desiccator for cooling down and weighed. After being weighed, the sample was put back into the furnace followed by step-two, in which the furnace temperature was programmed to increase up to 750^{o}C at the rate of 15^{o}C/min and then

maintained for 10hrs. Samples were then taken out and weighed again following the same procedure in the first step. The HCFA and SLAs after calcination have a tan-gold color as shown in Fig. 4.2. The LOI percentage of fly ash, which is also the value of carbon content present in HCFA, was calculated using Eq. 4.2 (ASTM D7348-08). In addition, after the LOI test had been completed on SLAs, the mass of HCFA in SLAs was calculated using Eq. 4.3 (Weingam 2002). After obtaining the mass of HCFA and plastics in SLAs, their percentage could then be derived using Eq. 4.4 and 4.5.

$$\mathbf{LOI_{HCFA}} = \frac{\mathbf{100}\ (\boldsymbol{C}-\boldsymbol{D})}{\boldsymbol{W}} \quad \textbf{(4.2)}$$

Where: W = mass of test specimen used, g;

C = mass of test specimen after drying in moisture test, g;

D = mass of HCFA residue after heating at 750^{o}C;

LOI_{HCFA} = percent loss of HCFA on ignition as determined in the test specimen;

$$\mathbf{M_{HCFA}} = \frac{\boldsymbol{M}_{\mathbf{LOI}}}{\mathbf{1}-\boldsymbol{LOI}_{\mathbf{HCFA}}} \quad \textbf{(4.3)}$$

$$\mathbf{\%HCFA} = \frac{\boldsymbol{M}_{\mathbf{FA}}}{\mathbf{1}-\boldsymbol{M}\mathbf{orig}} \quad \textbf{(4.5)}$$

$$\mathbf{\%Plastic = 1 - \%HCFA} \quad \textbf{(4.5)}$$

Where, M_{LOI} = total mass remaining after calcination of SLAs;

M_{HCFA} = mass of HCFA in SLAs before calcination.

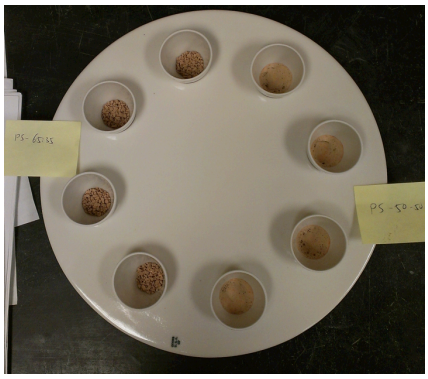

Fig. 4.2 Illustration of SLAs-HCFA/PS after Calcination

In addition, larger amounts (up to 150grams) of SLAs-HCFA/PS were subjected to the LOI procedure only for appearance comparison and specific gravity test. The SLAs after calcination was shown in Fig. 4.3.

Fig. 4.3 Illustration of large amount of SLAs-HCFA/PS after Calcination

4. 4 Confined Compression Test on Granulated SLA Particles – Sample Preparation

As discussed in Chapter 3, one objective of this research was to study the elastic modulus of SLAs. To evaluate this via laboratory tests, compression tests on solid SLAs need to be conducted to generate the necessary stress-strain curve and obtain the Yong's modulus. However, SLA exist as granular particles with irregular shapes. Therefore, the first step of performing compression tests in the laboratory was to produce solid SLAs specimens from granular SLAs that would be appropriate for testing. In this research granulated SLAs-

HCFA/PS 50:50, 65:35, and 80:20 particles that passed a No. 8 (2.36mm opening) sieve and were retained on the No. 16 (1.18mm opening) sieve were placed in a cylindrical mold and compressed into solid cylinders of SLA (12.7 mm in diameter and various lengths) for use in unconfined compression test.

4. 4. 1 Testing Equipment and Procedure

As illustrated in Fig. 4.4, two systems were used to measure the load-deformation response used in the confined comrpession test. One system was the load sensor and displacement sensor associated with the LoadTrac II (Geocomp Corp.) load frame used to apply and control the loading process. Another load and displacement sensor set was used with the load sensor placed under the mold, and the displacement sensor directly attached to the loading piston that compressed the SLAs in the mold. These sensors were connected to a separate data acquisition system (Geolog-6 reading box from Geocomp Corp.). For each test, a measured amount of graunlated particles were poured into the 12.7mm (0.5in) diameter cylindrical mold and compressed by a load piston. This confined compression was conducted at a constant rate of displacement. Applied stresses ranged from 0 to approximately 350MPa (50ksi) to obtain SLAs sample with essentially zero void ratio. Peak loading was maintained for 10min and then released. After unloading, the resulting solid sample was extruded out and measured. The test set-up was calibrated to account for maching compliance. Both sample weight before and after confined compression test was recorded, counting to the possible mass loss during the testing process. By utilizing this method, cylindrincal specimen of SLAs-HCFA/PS with designed mass ratio of 50:50, 65:35, 80:20 and pure PS was obtained.

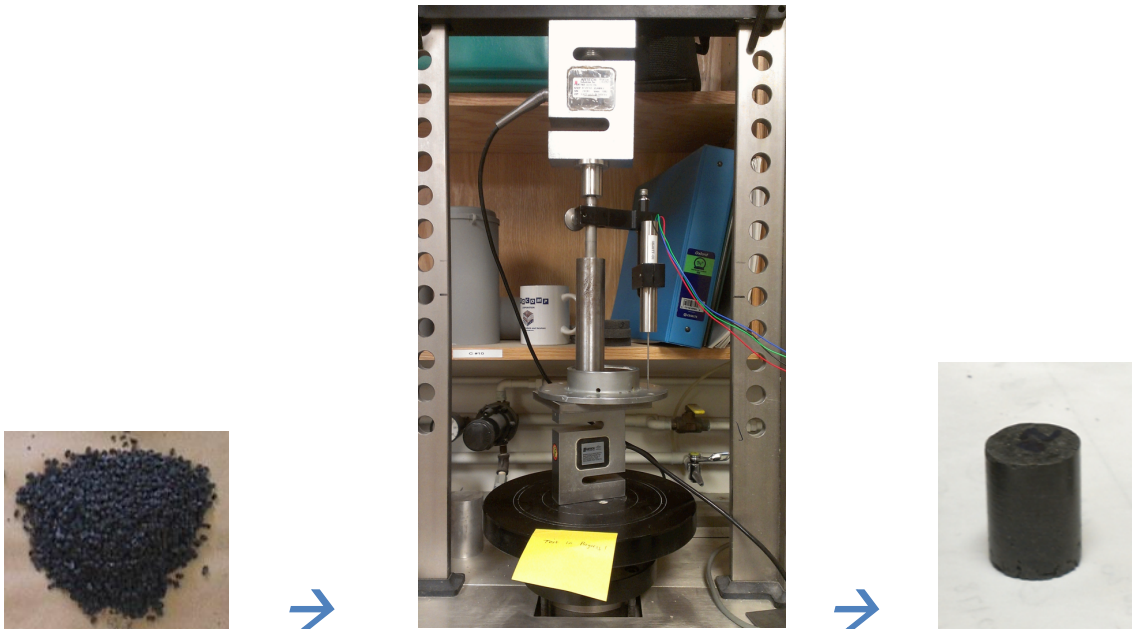

(a) Granulated SLAs (b) Confined Compression Equipment (c) Solid SLAs

Fig. 4.4 Illustration of Solid SLAs Sample Preparation

4. 4. 2 Specimen Measurement

The approximate dimensions of the solid SLAs cylinder was determined before testing so that the amount of granulated material could be measured. The dimensions of solid SLAs in this research were determined based on literature review, displacement sensor's measurablity, ASTM E111-04 "*Standard Test Method for Young's Modulus, Tangent Modulus, and Chord Modulus*", and ASTM E9-09 "*Standard Test Methods of Compression Testing of Metallic Materials at Room Temperature*". Trial tests had also been carried out to estimated the distance needed to compress the SLAs into an appropriately sized cylinder for testing.. Qi & Boyce (2005) studied the stress-strain behavior of thermoplastic polyurethanes and reommended a height/diameter ratio between 0.5 and 1 to eliminate potential buckling. In this research, a desirable height of 8mm was adopted for cylindrical specimen, generating the heigh/diamter ratio of 0.6 since the diamter of the specimen would be 12.7mm, which is as the same as the diamter of the mold. In

addition, specimen with a different height (18mm) and height /diamter ratio (1.4) were also produced to study the effect of specimen size on modulus. Due to the travel limit of displacement gauge (20.3mm), solid SLA specimens that had a height/diamter ratio of 1.4 were only obtained for SLAs-HCFA/PS(50:50). All specimens obtained from confined compression test was defined as "short" specimens according to ASTM E9-09.

In summary, the designed heights of 8mm and 18mm for SLAs-HCFA/PS(50:50), and 8mm for SLAs-HCFA/PS 65:35 and 80:20 were used. After finalizing the sizes of solid SLAs specimen, the amount of granulated material to use could be determined using Eq. 4.6.

$$\mathbf{M = 0.25\pi D^2 H\rho_w G_s} \qquad \mathbf{(4.6)}$$

Where, M = mass of granulated SLAs, mg;

G_s = specific gravity of the SLAs;

ρ_w = density of water, g/cm^3;

H = desired height of solid SLAs specimen, mm;

D = desired diamter of solid SLAs specimen, mm.

4. 4. 3 Testing Parameters

Other testing parameters such as side friction between particle and mold, and loading speed were studied in conducting the confined compression test. For example, it was found that to eliminate the effect of side friction, a thin film of oil could be applied around the inside of the cylindrical compression mold. In addition, the rate of displacement was varied with strain rates of 0.01mm/mm/min, 0.03mm/mm/min, and 0.05mm/mm/min used during loading and unloading process to evaluate the effect of displacement rate on the confined compression test.

4. 5 Unconfined Compression Test

The unconfined compression tests were carried out on pure PS and SLAs-HCFA/PS 50:50, 65:35, and 80:20 specimens obtained from the confined compression test. The purpose of the test was to experimentally determine the stress-strain behavior and obtain the Young's modulus of the materials. These experimental result of modulus will be used to compare with theoretical predictions from both analytical and FEM method.

The equipment used in unconfined compression test was INSTRON-3366, as shown in Fig. 4.5. Since no standard reference was available for materials like SLAs, various loading speeds had been tried and a strain rate of 0.015 per min was finalized as an appropriate rate to use. Before testing, the diameter, height, and mass were measured for each specimen, and its porosity could be calculated using the equations in soil mechanics as shown in Eq. 4.7 to 4.9. The reason to calculate the porosity is checking the initial porosity status of SLAs specimen, which will help to analyze the stress-strain curves. Since the specimens were acquired by compressing granulated particles instead of being obtained directly from solid material, it is possible that the granulated SLAs particles did not completely adhere to each other to create completely bound particle-to-particle surfaces or form zero-void solid specimens.

Each test was programed starting with a seat load of 5N, followed by a strain increment at the rate of 0.015 per min, and terminated when failure occurred. At least three samples were tested for each type of SLAs. After failure occurred, the specimens were collected with caution for being observed under scanning electron microscope (SEM).

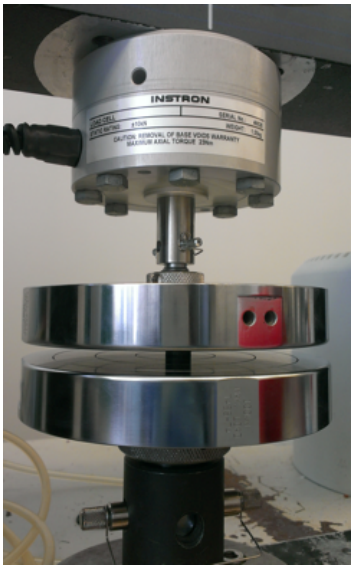

Fig. 4.5 Illustration of Unconfined Compression Test Equipment INSTRON-3366

$$\boldsymbol{n = \frac{V_v}{V} 100\% \ = \frac{V - V_S}{V} 100\%} \quad \textbf{(4.7)}$$

$$\mathbf{V_s = \frac{M}{Gs}} \quad \textbf{(4.8)}$$

$$\mathbf{V = 0.25\,\pi D^2 H} \quad \textbf{(4.9)}$$

Where, V = volume of SLA specimen, mm^3;

V_v = Volume of voids in the SLA specimen, mm^3;

V_s = Volume of SLAs solid, mm^3;

M = mass of granulated SLAs, g;

Gs = specific gravity of the SLAs;

H = height of solid SLAs specimen after compression, mm;

D = diamter of solid SLAs specimen after compression, mm.

4. 6 Scanning Electron Microscope (SEM) Test

Scanning Electron Microscope (SEM) test were conducted on HCFA and SLAs-HCFA/PS 50:50, 65:35, and 80:20 using a Zeiss Ultra55 SEM. HCFA particles before and after

calcination were both scanned to compare the different appearance of fly ash with and without the presence of carbon. The natural failure surfaces of unconfined compression test specimens of SLAs-HCFA/PS 50:50, 65:35, and 80:20 were also observed under microscope. The purpose was to study the bonding surface between HCFA and PS. In addition, the size and distribution of HCFA particle in the PS matrix was also observed. This will aid in evaluating the assumption that compressed SLAs specimens act as a homogenous isotropic material, and also help to detect the different degree of bonding between HCFA and PS in various HCFA/PS ratios. In addition, SEM micrographs contain a scale to evaluate the range in sizes of fly ash used in FEM modeling.

THEORETICAL COMPUTATION RESULT

5. 1 Introduction

This chapter presents the computed elastic moduli of SLAs at various volume fractions. Both analytical methods; including H-S upper bound, H-S lower bound, Mura expression, Counto equation, and Kerner equation, and FEM modeling in PLAXIS axisymmetric, ABAQUS axisymmetric, and ABAQUS 3D coordination systems were employed. The results from those two methods were then compared and discussed. The Young's moduli of SLAs-HCFA/PS at r/d ratio of 0.5, 0.8, and 0.98, corresponding to the volume fraction (f) of 0.083, 0.341, and 0.627 in axisymmetric coordination system; and 0.065, 0.268, and 0.493 in 3D coordination system were predicted. For each method, employed material properties such as elastic modulus and Poisson's ratio of HCFA and plastics were consistent and were taken as the assumed values as listed in Table 3.2 in Chapter 3.

5. 2. Analytical Computation Results

The elastic moduli of SLAs made of HCFA and various types of plastic, including HDPE, LDPE, PS, and mixture of plastic (MP) was computed at various volume fractions using different analytical methods. For comparison purpose, the maximum volume fraction was obtained when the fly ash had the maximum diameter in a unit cell, that is when the ratio of fly ash diameter (2r) to the edge of unit cell (2d) is 1, generating the volume fraction (f) of 0.667 in

axisymmetric and 0.524 in 3D coordination system, respectively. Hence, volume fraction from 0 to 0.7 was used for analytical analyses.

The calculated elastic results from analytical methods were summarized in APPENDIX (I) and the normalized moduli referred to the modulus of the corresponding matrix material are illustrated as in Figures 5.1 and 5.2. Fig. 5.1 shows elastic moduli for SLAs-HCFA/PS, SLAs-HCFA/LDPE, SLAs-HCFA/MP and SLAs-HCFA/HDPE at volume fraction from 0.1 to 0.7 for different the four analytical methods. It should be noted that the H-S upper bound method generates values that are 20 times more than those obtained from other methods and it is inappropriate to be used for SLAs elastic modulus prediction. It is apparent in Fig. 5.1 that all four methods; the Mura expression, Counto equation, and Kerner equation, and H-S lower bound method generate similar values. In general, the increase in fly ash content (higher fly ash volume fraction) leads to an increase in normalized modulus. For each method, SLAs composed with LDPE and HCFA have higher normalized elastic modulus values, indicating LDPE was stiffened most by the fly ash, followed by HDPE, MP, and PS. This indicates that HCFA stiffens the more ductile plastics more, especially at higher reinforcement levels. Furthermore, the impact of reinforcement level varies for the different methods; e.g., the H-S lower bounds generated the largest divergence; while the Kerner equation generated the most consistent results for all types of SLAs.

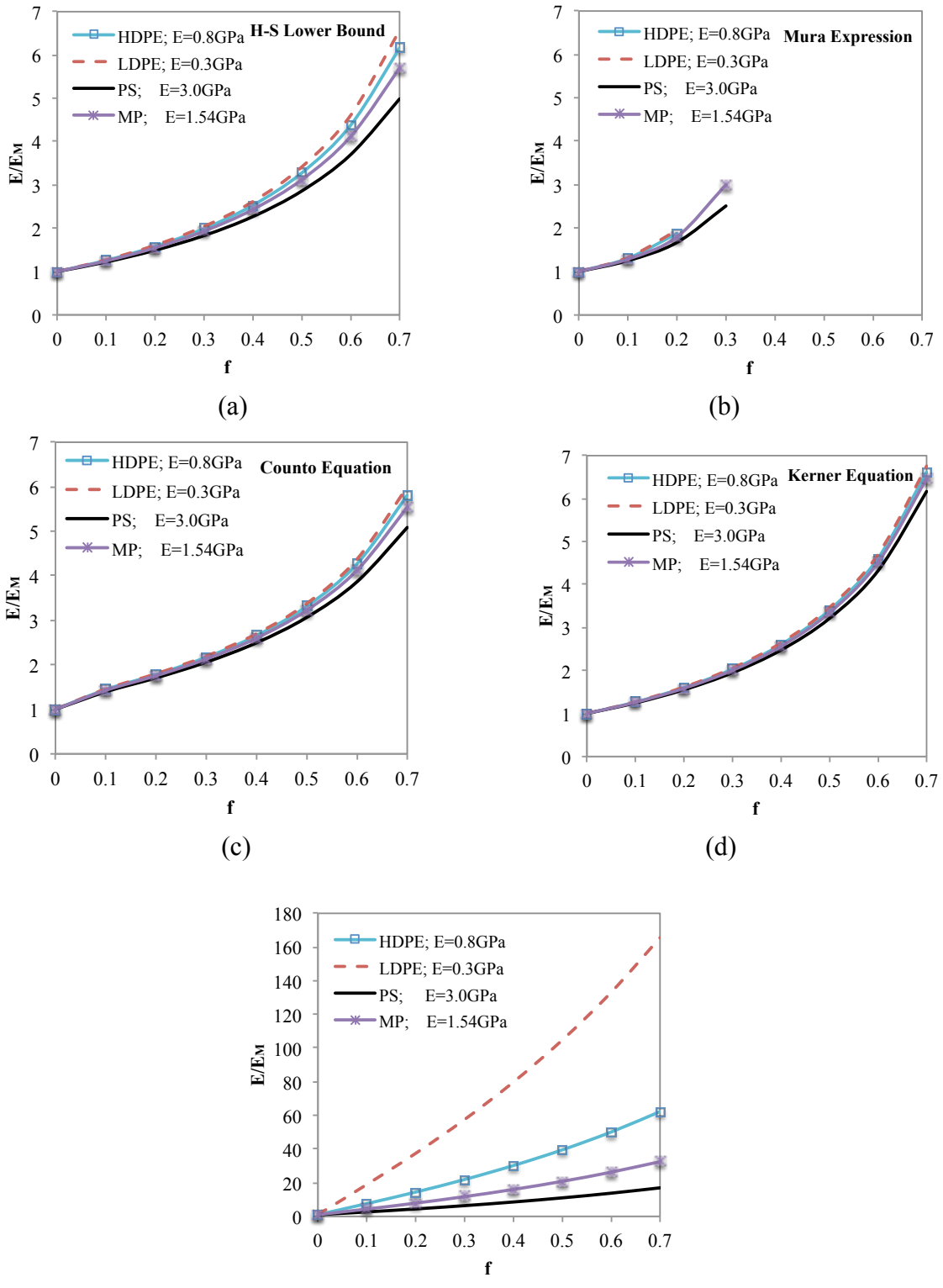

Fig. 5.1 Normalized Elastic Moduli of SLAs Computed from Different Methods: (a) H-S Lower Bound; (b) Mura Expression; (c) Counto Equation; (d) Kerner Equation; (e) H-S Upper Bound

Fig. 5.2(a)-(e) show the normalized elastic modulus computed by different methods for each type of SLA. All figures show that the elastic modulus of various types of plastic was increased from 1 to nearly 7 times when fly ash volume fraction increased from 0 to 0.7. The increment went up more rapidly when the volume fraction increased, especially for SLAs composed with HDPE and LDPE, which were more ductile plastics than the other two. In addition, the elastic modulus of these two types of plastics also had the most agreement when computed using different analytical methods.

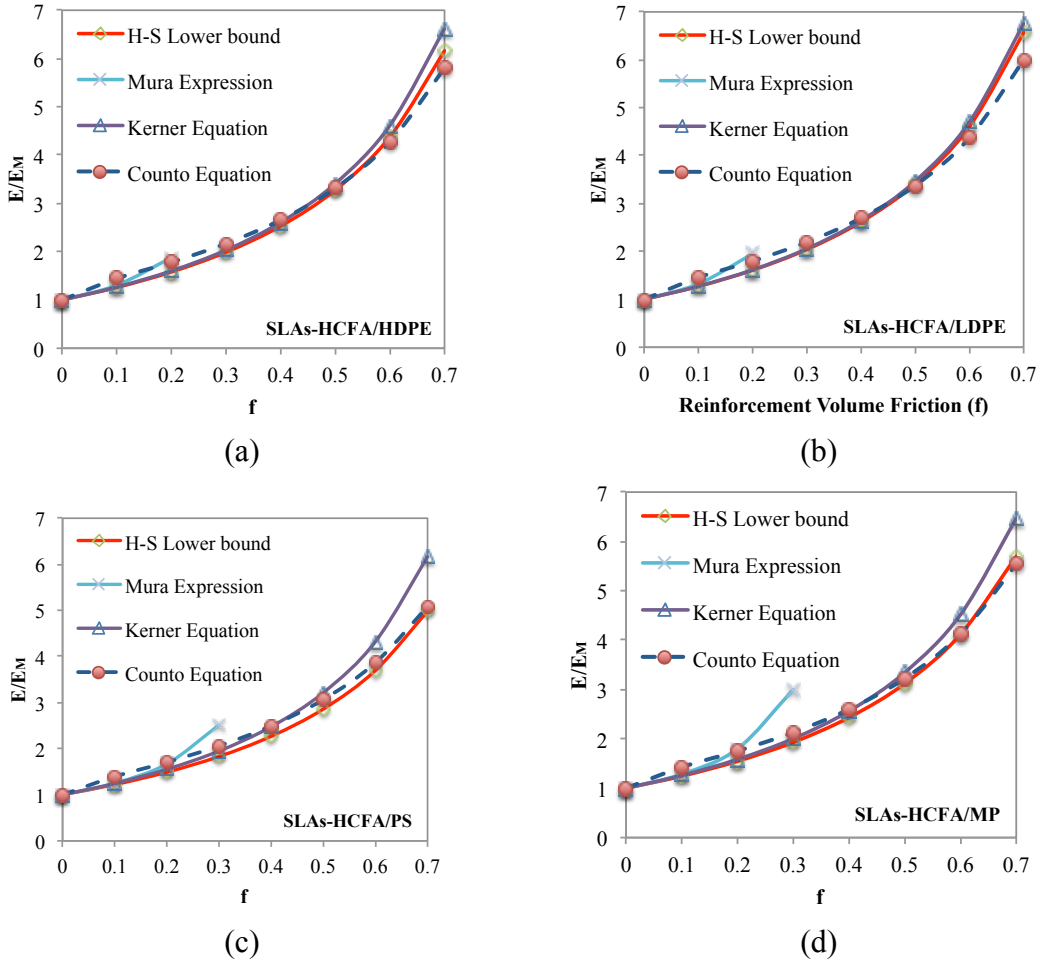

Fig. 5.2 Normalized Elastic Moduli of SLAs Computed from Different Methods (a) SLAs-HCFA/HDPE; (b) SLAs-HCFA/LDPE; (c) SLAs-HCFA/PS; (d) SLAs-HCFA/MP

The elastic modulus is also computed for the r/d = 0.5, 0.8, and 0.98 cases for SLAs-HCFA/PS. These results are detailed in APPENDIX (II). Generally, the Young's moduli calculated from the analytical methods fell in the range of 3.54~7.11GPa, 5.99~21.76GPa, and 11.98~43.84GPa at volume fraction of 0.083, 0.341, and 0.627; and 3.42G~6.21GPa, 5.14~17.20GPa, and 8.43~32.46GPa at volume fraction of 0.065, 0.268, and 0.98, corresponding to the r/d value of 0.5, 0.8, an 0.98 in 2-D axisymmetric and ABAQUS 3D analyses, respectively. These values will be used to compare with those obtained from FEM modeling to be discussed in the following section.

5. 3. FEM Computation Results

The elastic moduli of SLAs-HCFA/PS at various volume fractions were predicted using PLAXIS axisymmetric model, ABAQUS axisymmetric model, and ABAQUS 3D models, taking into account various roughness conditions of the HCFA and PS interaction surface. The elastic moduli of SLAs-HCFA/MP at various volume fractions were calculated using both ABAQUS 3D one-layer model and two-layer model, assuming perfect bound between HCFA and MP. These results are also detailed in APPENDIX (II).

5. 3. 1 Elastic Moduli of SLAs-HCFA/PS

As stated above, the elastic modulus of SLAs-HCFA/PS calculated using different FEM models is presented taking into account the effect of fly ash volume fraction, and computation parameters such as element type, coefficient of friction between HCFA and PS.

5. 3. 1. 1 PLAXIS Axisymmetric Model Computation Result

In PLAXIS axisymmetric models, elastic moduli of SLAs-HCFA/PS at volume fraction (f) of 0.083, 0.341, and 0.627, corresponding to the unit cell edge-to-particle diameter (r/d) ratio

of 0.5, 0.8, and 0.98 were computed. An example of displacement contour is illustrated in Fig. 5.3. The computed parameters of mesh fineness (coarse, medium, fine, and very fine) and element type (6-node and 15-node) were studied. In addition, the parameter R_{inte}, which is the strength reduction factor that accounts for the interaction between the reinforcement (fly ash) and matrix (plastic), indicated no significant influence on the modulus. Hence, the interaction between fly ash and PS is not a control parameter in the Plaxis modeling. These results are detailed in APPEDIX (II). The Young's modulus was 3.87~3.95GPa, 11.01~11.03GPa, and 18.06~18.33GPa for the SLAs with r/d ratio of 0.5, 0.8, and 0.98, respectively. These values are consistent with those predicted by the analytical methods. They also show the incremental increase in elastic moduli with the increase in HCFA volume fraction.

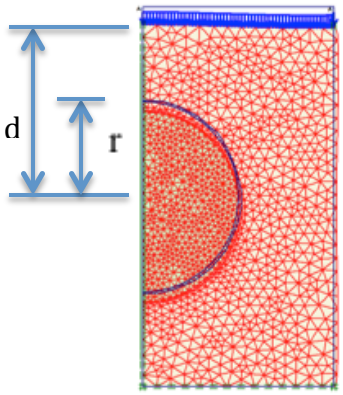

Fig. 5.3 Example of PLAXIS Axisymmetric Modeling Output (Displacement Contour)

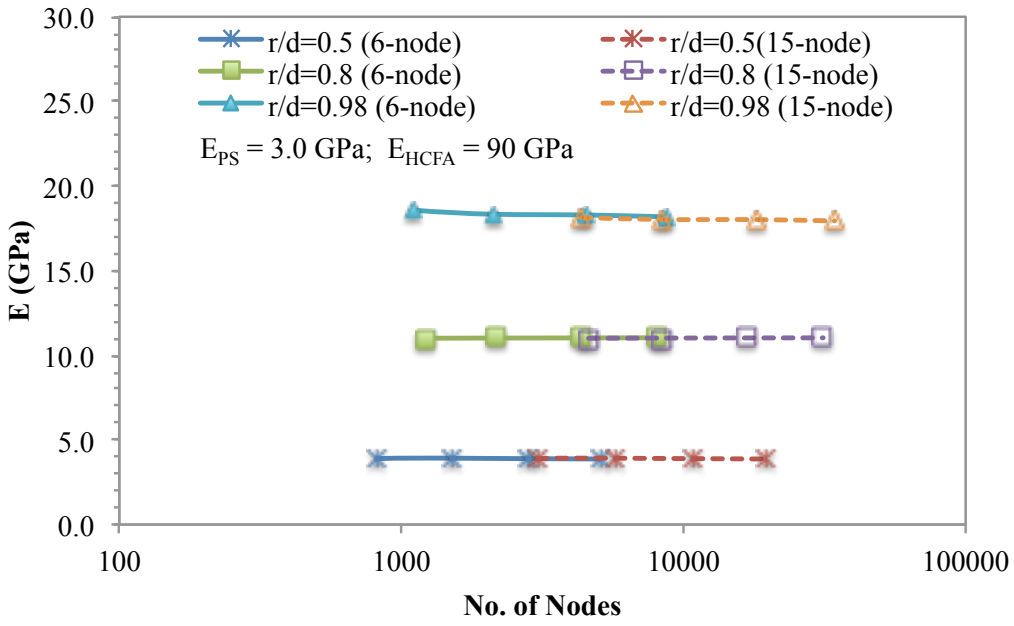

Fig. 5.4 PLAXIS Axisymmetric Modeling Result: E vs. No. of Nodes for r/d = 0.5, 0.8, and 0.98

The elastic modulus vs. number of nodes was plotted as shown in Fig. 5. 4. As shown, it exhibits consistently similar values of E at different mesh fineness and element type. Specifically, the results show that the 6-node and 15-node element model generated almost the same Young's moduli at r/d=0.5 and r/d=0.8. While for r/d=0.98, the 6-node model produced higher value of E than the 15-node model. However, the difference was very small, and was approximately within 2%. Hence, it can be concluded that the element type had no significant effect on the elastic modulus. For the models with r/d = 0.5 and 0.98, the Young's modulus decreased (3.95 to 3.87GPa, and 18.33 to 18.06GPa, respectively) with the increase of mesh fineness; while the model with r/d = 0.8 showed the opposite trend (11.01 to 11.03GPa). Hence, it is difficult to conclusively state that the mesh fineness affects computed Young's moduli. Nonetheless, the difference of E values caused by the different mesh fineness was very small,

which was 2.1%, 0.2%, and 1.5% for r/d = 0.5, 0.8, and 0.98 respectively. Hence, the influence of mesh fineness is limited and can be considered negligible for this study.

5. 3. 1. 2 ABAQUS Axisymmetric Model Computation Result

Similar to the PLAXIS axisymmetric computation outlined above, the elastic moduli of SLAs-HCFA/PS at volume fraction of 0.083, 0.341, and 0.627, corresponding to the r/d ratio of 0.5, 0.8, and 0.98 were computed using ABAQUS axisymmetric model. A displacement contour example is illustrated as in Fig. 5.5. One computation parameter different from the PLAXIS model is that variability of the bond between the fly ash and plastic, taken as coefficient of friction values of 0.1 (for weak bonding), 0.3, 0.5, 0.7, 0.9 and 1.0 (for perfect bound), can be considered. Fig. 5.6 shows the computed elastic moduli of SLAs-HCFA/PS at various coefficient frictions. Apparently, the modulus increases with the increase of friction between fly ash and PS. This is as expected because the stronger the bond between the two phases (fly ash and PS), the stiffer the composite should be. In addition, Fig. 5.6 also shows modulus increases more rapidly for the SLAs that have higher volume fractions compared to those with less fly ash content. For instance, when the roughness increased from 0.5 to 0.9, the E increased with 4%, 20%, and 88% for the fly ash volume fraction of 0.065, 0.268, and 0.493 respectively.

Another parameter that had been taken into account is element type. The element type of CAX3 (A 3-node linear axisymmetric triangle) and CAX6M (A 6-node modified quadratic axisymmetric triangle) was used in the ABAQUS axisymmetric models with a coefficient friction of 0.9. The computed Young's moduli are listed in Table 5.1, which shows the element type only caused slight differences (within 2.5%) on the moduli. The CAX6M models generated lower modulus than the CAX3 did for r/d = 0.5 and r/d = 0.98 case; while higher modulus for r/d = 0.8

case. This agrees with the PLAXIS results, in which the element type has similar effect on the E values, comparing different volume fractions

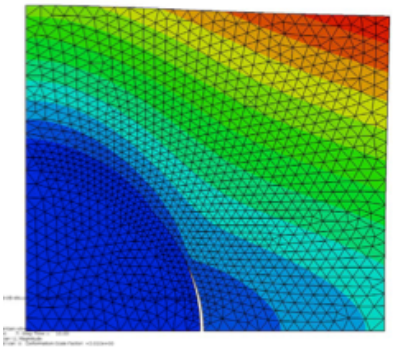

Fig. 5.5 Example of ABAQUS Axisymmetric Modeling Output (displacement contour)

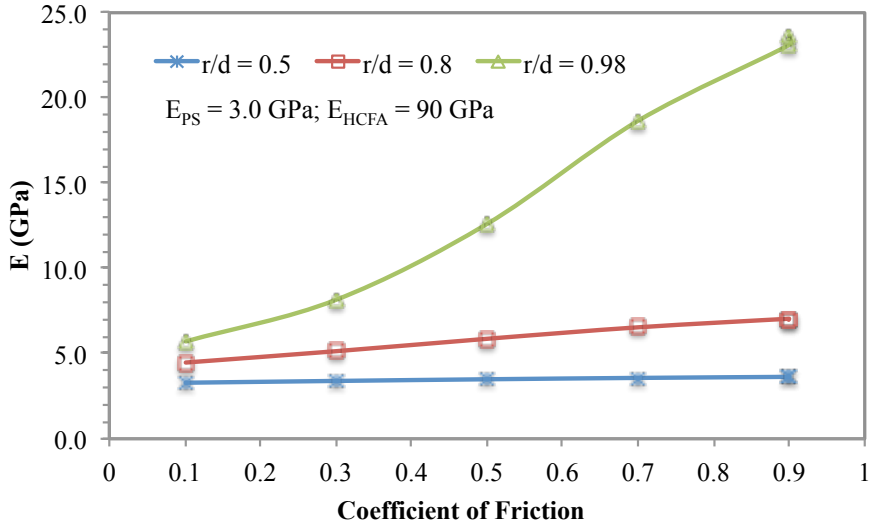

Fig. 5.6 ABAQUS Axisymmetric Modeling: E vs. Coefficient of Friction for r/d = 0.5, 0.8, and 0.98

Table 5.1 Young's Moduli of SLA (in GPa) for Different Element Types in ABAQUS

Element Type	r/d = 0.5	r/d = 0.8	r/d = 0.98
CAX3	3.63	7.05	23.12
CAX6M	3.63	7.02	23.67

5. 3. 1. 3 ABAQUS 3D Model Computation Result

In the ABAQUS 3D models, both stress-control and strain control models were adopted to examine the different effect of being applied with uniform stress and uniform strain during the simulation. The stress-control model had uniform stress on the top surfaces. And the elastic modulus was calculated for each node on the top surface. By averaging these nodal moduli, the elastic modulus of the whole unit cell was then obtained. On the other hand, the strain-control model was applied with uniform displacement on the top surface, and the elastic moduli were calculated based on the reaction force output. The total reaction force on the top surface was computed and divided by the area of the top surface, generating a stress value. The stress was then divided by the applied strain for the elastic modulus calculation. Fig. 5.7 below provides stress contour examples for these two cases.

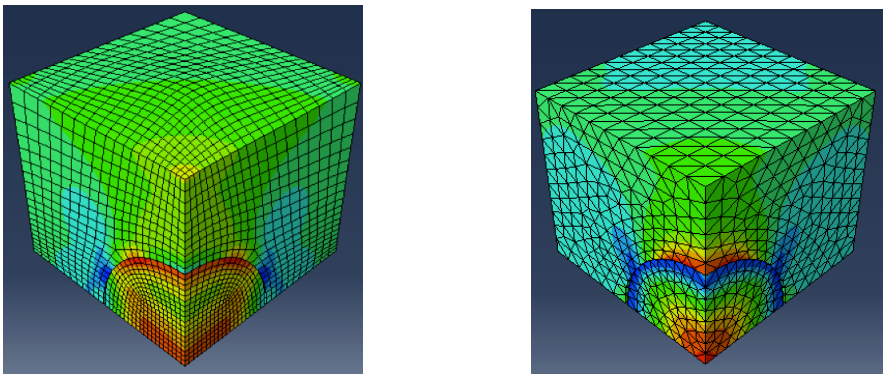

(a) Strain Control (b) Stress control

Fig. 5.7 Example of ABAQUS 3-D Modeling Output: (a) Strain-control (stress contour); (b) Stress-control (stress contour)

As mentioned, the effect of element type was also evaluated for ABAQUS 3D models, which had been meshed with linear hexahedral element type of C3D8 and quadratic tetrahedral element type of C3D10, respectively. And the calculated Young's moduli at various volume fractions and coefficient of frictions were compared as shown in Fig. 5.8. The results show that

the element type had no significant effect on the elastic moduli of the SLAs. In addition, at higher volume fraction, tetrahedral elements generated slightly higher stiffness, with the difference increasing from 2% to 10% with an increase of friction coefficient from 0.1 to 0.9.

Fig. 5.8 also shows the elastic modulus increases with the increase of coefficient of friction. In addition, the E value increased more rapidly for SLAs with higher HCFA volume fractions compared to those with lower HCFA volume fractions. This is consistent with the previous analysis on the ABAQUS axisymmetric models results.

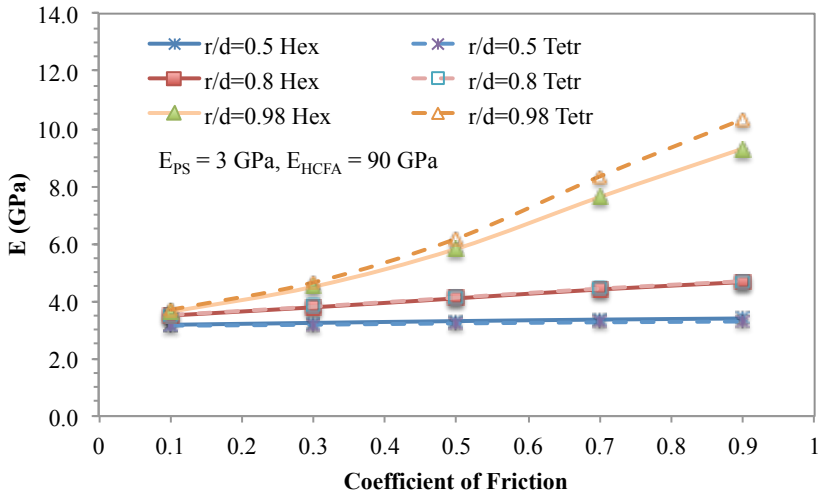

Fig. 5.8 ABAQUS 3-D Stress Control Result: E vs. Coefficient of Friction for r/d = 0.5, 0.8, and 0.98

5. 3. 2 Elastic Moduli of SLAs-HCFA/MP

The elastic moduli of SLAs-HCFA/MP at r/d of 0.3, 0.5, 0.65, 0.8, and 0.98 were calculated using ABAQUS 3D one-layer and ABAQUS 3D two-layer models, corresponding to HCFA volume fractions of 0.014, 0.065, 0.144, 0.268, and 0.493, respectively. The examples of stress contour are illustrated in Fig. 5.9. The elastic modulus at various r/d ratios was plotted in Fig. 5.10. As shown, the elastic modulus ranges from 1.5GPa to 3GPa at HCFA volume fractions

less than 0.268, while the stiffness dramatically increases when the volume fractions go above 0.268. In addition, the divergence between the results obtained from one-layer and two-layer model increases when the volume fractions increased. The computed elastic modulus was also compared to those from Weingam's (2003) prediction, in which the elastic modulus of SLAs-HCFA/MP that has volume fraction of 0.160 and 0.270 was given. As shown in Fig. 5.10, the one-layer model showed more agreeable result with the Weingam's results than the two-layer model does.

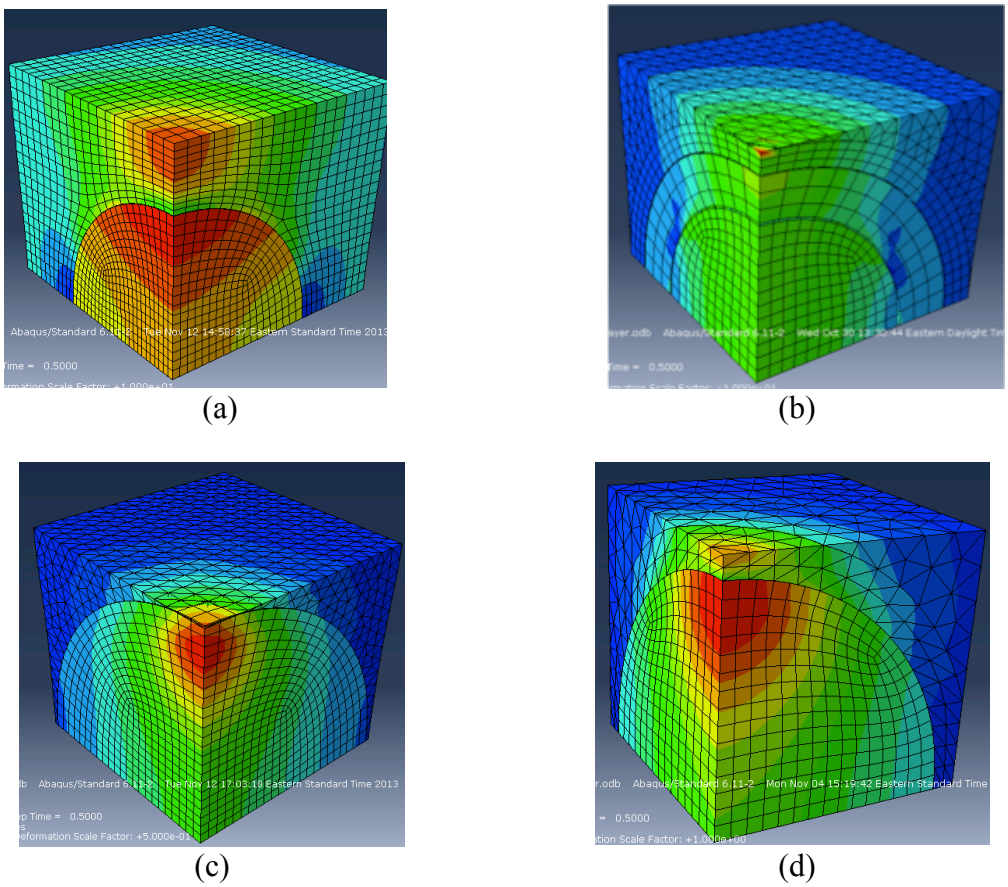

(a) (b) (c) (d)

Fig. 5.9 Examples of FEM Modeling Output for SLAs-HCFA/MP: (a) r/d = 0.65, one-layer of matrix; (b) r/d = 0.65, two-layer of matrix; (c) r/d = 0.98, one-layer of matrix; (b) r/d = 0.98, two-layer of matrix;

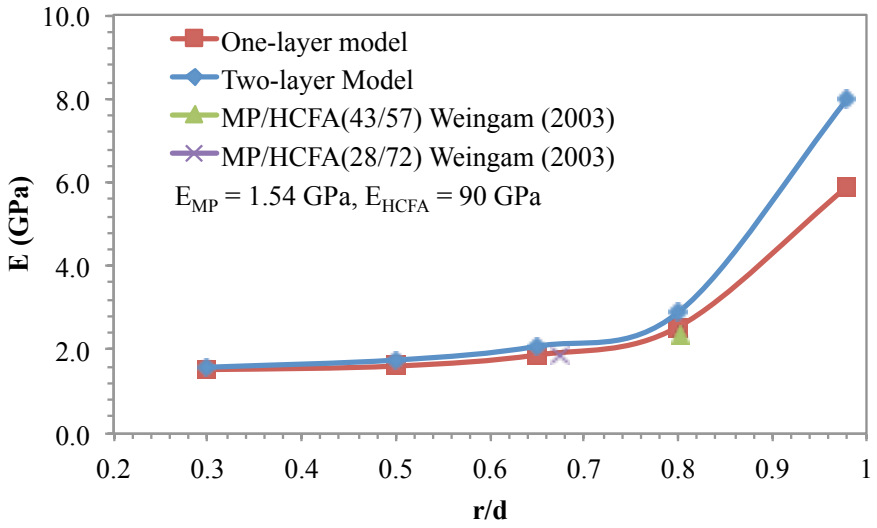

Fig. 5.10 SLAs-MP/HCFA Elastic Modulus vs. r/d from ABAQUS 3D

5. 4. Comparison of Analytical and FEM Results

The predicted Young's moduli from the FEM models were compared to those obtained from various analytical methods. The percentages of difference were calculated and plotted for SLAs-HCFA/PS and SLAs-HCFA/MP at different HCFA volume fractions.

5. 4. 1 Elastic Moduli Comparison for SLAs-HCFA/PS

Fig. 5.11 shows the differences between moduli of SLAs-HCFA/PS obtained from FEM prediction and those from various analytical methods. For each figure, the difference was calculated using the analytical E value minus the E values obtained from the FEM method and divided by the FEM values. For comparison purpose, the charts in Fig. 5.11 use the Young's moduli with an interaction option of "rough" for the ABAQUS 3D, and the Young's moduli computed for scenarios with a coefficient of friction of 0.9 for the ABAQUS Axisymmetric system. It shows that the Young's modulus difference increases accordingly with the increase of r/d ratio or fly ash volume fraction in most cases. In general, the analytical methods, including H-S lower bound, Counto equation, and Kerner equation had good agreement with the FEM

modeling prediction, especially at lower volume fractions (r/d = 0.5 and 0.8). For instance, the difference between these predictions was less than 15%, 16%, and 15% for ABAQUS axisymmetric, ABAQUS 3D stress control, and ABAQUS 3D strain control model, respectively. As shown, the FEM methods predict the E values either lower or higher than analytical methods do at lower volume fraction; while at high volume fraction (r/d = 0.98), the FEM methods generally generate higher E values. Furthermore, the ABAQUS 3D stress control had the best agreement with H-S Lower and Kerner equation, which was within 2% and 8% respectively. Comparatively, the ABAQUS 3D strain control had only 2% and 3% difference with the H-S lower and Kerner predictions at lower volume fraction. However, at large volume fraction (r/d = 0.98), the differences between analytical and FEM modeling prediction were relatively significant with computed E values up to 47%, 20%, and 35% greater than analytical E values for ABAQUS axisymmetric, ABAQUS 3D stress control, and ABQUS 3D strain control model, respectively. Overall, the Young's modulus from ABAQUS 3D showed better agreement (within 25% for stress control and 39% for strain control) with E values from analytical methods, especially with the Kerner method.

Additionally, the differences between the analytical predictions and ABAQUS 3D stress-control and strain control models was very small, especially at lower HCFA volume fractions; however, it rapidly increased for the strain-control model as volume fractions increased. Fig. 5.11(d) also includes the Young's modulus at r/d = 0.91 (f = 0.395) to show the dramatic increase of modulus divergence when the r/d ratio change from 0.91 to 0.98 (volume fraction f from 0.395 to 0.493). Overall, although the Kerner method might be the most agreeable analytical method with ABAQUS 3D modeling, it is more confident to say that the FEM modeling result is not consistently agreeable with one specific analytical method. Hence it is

necessary to rely on more than one analytical expression for evaluating the reasonability of FEM results.

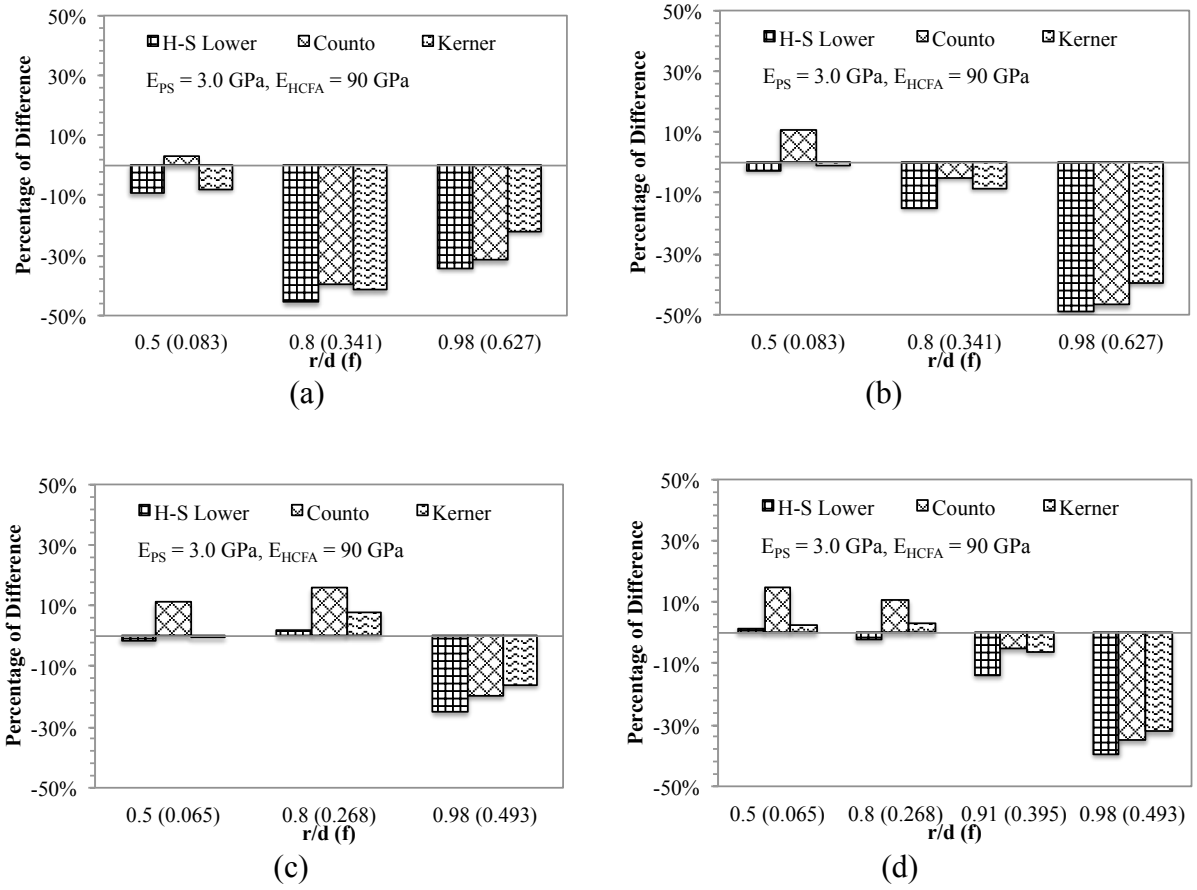

Fig. 5.11 Percentages of Young's Modulus Difference Computed from Analytical Predictions Compared to Predicted E Obtained from: (a) PLAXIS Axisymmetric; (b) ABAQUS Axisymmetric; (c) ABAQUS 3-D Strain-control; (d) ABAQUS 3-D Stress-control

5. 4. 2 Elastic Moduli Comparison for SLAs-HCFA/MP

The elastic modulus predicted by the ABAQUS 3D one-layer model and two-layer model was also compared with those calculated using analytical methods. Differences by percentage were plotted as illustrated in Fig. 5.12 and Fig. 5.13. As shown, the two-layer model showed better agreement with analytical methods than the one-layer model at lower volume fractions ($f \leq 0.268$), but it shows the opposite way at higher volume fraction ($f = 0.493$). Specially, the

difference between one-layer model results and analytical predictions was less than 34% when r/d is no greater than 0.8 ($f \leq 0.268$), and 37% at r/d of 0.98 ($f = 0.493$). However, for the ABAQUS two-layer model, the difference was within 19% at low volume fractions, and 53% at higher volume fractions. Moreover, the H-S lower method and Kerner equation showed better agreement with ABAQUS predictions at low volume fractions, but the Counto equation generated moduli that were most close to those from ABAQUS analysis at high volume fraction. This also supports the conclusion that more than one analytical expression should be used to evaluate the FEM models as discussed above.

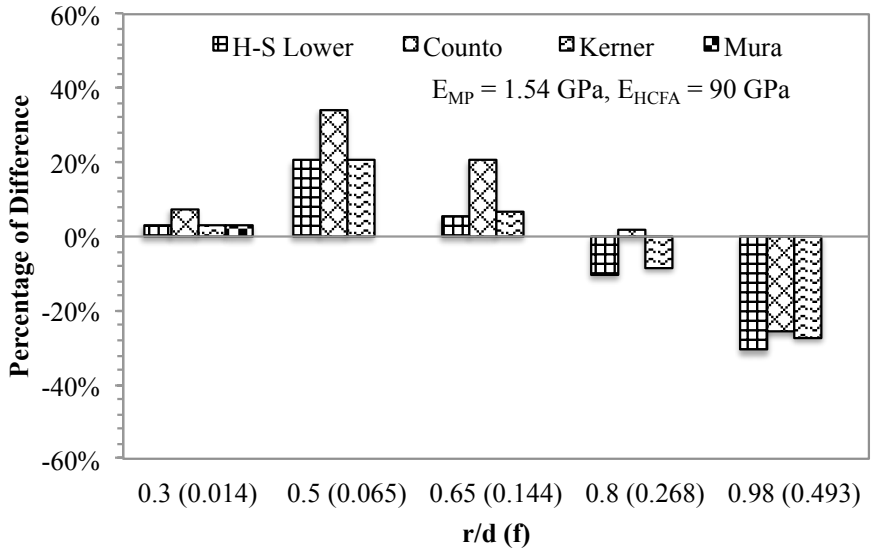

Fig. 5.12 Percentage Difference of Young's Modulus Computed From Analytical Methods Compared to ABAQUS 3D One-layer Model Prediction

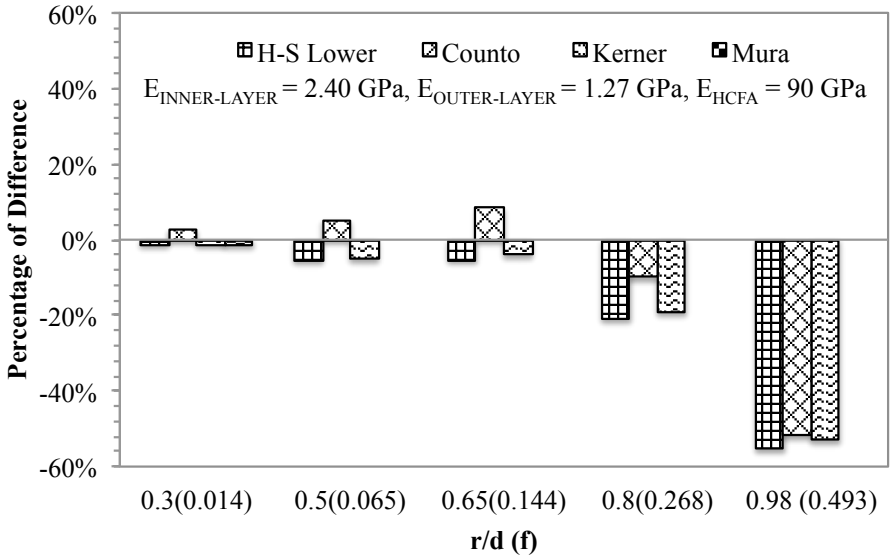

Fig. 5.13 Percentage Difference of Young's Modulus Computed From Analytical Methods Compared to ABAQUS 3D Two-layer Model Prediction

5. 5. Conclusions

In conclusion, the analytical and FEM methods both showed that the elastic modulus of SLAs increases with the increase in HCFA volume fraction, and this incremental increase became more pronounced as the HCFA volume fraction continued to increase. In addition, the analytical analysis indicated that the increase slightly varied with the matrix material; i.e., the plastic type. The FEM analysis showed that the element type and mesh fineness had no significant effect on the elastic modulus of SLAs. However, the roughness of interface between HCFA and plastic influenced the stiffness of the composite SLAs dramatically. This influence increased as the fly ash volume fraction increased. Finally, the comparison between analytical and FEM results shows that the ABAQUS axisymmetric and 3D models had better agreement with analytical results, especially at lower volume fraction (less than 0.395). However, the difference in E values increased significantly as the volume fraction increased (especially for an r/d of 0.98). In addition, the FEM methods generally produced E values greater than analytical

predictions. Summarily, since no specific analytical method had shown consistent agreement with FEM predictions, it is suggested that all analytical methods discussed herein should be used when evaluating the applicability of the FEM models in this research. In the next chapter, the ABAQUS 3D models are used for further study with the strain-control method adopted in the simulation of laboratory tests.

LABORATORY RESULTS AND COMPARISON WITH COMPUTATIONAL RESULTS

6. 1 Introduction

This Chapter introduces the results from laboratory tests performed on SLAs-HCFA/PS with nominal HCFA / PS mass ratios of 50:50, 65:35, and 80:20. Based on the specific gravity and LOI test results, actual HCFA and PS contents in SLAs were obtained. Accordingly, the dimensions of unit cell model in ABAQUS 3D coordination system were adjusted to simulate the stress-strain behavior of SLAs-HCFA/PS(50:50) and SLAs-HCFA/PS(65:35). In addition, the elastic modulus of PS obtained from unconfined compression test was also used as a computation parameter in ABAQUS and analytical method to compute the elastic modulus of SLAs. Finally, comparisons between the stress-strain behavior obtained from laboratory test and those from ABAQUS modeling were made; specifically, between the elastic modulus obtained from laboratory test, ABAQUS modeling, and analytical method; and between the Poisson's ratio obtained from analytical method and ABAQUS modeling.

6. 2 Laboratory Test Results

The laboratory test results include those obtained from specific gravity test and Loss of Ignition (LOI) test on SLAs-HCFA/PS and SLAs-HCFA/MP; confined compression test, and unconfined compression test on SLAs-HCFA/PS.

6. 2. 1 Specific Gravity

Specific gravity tests were performed on HCFA, PS, and SLAs that are composed of various proportions of HCFA and PS or MP. The tested specific gravities are summarized below in Table 6.1. As shown, the average specific gravities of PS and HCFA are 1.06 and 2.2, respectively. The specific gravities of SLAs-HCFA/PS and SLAs-HCFA/MP falls in the range of 1.29~1.79 and 1.45~1.72 respectively. It is apparent that SLAs with higher HCFA content have higher specific gravity. However, the laboratory tests show that SLAs-HCFA/MP(65:35) has higher specific gravity than SLAs-HCFA/MP(80:20), which indicates the uncertainty of components' content in SLAs products. Hence, to obtain the actual compositions of these SLAs (and others), LOI tests were conducted.

Table 6.1 Specific Gravity Test Results

	PS	HCFA	SLAs-HCFA/PS (50:50)	SLAs-HCFA/PS (65:35)	SLAs-HCFA/PS (80:20)	SLAs-HCFA/MP (50:50)	SLAs-HCFA/MP (65:35)	SLAs-HCFA/MP (80:20)
Gs	1.06	2.20	1.29	1.58	1.79	1.45	1.72	1.67

6. 2. 2 Loss of Ignition (LOI)

The LOI tests had been performed on HCFA, SLAs-HCFA/PS and SLAs-HCFA/MP. The LOI tests on the fly ash consistently indicated a carbon content in the HCFA of 16.9%. Since the specific gravity of fly ash had also been measured, the HCFA and plastics contents were now able to be calculated. In summary, the actual proportions of fly ash and plastics are listed in Table 6.2. As shown, the designed mass ratio of plastic to HCFA is different than anticipated from the SLAs' believed composition, especially for SLAs with significant HCFA. For example, for the SLAs-HCFA/MP (80:20), that was to be have been designed to contain 80% of HCFA by mass, only contained approximately 70% of HCFA. And according to the

specific gravity and carbon content values in SLAs-HCFA/MP(65:35), the SLAs-HCFA/MP(80:20) and SLAs-HCFA/MP(65:35) might be mislabeled because they have HCFA:MP ratios of approximately 70:30, and 75:25 respectively. This explains why the specific gravity of SLAs-HCFA/MP(65:35) is greater than the one of SLAs-HCFA/MP(80:20) as listed in Table 6.1.

Table 6.2 LOI Test Results

% of Mass	SLAs-HCFA/PS (50:50)	SLAs-HCFA/PS (65:35)	SLAs-HCFA/PS (80:20)	SLAs-HCFA/MP (50:50)	SLAs-HCFA/MP (65:35)	SLAs-HCFA/MP (80:20)
HCFA (%)	43.5	61.8	76	48.3	74.9	70.2
PS (%)	56.5	38.2	24.0	-	-	-
MP (%)	-	-	-	51.7	25.1	29.8

6. 2. 3 Confined Compression Test – Sample Preparation

As mentioned, individual, granular SLAs particles were compressed, via a confined compression, into solid specimens to be used in unconfined compressive tests. Solid specimens were created from SLAs-HCFA/PS with nominal mass ratios of 50:50, 65:35, and 80:20 and pure PS (also in a granulated state). The stress-strain curves of the confined compression tests are shown in Fig. 6.1 to Fig. 6.3. As shown, approximately 55% axial strain was required for granulated SLAs to become compressed into solid specimens. All stress-strain curves show that when strain reached up to 50%, the stress increased exponentially; reaching maximum load capacity of the loading device with relatively little additional strain. In addition, as illustrated in Fig. 6.1, for SLAs-HCFA/PS(50:50) specimens where the compression mold was not oiled showed significantly higher rates of strain-hardening than cases where the mold was oiled . This was not noted for the 65:35 and 80:20 SLAs mixtures. This indicates that the SLAs-HCFA/PS

with less fly ash content was more likely to be influenced by the friction between the SLAs and molds.

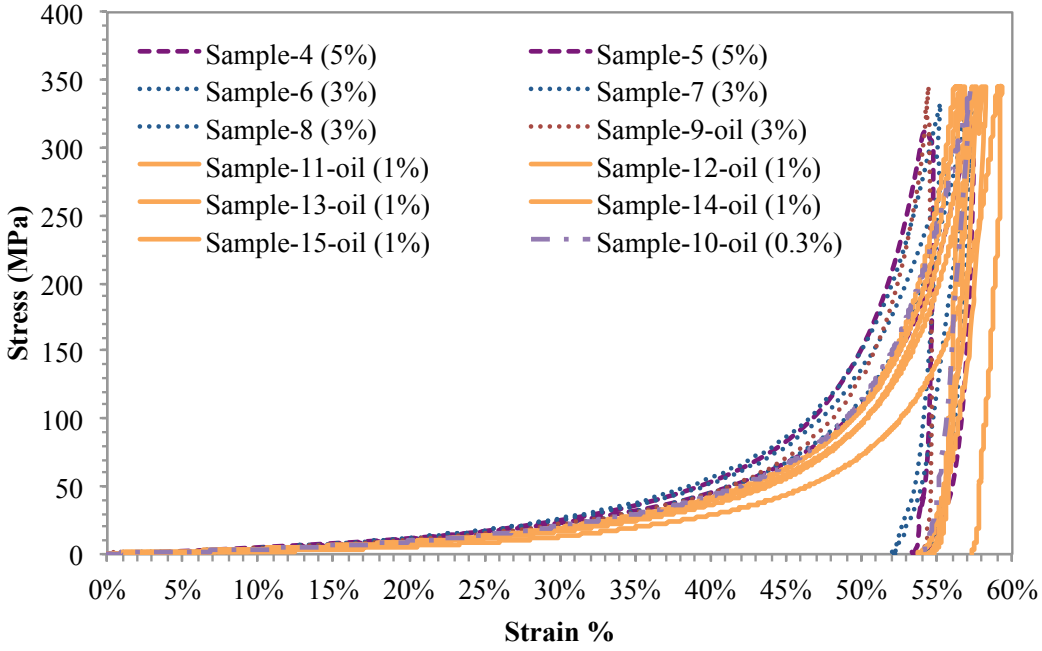

Fig. 6.1 Constrained Stress vs. Strain Curves of SLAs-HCFA/PS(50:50)

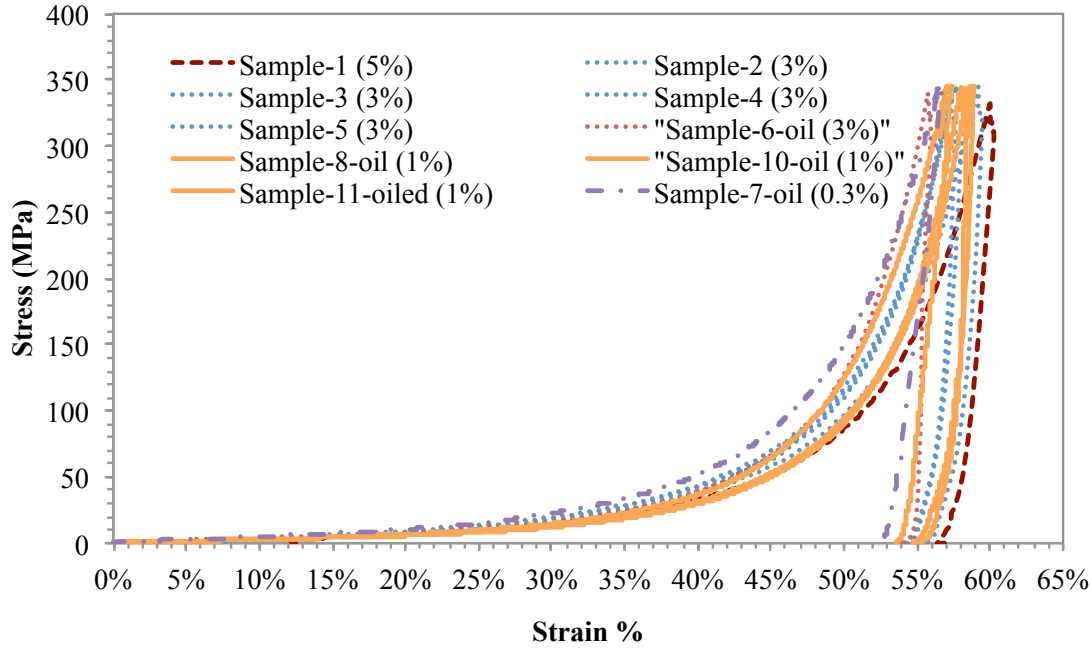

Fig. 6.2 Constrained Stress vs. Strain Curves of SLAs-HCFA/PS(65:35)

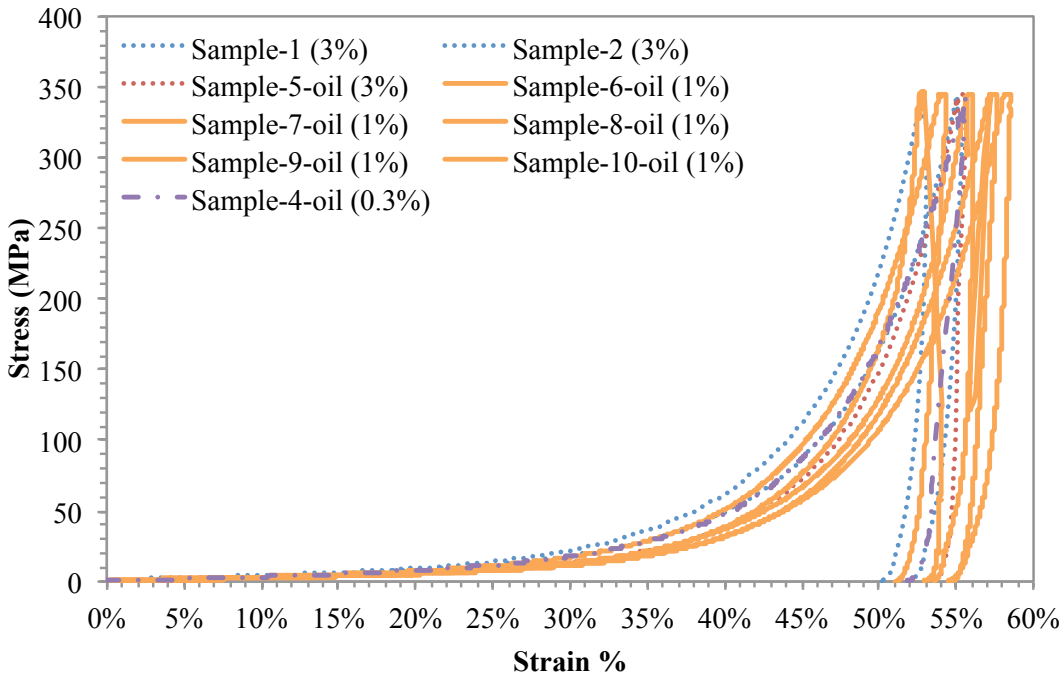

Fig. 6.3 Constrained Stress vs. Strain Curves of SLAs-HCFA/PS(80:20)

Furthermore, the porosity at different states, including maximum stress, maximum strain, unloading to zero stress, at the end of test, and after extruding from the mold, was calculated, using Eq. 4.7 to 4.9 in Chapter 4, and were plotted in Fig. 6.4 to Fig. 6.6. As shown, the specimen was compressed most after the maximum stress had been reached and maintained for at least 10min. The sample then rebounded during the unloading process, and the porosity reached its highest post-compression value after extrusion. The average mass, dimensions, and porosity of SLAs after extrusion are listed in Table 6.3. As can be seen, the SLAs that contain less HCFA compressed more and maintained nearly zero void ratio after extrusion.

An interesting case is shown by specimens created with SLAs-HCFA/PS(50:50) which were able to reach negative porosities. In addition, Fig. 6.4 and 6.5 also shows that other 50:50, and 65:35 SLA specimens reached negative porosity at high pressure during the compression

process. The rationale for negative porosities is as follows. According to the equations for porosity calculation, negative porosity could be obtained when the volume of solid ($V_S = M/G_S$) is larger than the volume of SLAs ($V = 0.25\ \pi D^2 H$). This is possible when the measured G_S, which is used to calculate the volume of solid, is less than the specific gravity of the actual solid SLAs. Theoretically, this can happen when air is trapped inside SLA grains, taking up space during specific gravity testing, but compressed during compression tests. Hence, the negative porosities in 50:50 and 65:35 cases indicate entrapped air voids in SLAs. On the other hand, as illustrated in Fig. 6.6, no SLAs-HCFA/PS(80:20) specimen had shown negative porosity. This can be explained by two potential aspects of this SLA: first, no entrapped air voids exists in SLAs-HCFA/PS(80:20); or second, the material was not completely compressed and no entrapped air voids could be detected. Actually, the higher porosities of compressed SLAs-HCFA/PS(80:20) specimens indicate the difficulties of getting solid SLAs specimen due to the presence of higher concentrations of fly ash particles, creating SLA grains which could not be tightly compressed together and may leave voids between SLA grains. Fig. 6.4 to 6.6 also shows that the test with non-oiled mold generated samples with higher porosity, which is 24.9% and 1.6% for 65:35 and 80:20 cases respectively. However, for the SLAs-HCFA/PS(50:50), the friction between the mold and compressed samples may contribute to the negative porosity (46 times less than the oiled case) in extruded SLAs solid. This indicates various side-friction effects on SLAs with different proportion of fly ash and plastic components. In general, the side friction has less significant influence on specimen that has higher amount of HCFA.

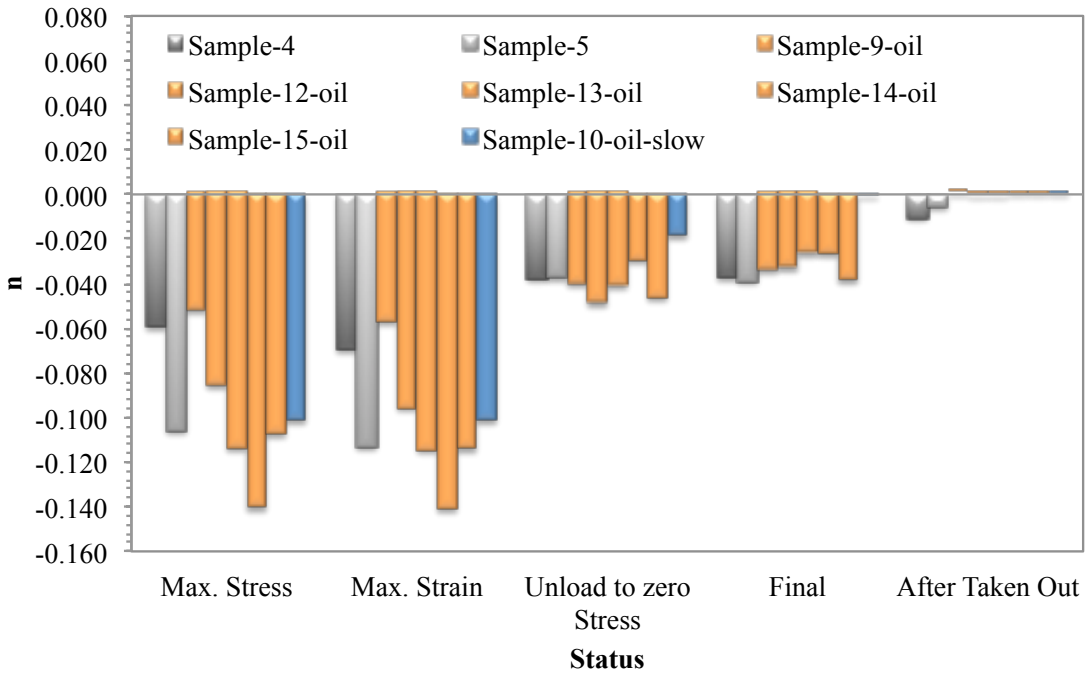

Fig. 6.4 Porosity at Different Status at Constrained Compression of SLAs-HCFA/PS(50:50)

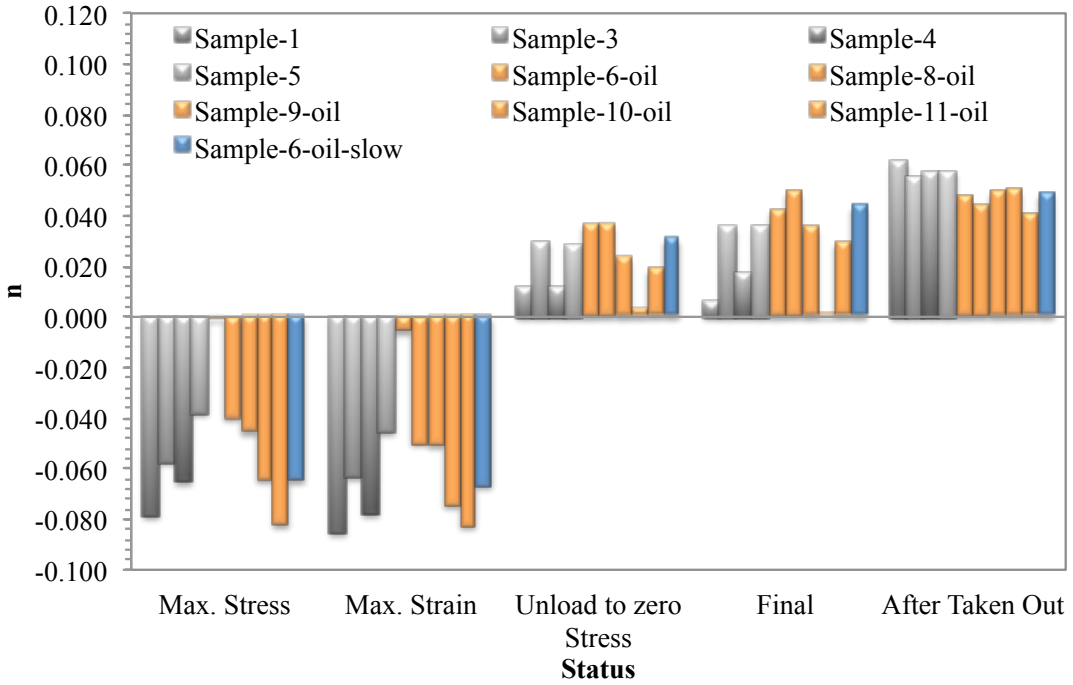

Fig. 6.5 Porosity at Different Status at Constrained Compression of SLAs-HCFA/PS(65:35)

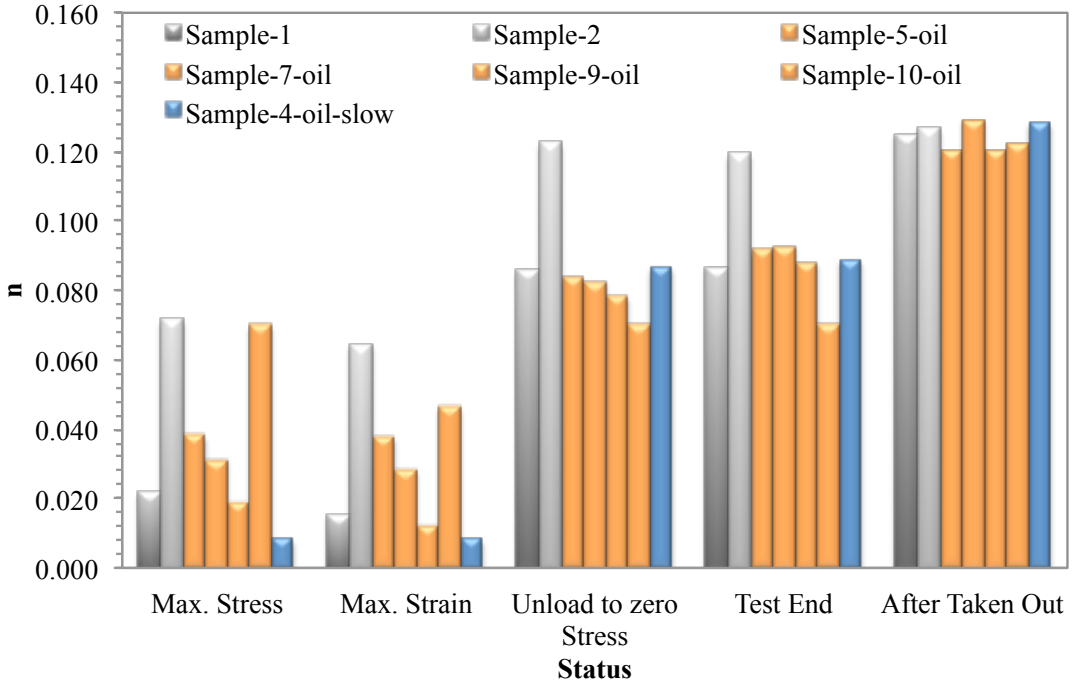

Fig. 6.6 Porosity at Different Status at Constrained Compression of SLAs-HCFA/PS(80:20)

Table 6.3 Mass, Dimensions, and Porosity of Prepared SLAs-HCFA/PS Samples

	SLAs-HCFA/PS (50:50)	SLAs-HCFA/PS (65:35)	SLAs-HCFA/PS (80:20)
Mass (g)	56.5	38.2	24.0
Diameter (mm)	13.07	13.08	13.13
Height (mm)	7.47	7.95	8.47
Porosity n (oiled)	0.0002	0.046	0.124
Porosity n (non-oiled)	-0.009	0.057	0.126

Table 6.4 Mass, Dimensions Prepared SLAs-HCFA/PS Samples

	SLAs-HCFA/PS (50:50)	SLAs-HCFA/PS (50:50)_H	SLAs-HCFA/PS (65:35)	SLAs-HCFA/PS (80:20)
Mass (g)	56.5	56.5	38.2	24.0
Diameter (mm)	13.07	13.07	13.08	13.13
Height (mm)	7.47	7.47	7.95	8.47

From the stress-strain curves, constrained moduli (D) were calculated with two methods: (1) using the last part of the compression loading curve; i.e., the linearized component of the

curve that occurred within the last 3% strain in average prior to reaching the maximum applied stress; (2) using the unloading curve; i.e., the linearized component of the curve that occurred with the stress release from maximum stress to 150MP. The constrained modulus vs. loading rate graph for SLAs-HCFA/PS with different HCFA/PS ratios is plotted in Fig. 6.7.(a) and Fig. 6.7.(b). Fig. 6.7.(a) shows that SLAs-HCFA/PS(65:35) and SLAs-HCFA/PS(80:20) have relatively consistent constrained modulus, even at different loading rates, compared to the SLAs-HCFA/PS(50:50). The differences in constrained moduli were below 20% for the SLAs-HCFA/PS(65:35) and SLAs-HCFA/PS(80:20) when loading rate varied from strain rate of 0.35%/min to 3.68%/min in oiled condition, and within 28% in non-oiled condition. The difference in D values for SLAs-HCFA/PS(50:50) is 38% and 25% in oiled and non-oiled condition, respectively. This indicates the degree of smoothness of the interaction surface between compressed specimen and mold had a significant influence on SLAs-HCFA/PS(50:50) than the other two. This is consistent with the previous conclusion drawn from the porosity analysis. In addition, although in general the stiffness of composite material increases with the amount of reinforcement as discussed in Chapter 2 (and shown computationally in Chapter 5), Fig. 6.7.(a) shows the opposite result because the SLAs-HCFA/PS(50:50) had higher constrained modulus than the other two. The unconfined compression test results, which will be discussed later, show a similar trend. Comparatively, Fig. 6.7.(b) showed scattered constrained modulus values at different strain rate for various types of SLAs. This indicates that D may not be determinable via the compression test. Other critical factors influence the variability in D values are the coefficient of friction between HCFA and plastic, and possible difference in the coefficient of friction as the proportions of fly ash and plastics change. In addition, it is suspected that variations in interface conditions between SLA grains may also be a cause of the

unpredictable modulus trend shown in the laboratory tests. That is, many of the compressed specimens did not have near-zero-porosities; therefore, grain-to-grain contacts of the SLA may still be governing the measured D values.

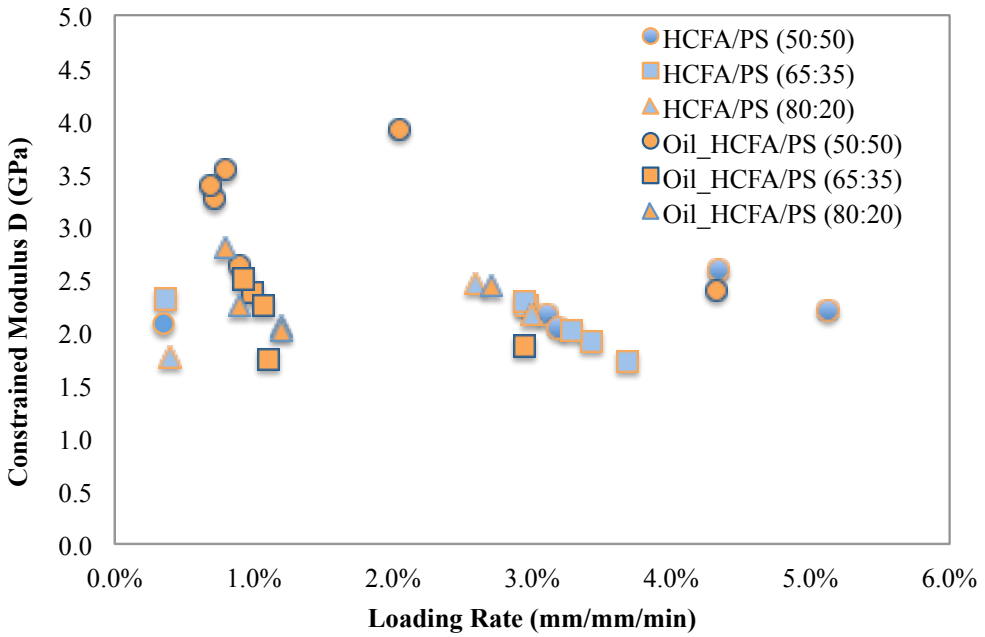

Fig. 6.7.(a) Constrained Modulus of SLAs-HCFA/PS vs. Loading Rate

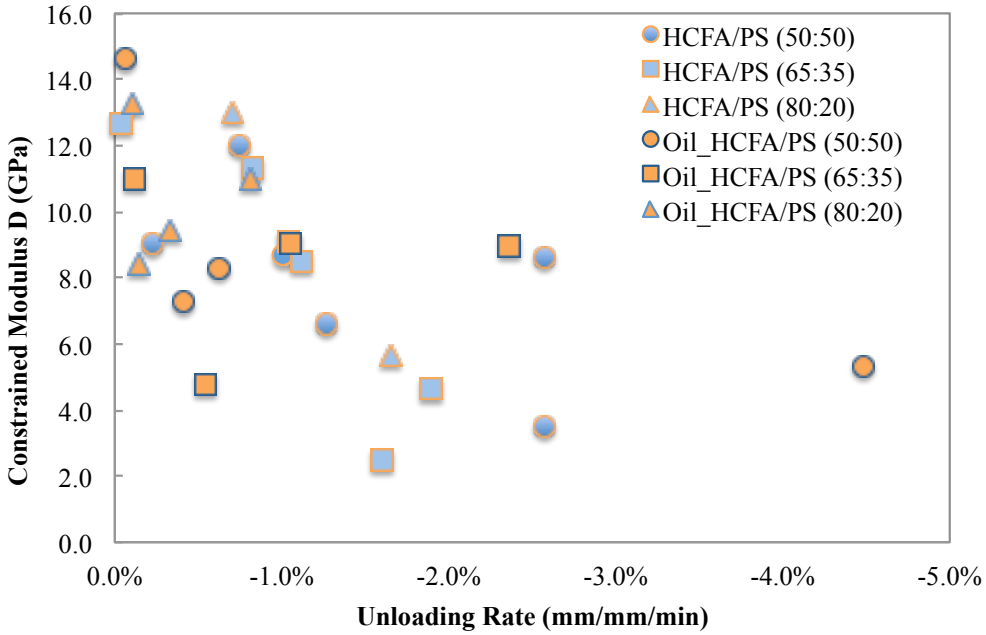

Fig. 6.7.(b) Constrained Modulus of SLAs-HCFA/PS vs. Unloading Rate

Constrained moduli are correlated to the elastic modulus by using Eq. 6.1, assuming Poisson's ratio of 0.33 and homogenous isotropic condition. In summary, the elastic modulus range is 1.38~2.64GPa, 1.16~1.70GPa, and 1.20~1.88GPa from loading curve, and 2.36~9.89GPa, 1.67~8.53GPa, and 3.83~8.94GPa from unloading curve, for SLAs-HCFA/PS with designed mass ratio of 50:50, 65:35, and 80:20, respectively. And the average and standard deviation was calculated and listed in Table 6.4.(a) and 6.4.(b). The values will be used to compare with those obtained from the unconfined compression test result. However, as shown, the standard deviation of elastic modulus obtained from loading part is 10%~18% differentiated with the average E value; while those from unloading part is 20%~50% different with the average. Since only the elastic moduli obtained from loading part will be used for future comparison.

$$E = \frac{D(1-2\nu)\,(1+\nu)}{1-\nu} \qquad \textbf{(6.1)}$$

Where, E is elastic modulus, D is constrained modulus, and ν is Poisson's ratio.

Table 6.5.(a) Constrained Modulus (D) in GPa and Elastic Modulus (E) in GPa of SLAs-HCFA/PS Obtained from Constrained Compression Test Loading Curve

		SLAs-HCFA/PS (50:50)		SLAs-HCFA/PS (65:35)		SLAs-HCFA/PS (80:20)	
		Average	SD	Average	SD	Average	SD
Oiled	D	3.19	0.57	2.27	0.24	2.31	0.31
	E	2.15	0.38	1.53	0.16	1.56	0.21
Non-oiled	D	2.22	0.22	1.99	0.24	2.13	0.35
	E	1.50	0.15	1.35	0.16	1.44	0.23

Table 6.6.(b) Constrained Modulus (D) in GPa and Elastic Modulus (E) in GPa of SLAs-HCFA/PS Obtained from Constrained Compression Test Unloading Curve

		SLAs-HCFA/PS (50:50)		SLAs-HCFA/PS (65:35)		SLAs-HCFA/PS (80:20)	
		Average	SD	Average	SD	Average	SD
Oiled	D	8.89	4.03	8.43	2.60	10.53	2.09
	E	6.00	2.72	5.69	1.75	7.10	1.41
Non-oiled	D	8.06	2.83	8.11	3.90	9.36	5.21
	E	5.44	1.91	5.47	2.63	6.31	5.21

6. 2. 4 Unconfined Compression Test

Unconfined compression tests were carried out on solid specimen of pure PS, and SLAs-HCFA/PS with PS and HCFA mass ratios of 50:50, 65:35, and 80:20. Specimens were obtained from confined compression tests. All specimens had a diameter of approximately 13mm and height of approximately 8 mm, as listed in Table 6.3. In addition, one set of specimens for SLAs-HCFA/PS(50:50) had a diameter of approximately 13mm and height of approximately 18mm) in order to evaluate the effect of sample height on the stress-strain behavior of SLAs. The stress-strain curves of SLAs are plotted in Fig. 6.8. As illustrated, all stress-strain curves begin with strain-hardening, followed by a linear section and then strain-softening to a peak value (failure) and then continued softening until specimens no longer had any integrity under loading. The initial strain-hardening is likely due to a number of mechanical variables including machine compliance and specimen seating. In addition, this phenomenon may indicate the existence of air voids in samples that needed to be compressed before the specimens provided the more linear elastic response. This linear component of the curve was used for elastic modulus calculations. As can be observed, the elastic modulus was taken as the ratio of increased stress to the increased strain between two labeled points on the curves. The elastic moduli were summarized in Table 6.5. As can be seen, all SLAs-HCFA/PS have slightly higher modulus than the pure PS does. For

the specimen with identified dimensions, the modulus increase was 45%, 40%, and 9% for SLAs with HCFA/PS mass ratio of 50:50, 65:35, and 80:20, respectively. It is apparent that the stiffness decreased with the increase in HCFA content in the SLAs. It indicates that the PS was enhanced to a similar degree when 65% and 50% of HCFA by weight was added. However, when 80% of HCFA was added, the stiffness of the material rapidly decreased compared the other two SLAs, but slightly increased compared to the pure PS. This agrees with the modulus vs. HCFA content trends obtained from the confined compression tests. However, the elastic moduli from unconfined compression tests were much less than those obtained from constrained compression test. Potential reasons that contribute to this large bias include: 1) the elastic modulus calculation from the constrained modulus that was based on the assumption that the material is isotropic, homogenous, and has Poisson's ratio of 0.33 may not be applicable in this case; and 2) a critical material parameter - the interaction between HCFA and PS, may be different under different loading conditions (confined or unconfined), which may generate different bonding ability between the components, and in turn affect the elastic modulus of the composite material.

Fig. 6.8 also shows that the failure occurred at strains of 12%~14%, 10%~11%, and 8%~9%, and the compressive strength was 39~63MPa, 35~52MPa, and 23~31MPa, for 50:50, 63:35, and 80:20 SLAs, respectively. This shows that the increased HCFA content may contribute to the decrease of the strain at failure. This agrees with the analysis on the material composed of high-lime fly ash enriched RPET by White (2000), who proposed a method of calculating the elastic modulus of composite material using the compressive strength and percentage of fly ash content, as shown in Eq. 6.2.

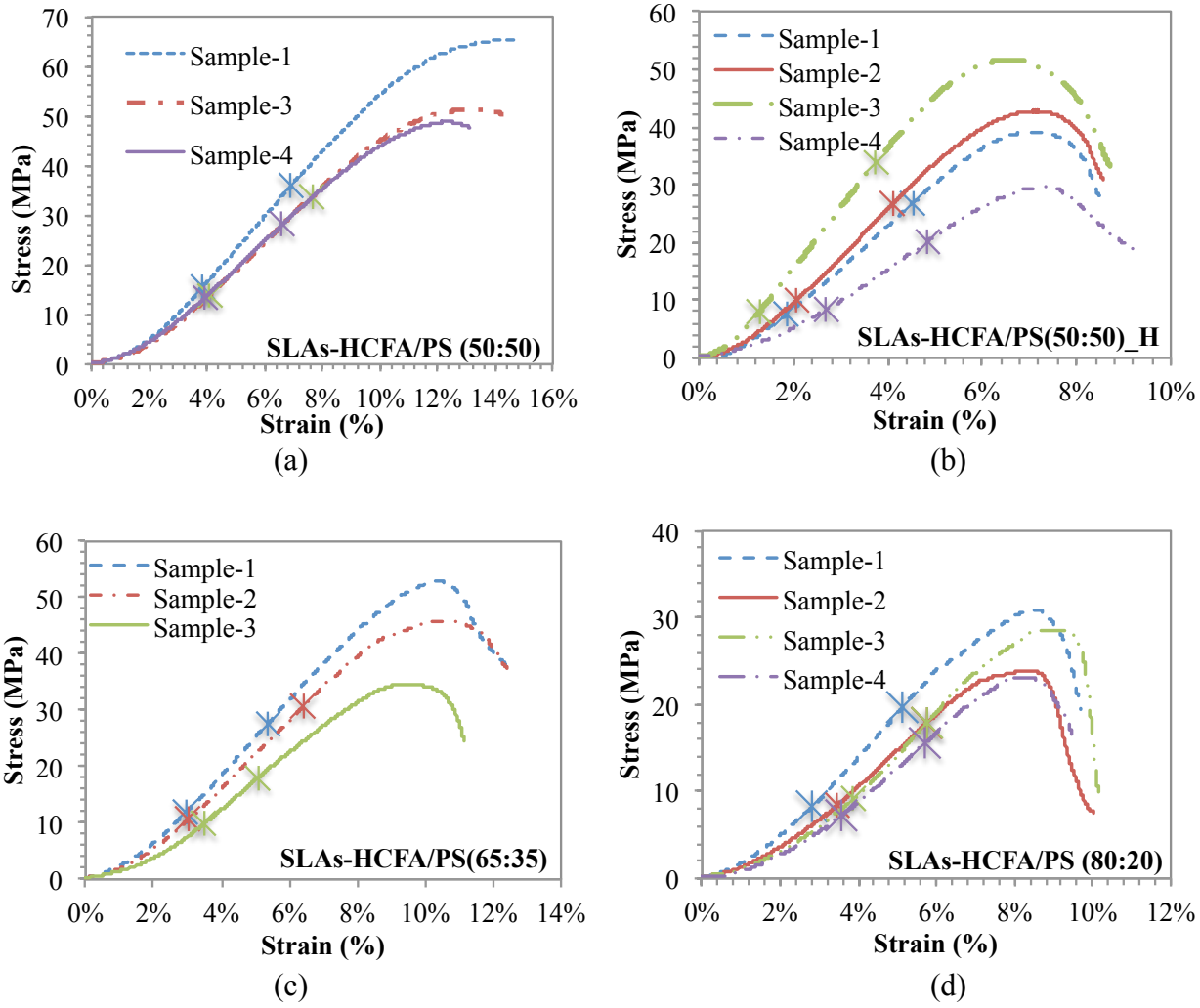

Fig. 6.8 Stress-strain Curve of SLAs-HCFA/PS: (a) SLAs-HCFA/PS(50:50) $D_0 \approx 13$mm, $H_0 \approx 7.5$mm; (b) SLAs-HCFA/PS(50:50) $D_0 \approx 13$mm, $H_0 \approx 18$mm ; (b) SLAs-HCFA/PS(65:35) $D_0 \approx 13$mm, $H_0 \approx 8.0$mm; (b) SLAs-HCFA/PS(80:20) $D_0 \approx 13$mm, $H_0 \approx 8.5$mm ;

$$E_c = 125 - 135\,(1 + \frac{C_{FA}}{100})\sqrt{f'_C} \qquad \textbf{(6.2)}$$

Where, E_c = the elastic modulus (MPa);

C_{FA} = the percentage of fly ash content by weight (%);

f'_c = the compressive strength (MPa) obtained from unconfined compression test.

According to this method, the elastic modulus of SLAs-HCFA/PS ranged from 1.14~1.48GPa, 1.00~1.35GPa, and 0.85~1.00GPa for 50:50, 65:35, and 80:20 SLAs, respectively. Average

values of E are listed in Table 6.5. As can be seen, the elastic moduli calculated using White (2000) method are in good agreement with those calculated using constrained modulus as listed in Table 6.4. But there is up to 100% bias compared to those obtained from linear regression of unconfined compression stress-strain curves. However, the results also show the trend that higher fly ash contents generate SLAs with less stiffness, which is as discussed above.

The elastic modulus of SLAs-HCFA/PS(50:50)_H specimens with height of 18mm (H/D ratio of 1.38), also listed in Table 6.5, are 28% greater than specimens with height of 7.5mm (H/D ratio of 0.58); however, moduli were 17% less when using White (2000) method. Hence, the data is inconclusive in this research as to the effect of specimen dimension on the results. In addition, as illustrated in Fig. 6.8(b), the sample with larger height/diameter ratio exhibits highly scattered stress-strain curves compared to the others as shown in Fig. 6.8(a), (c), and (d). Therefore, tests on shorter specimens produce more consistent responses and corresponding E values; therefore, are more appropriate.

Table 6.7 Elastic Modulus (E) of SLAs-HCFA/PS Obtained from Laboratory Test

	Method	Pure PS	SLAs-HCFA/PS (50:50)	SLAs-HCFA/PS (50:50)_H	SLAs-HCFA/PS (65:35)	SLAs-HCFA/PS (80:20)
E (GPa)	Linear Regression	0.43	0.63	0.81	0.60	0.47
	White (2000)	-	1.39	1.16	1.17	0.92

6. 2. 5 Scanning Electron Microscope (SEM)

Fig. 6.9 (a), (b), and (c) present SEM images of SLAs-HCFA/PS with designed mass ratios of 50:50, 65:35, and 80:20. The tested material was taken from test specimens after testing in unconfined compression. The images show that the HCFA particles have a variety of sizes and

are random in distribution. The HCFA particles and the contact surface between HCFA and plastic are also clearly seen from the images. In general, the images indicate the lower the HCFA content in SLAs, the more integrated and bounded individual particles become in plastic matrix. The image of the 80-20 SLA's failure surface in Fig. 6.9 (c) shows that some HCFA particles stay together and are bounded as a group of particles instead of distributing as individual particles in the matrix. This phenomenon more likely happens in the 80:20 and 65:35 SLAs because of the larger volume of HCFA.

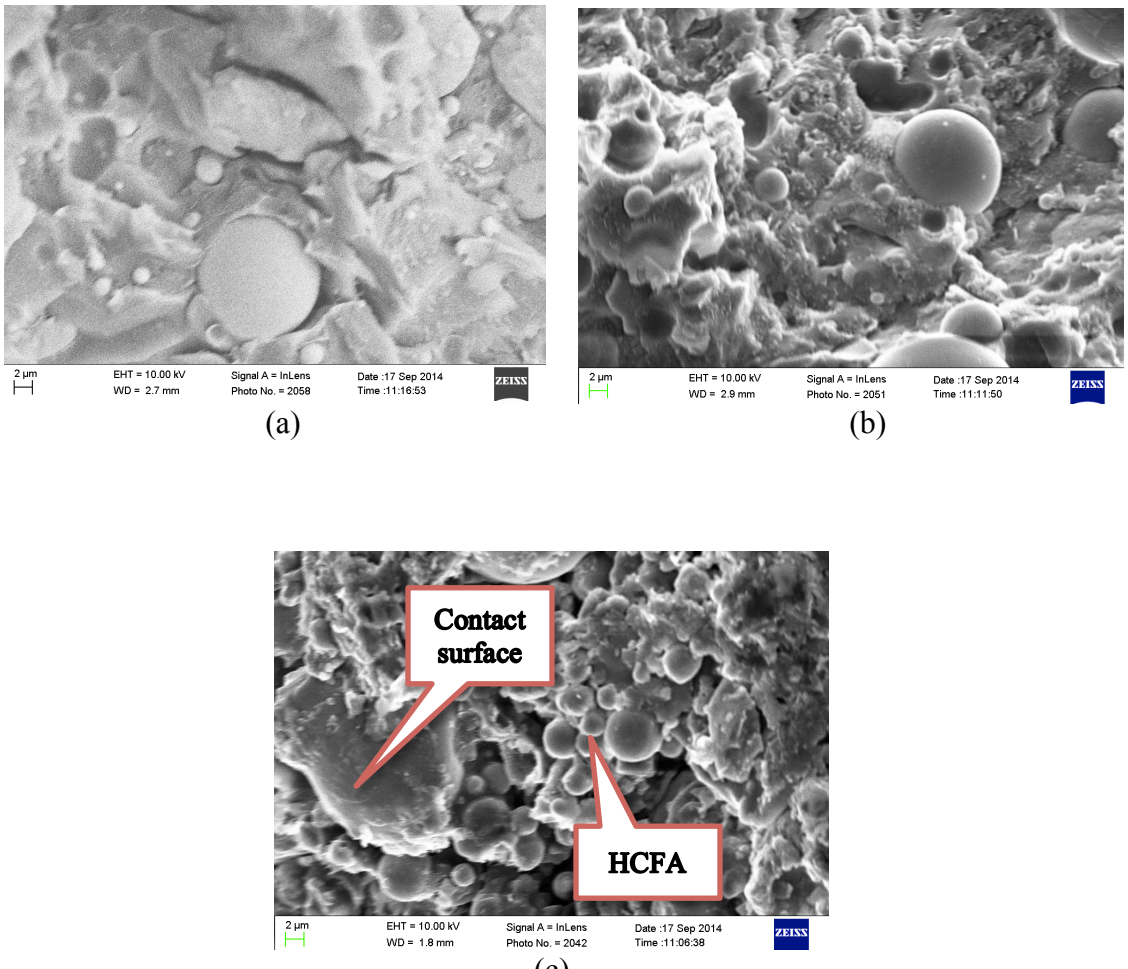

Fig. 6.9 SLAs-HCFA/PS Taken on SEM: (a) HCFA/PS(50:50); (b) HCFA/PS(65:35); (c) HCFA/PS(80:20)

To check if alterations of the HCFA particles' occur after they undergo calcination at temperature of 750^{o}C, SEM images were taken for particles before and after calcination, as shown in Fig. 6.10. Fig. 6.10 (a)-1 and (a)-2 shows an abundance of cluster-like particles, which have been taken to represent unburned carbon; compared to the Fig. 6.10 (b)-1 and (b)-2 where the presence of such clusters is reduced. These cluster-like particles are similar in appearance as those in SEM micrographs of unburned carbon presented by Huwang et al. (2002) and Ahn et al. (1999) [presented as Fig. 2.5 (a) and Fig. 2.5 (b), respectively, in Chapter 2]. As can be seen, some fly ash particles are embedded in clusters of unburned carbon. This also indicates that the existence of unburned carbon is another component of this composite SLAs and may affect the uniform distribution of fly ash in plastic, further questioning whether SLAs can be considered as a type of homogenous isotropic material.

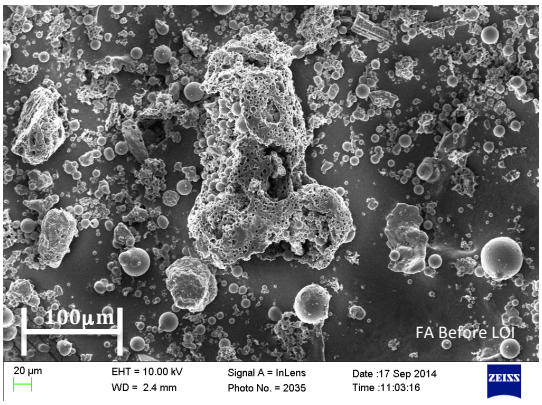

(a)-1

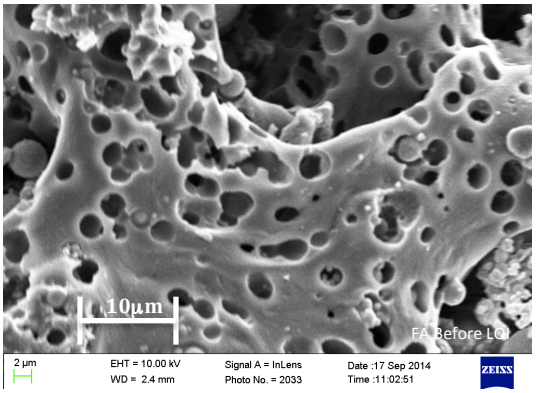

(a)-2

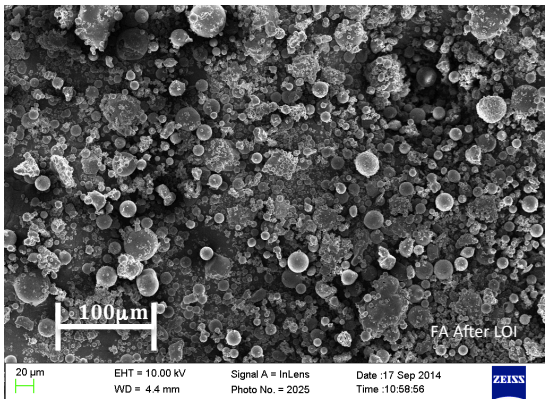

(b)-1

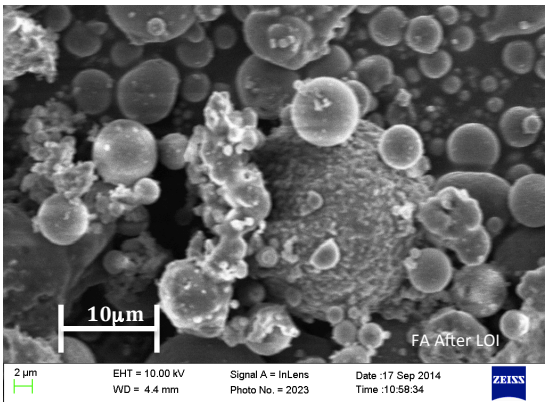

(b)-2

Fig. 6.10 HCFA Particles Taken on SEM: (a)-1. Before Calcination (20µm scale); (a)-2 Before Calcination (2µm scale); (b)-1. After Calcination (20µm scale); (b)-2 After Calcination (2µm scale);

6. 3 Theoretical Computation

As stated previously, the proportion of actual HCFA and PS were determined after specific gravity and LOI test were conducted. Correspondingly, FEM model can be adjusted by modifying the dimensions of fly ash and matrix in the unit cell model, so that it can simulate the behavior of SLAs more accurately. This procedure was done for SLAs-HCFA/PS with nominal mass ratios of 50:50 and 65:35 in ABAQUS 3D modeling system and the results are presented

herein. Furthermore, results were compared to calculations performed using previously discussed analytical methods.

6. 3. 1 Computational Parameters

As shown in LOI test results, the actual mass ratio of HCFA to PS in SLAs-HCFA/PS(50:50) and SLAs-HCFA/PS(65:35) is 44:56, and 62:38 respectively. Accordingly, the volume fraction f is 0.27, and 0.44, corresponding to the r/d value of 0.81 and 0.95 in unit cell model. In addition, the elastic modulus of PS was changed from an assumed 3GPa to the tested value of 0.4GPa in the following study. The Poisson's ratio of 0.22 (Matweb, 2015) was used for PS, assuming a molded, unreinforced PS.

Note: The SLAs-HCFA/PS(80:20) is not covered in this phase of the studywork because its actual volume fraction (0.61) goes beyond the scope of the cubic edge array model, which, for the unit cell geometry used to simulate SLAs, would be a volume fraction that is less than 0.52 (r/d = 1.0) only.

6. 3. 2 Analytical Computation

The elastic modulus of SLAs-HCFA/PS(50:50) and SLAs-HCFA/PS(65:35) were calculated using the analytical methods, including H-S upper bound, H-S lower bound, Counto equation, and Kerner equation. Mura's expression was not considered since the HCFA volume fraction of 0.27 was close to exceeding the expression's upper volume fraction limit. The values of E are summarized in Table 6.6. Poisson's ratios of SLAs are presented in Table 6.7. Ratios were computed using Eq. 6.5, where the value of bulk modulus (K) and elastic modulus (E) was obtained using H-S upper bounds and lower bounds method. In order to study the Poisson's ratio of composite material more comprehensively, two Poisson's ratio values (0.22 and 0.38) were used for PS. As can be seen, the Poisson's ratio of SLAs-HCFA/PS(65:35) is greater than that of

PS. This indicates the possibility that the mixture of two different materials may generate a composite material that has Poisson's ratio greater than the matrix. These values will be compared with those obtained from the ABAQUS 3D modeling as well.

$$\nu = \frac{3K-6E}{6K} \quad \textbf{(6.5)}$$

Where, v = Poisson's ratio; E = elastic modulus; and K = Bulk modulus.

Table 6.8 Elastic Modulus (E) of SLAs-HCFA/PS Obtained from Analytical Method Compared to Those from Unconfined Compression Test

	Method	H-S Upper Bound	H-S Lower bound	Counto Equation	Kerner Equation	Unconfined Compression
E (GPa)	SLAs-HCFA/PS (50:50)	14.93	0.70	0.84	0.71	0.63 (H/D =0.58) 0.81 (H/D = 1.38)
	SLAs-HCFA/PS (65:35)	26.40	1.26	1.20	1.06	0.60

Table 6.9 Poisson's Ratio (ν) of SLAs-HCFA/PS Obtained from H-S Bounds Method

	Poisson's Ratio of PS	SLAs- HCFA/PS (50:50)		SLAs- HCFA/PS (65:35)	
		H-S Upper Bound	H-S Lower Bound	H-S Upper Bound	H-S Lower Bound
ν	0.22	0.21	0.22	0.21	0.47
	0.38	0.21	0.34	0.21	0.47

6. 4 ABAQUS 3D Results and Comparison to the Laboratory and Analytical Results

The ABAQUS 3D models were used to simulate the stress-strain behavior of SLAs. In the modeling, a unit cell model parameter r/d of 0.81 (f = 0.27) was used for SLAs-HCFA/PS(50:50), and a r/d of 0.95 (f = 0.44) was used for SLAs-HCFA/PS(65:35). In addition, various bounding conditions, including coefficient friction of 0.1 (coeff-01), 0.2 (coeff-02), 0.3

(coeff-03), 0.4 (coeff-04), 0.5 (coeff-05), 0.6 (coeff-06), 0.7 (coeff-07), 0.8 (coeff-08), and perfect bounding (rough) between fly ash and PS were also used.

6. 4. 1 Stress Strain Behavior

The stress-strain curves of SLAs-HCFA/PS(50:50) are shown in Fig. 6.11. The stress-strain curves obtained from laboratory tests were also plotted on the same figures for comparison. Similarly, Fig. 6.12 show the stress-strain behavior of SLAs-HCFA/PS(65:35) obtained from ABAQUS 3D simulations. As can be seen, the stress obtained from ABAQUS generally has higher values than the experimental values at the same strain. And the SLAs exhibit stiffer stress-strain behavior when the friction coefficient between fly ash and PS is higher. In addition, the SLAs' stiffness increases with the increment of loading strain. And this increase is more dramatic as the SLAs' friction coefficient increases.

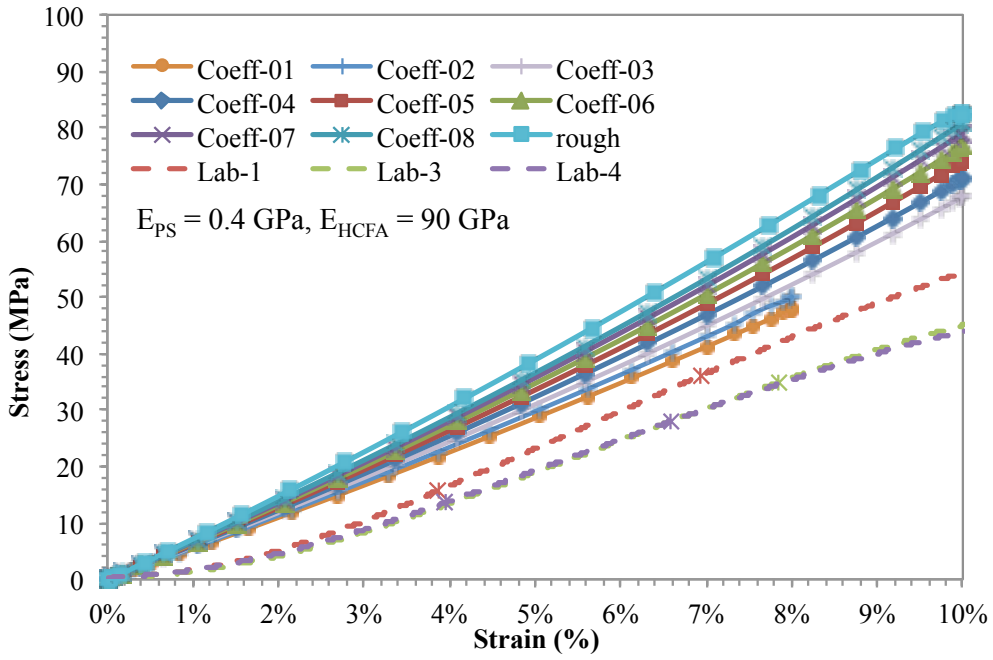

Fig. 6.11 Stress-strain Curves of SLAs-HCFA/PS(50:50)

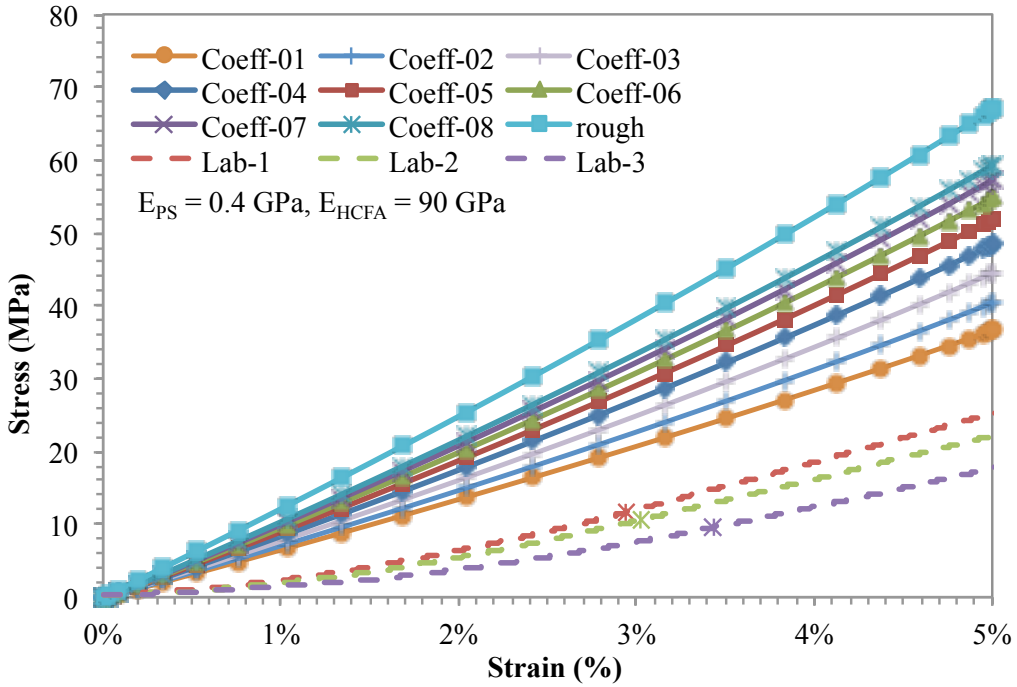

Fig. 6.12 Stress-strain Curves of SLAs-HCFA/PS(65:35)

6. 4. 2 Elastic Modulus

As shown in the stress-strain curves, the initial stiffness of SLAs increase with loading. The tangent moduli at various strains were calculated for SLAs simulated in each model. Taking the scenario that the coefficient of friction between fly ash and PS of 0.1 as a reference, the moduli increase (by percentage) is plotted in Fig. 6.13. Generally, Fig. 13(a) shows that the tangent modulus of SLAs-HCFA/PS(50:50) increases with an increase in strain, and the rate of increase is enhanced as the strain or coefficient of friction increases. Overall, within the first 5% of specimen strain, the difference of modulus is less than 30% for elastic model when coefficient of friction changes from 0.1 to 0.8; and the modulus change is less than 14% as the strain changes from 0% to 5% at a given coefficient of friction between HCFA and PS. Comparatively, Fig. 6.13(b) show that the variation of tangent moduli of SLAs-HCFA/PS(65:35) become more

consistent as strain increases. For a given coefficient of friction, the computed moduli changes are less than 4% the strain increases from 0% to 5%. However, the difference of modulus is 60% when coefficient of friction changes from 0.1 to 0.8 for SLAs-HCFA/PS(65:35).

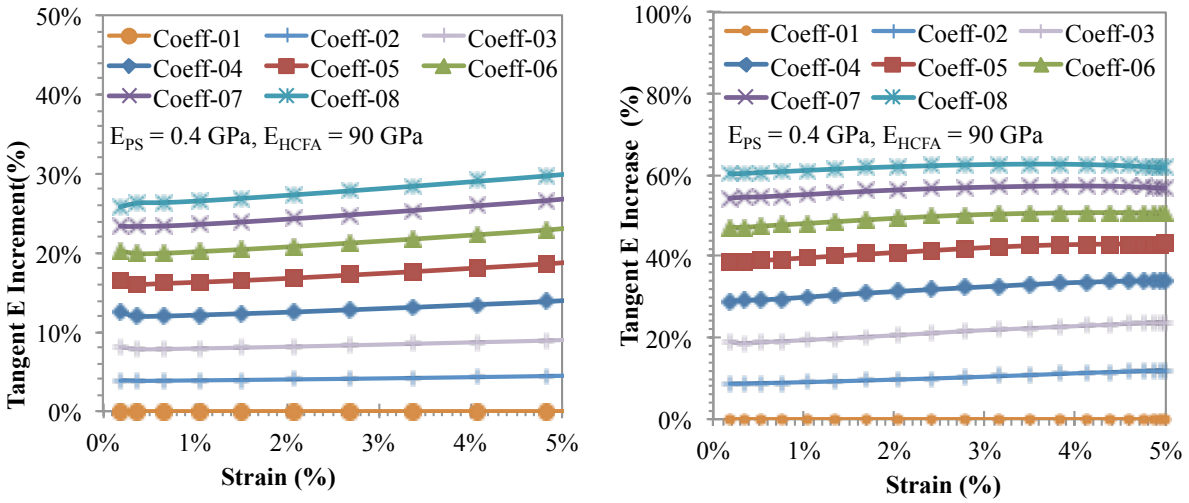

(a) (b)

Fig. 6.13 Increment of Tangent Modulus by Percent Compared to the Coeff-01 (Coefficient of Friction between HCFA and PS is 0.1) Scenario: (a) SLAs-HCFA/PS(50:50); (b) SLAs-HCFA/PS(65:35)

As discussed above, the tangent modulus changes when the applied strain is changed. In order to compare the modulus obtained from ABAQUS simulation with those from laboratory test, linear regression was taken in the strain range that is comparable to the linear part on the stress-strain curve obtained from laboratory test for each type of SLAs-HCFA/PS. Specifically, the elastic modulus was calculated using the linear regression of stress-strain curves with strain range of 4%~7% and 3%~5% for SLAs-HCFA/PS(50:50) and SLAs-HCFA/PS(65:35) respectively. The results were summarized in Table 6.8. Overall, the elastic modulus obtained from various methods, including ABAQUS 3D modeling, analytical methods, and laboratory

tests are plotted in Fig. 6.14 for SLAs-HCFA/PS(50:50) and in Fig. 6.15 for SLAs-HCFA/PS(65:35).

Table 6.10 Elastic Modulus (E) of SLAs-HCFA/PS Based on a Regression of Linear Portion of Stress-Strain Response From ABAQUS 3D Modeling

	SLAs- HCFA/PS (50:50)	SLAs- HCFA/PS (65:35)
Coeff-01	0.62	0.80
Coeff-02	0.65	0.89
Coeff-03	0.68	0.99
Coeff-04	0.72	1.07
Coeff-05	0.75	1.15
Coeff-06	0.78	1.21
Coeff-07	0.80	1.26
Coeff-08	0.82	1.30
Perfect Bound	0.86	1.45

As shown in Fig 6.14, for ABAQUS 3D cases, the predicted elastic modulus obtained using ABAQUS 3D models generated agreeable results with those obtained from analytical methods (H-S lower, Counto, Kerner); especially for ABAQUS model results in which the coefficient of friction is greater than 0.3 for SLAs-HCFA/PS(50:50) and between 0.2 and 0.5 for SLAs-HCFA/PS(65:35). However, the elastic modulus determined from laboratory test was generally lower than the ABAQUS and analytical prediction when the specimen's height-to-diameter ratio (H/D) of 0.6; but lay within the predicted value range when the sample had H/D of 1.4 for SLAs-HCFA/PS(50:50) scenario.

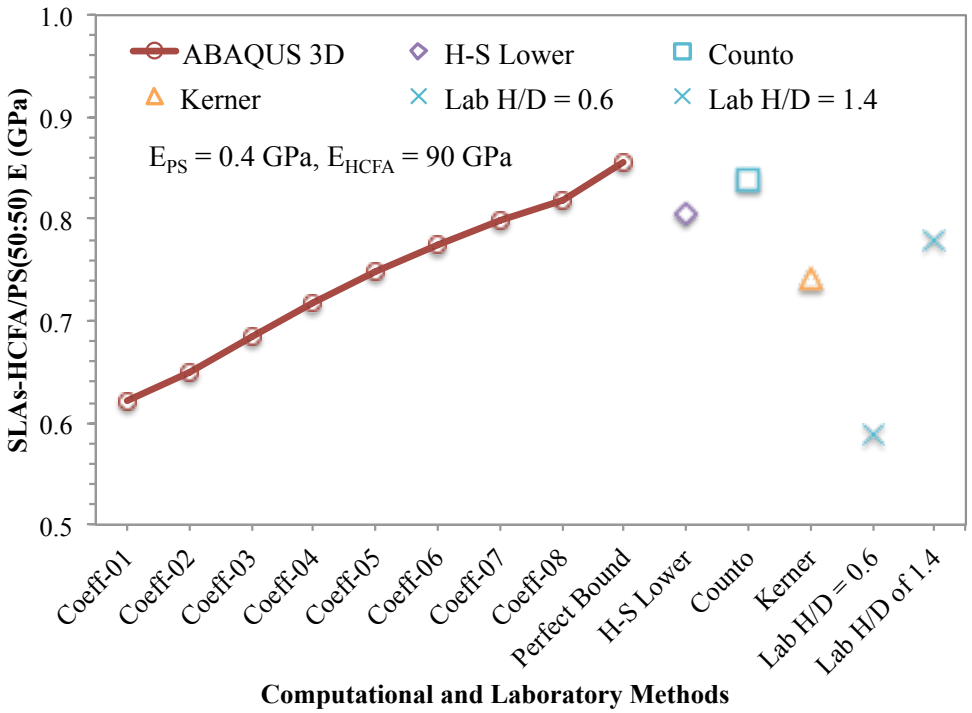

Fig. 6.14 Elastic Modulus of SLAs-HCFA/PS(50:50) from Different Methods

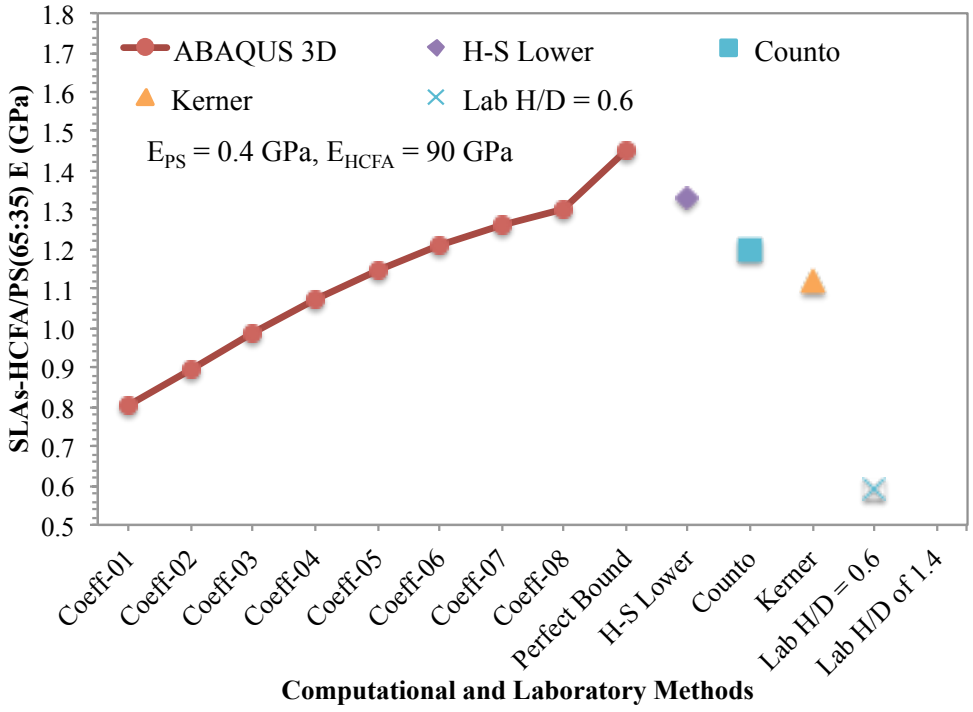

Fig. 6.15 Elastic Modulus of SLAs-HCFA/PS(65:35) from Different Methods

6. 4. 3 Poisson's Ratio

The Poisson's Ratio was also computed for SLAs-HCFA/PS(50:50) and SLAs-HCFA/PS(65:35) using data obtained from ABAQUS 3D models with two bounding conditions between fly ash and PS: perfect bound and coefficient of friction of 0.8 (coeff-08). As introduced in Chapter 3, uniform displacement along Y-axis was applied in each model. After simulation process, the displacement on the direction that is perpendicular to the Y-axis was obtained. And this displacement was averaged and divided by the applied displacement along Y-axis to acquire Poisson's ratio. Similarly with the elastic modulus, the Poisson's ratio had been calculated at different strain, but consistent values were generated. However, for different bounding conditions between fly ash and PS, the Poisson's ratios were different. The results were summarized in Table 6.9. As shown, the perfect bound condition generated composite material with Poisson's ratio that is close to but less than that of the PS matrix. However, in the coeff-08 case, the SLA has a Poisson's ratio that is greater than that of PS. Compared to the Poisson's ratio obtained from H-S upper and lower bounds method as listed in Table 6.7, the ABAQUS predicted values lies between 0.21 (obtained from upper bound method) and 0.47 (obtained from lower bound method) for SLAs-HCFA/PS(65:35). However, most Poisson's ratio prediction from ABAQUS 3D went above the Poisson's ratios obtained from H-S upper and lower bound method. Hence, the suitability of using ABAQUS 3D to predict the Poisson's ratios of SLAs might be affected by the composition of the material.

Table 6.11 Poisson's Ratio (ν) of SLAs-HCFA/PS Obtained from ABAQUS 3D

	Poisson's Ratio of PS	SLAs- HCFA/PS (50:50)		SLAs- HCFA/PS (65:35)	
		Perfect Bound	Coeff-08	Perfect Bound	Coeff-08
ν	0.22	0.22	0.27	0.21	0.33
	0.38	0.37	0.46	0.29	0.47

6. 5 Conclusions

In conclusion, using results from specific gravity and LOI tests, the actual fly ash and plastic contents could be determined more accurately, and, as found, it is apparent that desired SLA formulations with high fly ash content were difficult to produce. The elastic modulus calculated from the confined compression test is consistent with those calculated using the White (2000) method in unconfined compression test. However, these elastic moduli were greater than those obtained from linear regression method using unconfined compression stress-strain curves. In fact, calculations based on measured compression test responses indicate that SLAs with higher fly ash contents had lower-than-expected stiffness. This indicates that different bounding condition, between the reinforcement (HCFA) and matrix (PS) and between individual SLA grains, should be considered for the different types of SLA. Reinforcement/matrix bounding issue was explored further via ABAQUS 3D analysis with the analysis suggesting that for coefficients of friction greater than 0.3 for SLAs-HCFA/PS(50:50) and between 0.2 and 0.5 for SLAs-HCFA/PS(65:35), good agreement of elastic modulus results could be found. In addition, a prediction of Poisson's ratio was performed via ABAQUS 3D modeling with results found to be consistent with those from the H-S analytical method.

Possible explanations of a lower moduli from unconfined compression tests include: 1) the stiffness of SLAs might be affected by the presence of air pores in individual SLA grains, indicated from responses found in both confined and unconfined compression tests; 2) the pre-existing failure condition may between SLA particles thus reducing the initial and peak stress-strain responses of confined and unconfined compression testing; 3) the existence of poor bounding between the HCFA and PS matrix; and 4), at higher fly ash contents, individual fly ash particles may not be entirely enclosed in the PS matrix, but may exist as 'clumps' of particles

which may rub against each another during loading, a condition hypothesized when observing the SEM micrographs.

SUMMARY, CONCLUSIONS AND RECOMMENDAITONS

7. 1 Summary

This research focused on elastic moduli of SLAs – a composite material consisting of high carbon fly ash (HCFA) and various types of recycled plastic, including high density polyethylene (HDPE), low density polyethylene (LDPE), polystyrene (PS) and mixtures of recycled plastics (MP). Both theoretical computation and laboratory test were performed. Theoretical computations included both analytical calculations (H-S upper bound, H-S lower bound, Mura expression, Counto equation, and Kerner equation) and FEM simulations (FEM software of PLAXIS, ABAQUS). Analyses included: (I) computations based on assumed elastic properties of HCFA and plastic; and (II) computations based on experimentally-obtained values of elastic moduli of PS and specific SLAs-HCFA/PS specimens. In part (I), analytical calculation had been performed on each type of SLA; and FEM simulation using various unit cell models were carried out on SLAs-HCFA/PS and SLAs-HCFA/MP. Specifically, PLAXIS axisymmetric, ABAQUS axisymmetric, and ABAQUS 3D models were used for SLAs-HCFA/PS with r/d ratio of 0.5 (volume fraction, f = 0.083), 0.8 (f = 0.341), and 0.98 (f = 0.627); an ABAQUS 3D one-layer of matrix model and ABAQUS 3D two-layer of matrix model were performed in an attempt to predict the behavior of SLAs-HCFA/MP. In part (II), the ABAUQS 3D model was used to simulate the stress-strain behavior of specific type of SLAs-HCFA/PS, which have designed mass ratios of HCFA to PS as 50:50 and 65:35. In addition, the SLAs-HCFA/PS

studied in part (II) had been physically tested so that its actual component proportions are known and could be employed in FEM simulations.

7. 2 Conclusions

As summarized above, the investigations of SLAs' elastic moduli included: (1) Theoretical computation on various types of SLA, including analytical computation of elastic modulus of all types of SLAs and FEM prediction on elastic modulus of SLAs-HCFA/PS and SLAs-HCFA/MP with various volume fractions, using assumed elastic properties of HCFA and recycled plastics; (2) laboratory tests on SLAs-HCFA/PS and SLAs-HCFA/MP; (3) theoretical study on specific SLAs-HCFA/PS(50:50) and SLAs-HCFA/PS(65:35) and its comparison with experimental results. The main conclusions are listed below:

7. 2. 1 Theoretical Computation on Various Types of SLA

1. Both analytical and FEM methods showed an increase of elastic modulus with increasing fly ash volume fraction, with the rate of increase becoming higher as HCFA content increases.
2. The analytical computations showed that the HCFA reinforced the various types of recycled plastics to different degrees: generally, the stiffer the plastic, the less it was reinforced.
3. The computational geometry used in FEM modeling such as the element type of CAX3 or CAX6M in ABAQUS 2D, C3D8 or C3D10 in ABAQUS 3D, and the fineness of mesh did not significantly impact the elastic moduli of SLAs. Hence the element type and meshing technique that is more efficient for calculation is preferred. For example, in ABAQUS 3D the usage of C3D8 element can save up to several

hours compared to the C3D10. Therefore, the C3D8 element is recommended in ABAQUS 3D modeling.

4. The roughness of interface between HCFA and plastic significantly influenced the stiffness of the SLAs with the significance increasing as fly ash content increased.
5. Different loading mode such as stress-control and strain-control caused different stress distribution in the PS and fly ash particle, but had no significant effect on the elastic moduli of the composite;
6. The SLAs' elastic modulus predicted using FEM modeling showed consistent values with those obtained from analytical methods, especially when SLAs had lower HCFA content. Amongst the various models, ABAQUS 3D showed the best agreement.
7. The ABAQUS 3D one-layer-matrix model showed better agreement with analytical methods than the two-layer-matrix model did on elastic modulus prediction for SLAs-HCFA/MP, especially for those with higher fly ash volume fractions.
8. The ABAQUS modeling showed that the effect of plastic stiffness had more influential and consistent impact on the stiffness of SLAs than the HCFA's stiffness did.

7. 2. 2 Laboratory Test on SLAs-HCFA/PS

1. The specific gravity test showed that the specific gravities of SLAs-HCFA/PS and SLAs-HCFA/MP range between 1.29~1.79 and 1.45~1.72, respectively.
2. The specific gravity and LOI test determined that the actual proportions of plastic and HCFA in SLAs are not as the same as their nominally titled designations, but are within a 5% of these designations. However, for SLAs with designed HCFA content of 80%, the real fly ash content is consistently less;

3. Confined compression tests showed that the side friction between the inside of the compression mold and the compressing samples reduced as with increasing HCFA content. This might be because the spherical shape of HCFA helps in reducing the effects of side friction during compression.
4. When the granulated SLAs were compressed under high pressure (350MPa), those containing less fly ash compressed more leading to porosities less than zero. But the samples' final porosity was also affected more because of the friction between the sample and mold. It is also hypothesized that the presence of more fly ash interferes with the ability of SLA to get to lower porosity value;
5. Both constrained compression and unconfined compression tests on SLAs-HCFA/PS showed that the more HCFA in a SLA, the lower its elastic modulus. This indicates the critical effect of the friction coefficient between fly ash and plastic and the coefficient of friction might be dependent on the SLAs HCFA content as the higher the fly ash content, the lower the coefficient of friction. This observation is potentially explained by the reduced bond between ash and plastic, which effectively lowers the coefficient of friction between the fly ash and plastic and allows fly ash particles to rub against other fly ash particles as the composite is strained;
6. The SEM images illustrate that the lower fly ash content in SLAs, the more bounding area between fly ash and plastic in SLAs exists. On the other hand, in the SLAs that have more fly ash, the lack of bonding area between fly ash and plastic leads to the lower measured modulus, as the spherical, and smoother, ashes are allowed to move against and travel around each other, leading to a weaker composite and lower modulus.

7. The SEM micrographs of HCFA show that some fly ash particles are embedded in unburned carbon, which is porous-structured and in cindered clusters;
8. The stress-strain curves obtained from laboratory test exhibited a strain-hardening phenomena at lower strain (< 3%), this might due to the compression of entrapped air in SLAs. Otherwise, the curves had good agreement in shape with those from ABAQUS simulation;

7. 2. 3 Elastic Modulus Study on SLAs-HCFA/PS(50:50) and SLAs-HCFA/PS(65:35)

1. The ABAQUS 3D modeling showed an increased stiffness of SLAs with an increase in loading strain, especially for those SLAs with a rougher interface (i.e., coefficient of friction) between fly ash and plastics. This change was more significant for SLAs-HCFA/PS(50:50) (5%~26%) than for SLAs-HCFA/PS(65:35) (7%~17%).
2. The ABAQUS and analytical method generated good agreement on the prediction of SLAs' elastic modulus. Specifically, the ABAQUS model which had coefficients of friction greater than 0.3 for SLAs-HCFA/PS(50:50); and the model which had coefficients of friction between 0.2 and 0.5 for SLAs-HCFA/PS(65:35) generated the good agreement with the analytical method. However, the laboratory test using specimens with H/D of 0.6 provided lower modulus values than the theoretical predictions; while the test using SLAs-HCFA/PS(50:50) specimen with H/D of 1.7 generated modulus (0.81GPa) provided modulus values that lie within the predicted values (0.67~0.94GPa).
3. In summary, the elastic moduli of SLAs-HCFA/PS was calculated using three methods: (1) using constrained moduli obtained from confined compression tests and an assumption of Poisson's ratio (0.33); (2) using the linear regression of stress-strain

curves obtained from unconfined compression test; (3) using the unconfined compressive strength and fly ash content (%) stated by White's (2000) method. The elastic modulus values obtained from three methods were different and decreased in the sequence of method (1) → method (3) → method (2), but they all show the same trend that the elastic modulus of SLAs decreases with the increase amount of fly ash content, suggesting that different bonding conditions should be considered for SLAs as the fly ash content changes.

4. The Poisson's ratio prediction on SLAs-HCFA/PS(50:50) showed that the ABAQUS 3D scenario with perfect bonding between the fly ash and plastics had good agreement with those obtained from analytical predictions (less than 9% difference), especially when the assumed Poisson's ration of the plastic is lowered to 0.22. As for the SLAs-HCFA/PS(65:35), the ABAQUS modeling that assumed coeff-08 or perfect bonding conditions lead to Poisson's ratio that lie with analytical predictions.
5. Generally, the unit cell model created in ABAQUS 3D system predicted elastic moduli in good agreement with those from analytical calculations. However, the laboratory test results showed much lower moduli than both theoretical methods (FEM modeling and analytical method). The possible reasons include: (1) pre-existing failure surfaces between granular SLA particles maintained during the production of solid SLAs specimen; and (2) irregular distribution of HCFA particles in plastic resin that may cause direct interaction between fly ash particles, which rub against and travel around each other and lessen the stiffness of SLAs.

Overall, according to its good agreement with the analytical analysis, the unit cell model developed in ABAQUS 3D is applicable to predicting the elastic moduli of SLAs. In addition, it

is an efficient way to simulate the stress strain behavior of SLAs composed with various types of plastics and various fractions of fly ash reinforcement. In addition, by using the FEM model, the effect of different parameter such as the bond between fly ash and recycled plastics, the elastic modulus of each composite component, and the volume fraction of HCFA reinforcement can be evaluated. However, to further improve its applicability, laboratory tests should be performed on solid specimens.

7. 3 Recommendations

According to the possible reasons that generated the divergence between theoretical and laboratory tests, recommendations are given below for future study:

1. Instead of compressing small SLAs particle into a solid particle, SLAs specimen may be obtained by directly forming solid SLAs specimens by casting the still malleable (viscous fluid) SLAs composite into cylindrical molds as it exits the compounding device.
2. SLAs specimens with different height-to-diameter ratios should be produced for unconfined compression tests so that the effect of specimen dimension could be further studied and compared. This will allow optimization of the appropriate height-to-diameter ratio leading to the creation of a reference value for SLAs' elastic modulus studies.
3. Establish an ABAQUS model that contains reinforcement with various sizes and random distributions at the macroscopic scale using statistical method, in which a mesh generating tool can be utilized. A desktop software application, OOF3D (Object Oriented Finite Elements 3D) provided by NIST (National Institute of Standards and Technology) is recommended.

REFERENCES

ACAA (2013). "2013 Coal combustion product (CCP) production & use survey report." <https://www.acaa-usa.org/Portals/9/Files/PDFs/2013ReportFINAL.pdf> (Oct. 5, 2015).

ACAA (2013). "2013 Coal combustion product (CCP) production and use chart." <https://www.acaa-usa.org/Portals/9/Files/PDFs/1966-2013_FlyAsh_Prod_and_Use_Charts.pdf> (Oct. 5, 2015).

Adam, T. H. (2014). "Coal ash association applauds EPA deadline for finalizing regulations." *American Coal Ash Association*, <https://www.acaa-usa.org/Portals/9/Files/PDFs/News-Release-ACAA-Coal-Ash-Rulemaking-Deadline.pdf> (Sep. 17, 2015).

Alkan, C., Arslan, M., Cici, M., Kaya, M., and Aksoy, M. (1995). "A study on the production of a new material form fly ash and polyethylene." *Resource, Conservation and Recycling*, Vol. 13, pp. 1470154.

ASTM C618-12a, Standard Specification for Coal Fly Ash and Raw or Calcined Natural Pozzolan for Use in Concrete, ASTM International, West Conshohocken, PA, 2012, www.astm.org

ASTM D3878-15, Standard Terminology for Composite Materials, ASTM International, West Conshohocken, PA, 2015, www.astm.org.

ASTM D7348-08, Standard Test Methods for Loss on Ignition (LOI) of Solid Combustion Residues, ASTM International, West Conshohocken, PA, 2008, DOI: 10.1520/D7348-08, www.astm.org

ASTM D7611 / D7611M-13e1, Standard Practice for Coding Plastic Manufactured Articles for Resin Identification, ASTM International, West Conshohocken, PA, 2013, www.astm.org.

ASTM E9-09, Standard Test Methods of Compression Testing of Metallic Materials at Room Temperature, ASTM International, West Conshohocken, PA, 2009, DOI: 10.1520/E0009-09 www.astm.org.

ASTM E111-04 (2010), Standard Test Method for Young's Modulus, Tangent Modulus, and Chord Modulus, ASTM International, West Conshohocken, PA, 2010, www.astm.org.

Bhatty, J. I., Gajda, J., and Miller, F. M. (2002). "Commercial use of high-carbon fly ash in cement manufacturing." <https://www.netl.doe.gov/publications/proceedings/02/ubc/bhattysummary.pdf> (Sep. 16, 2015).

Cantor, K. M., and Watts, P. (2011). "Plastics materials." *Applied plastics engineering handbook*, Kutz, M., Elsevier Science, pp. 3-5.

Chauhan, S. R., Kumar, A., Singh, I., and Kumar, P. (2010). "Effect of Fly Ash Content on Friction and Dry Sliding Wear Behavior of Glass Fiber Reinforced Polymer Composites - A Taguchi Approach." *Journal of Minerals & Materials Characterization & Engineering*, Vol. 9, No.4, pp.365-387.

Chawla, N. and Shen, Y.–L. (2001). "Mechanical behavior of particle reinforced metal matrix composites," *Advanced Engineering Materials*, 3, No. 6.

Choi, Y. W., Moon, D. J., Kim, Y. J., and Lachemi, M. (2009). "Characteristics of mortar and concrete containing fine aggregate manufactured from recycled waste polyethylene terephthalate bottles," *Construction and Building Materials*, Vol. 23, pp. 2829-2835.

Clean Up Australia Ltd. (2009). "Plastic recycling fact sheet," <http://www.cleanup.org.au/PDF/au/cua_plastic_recycling_fact_sheet.pdf> (Sep. 22, 2015).

Counto, U. J. (1964). "The effect of the elastic modulus of the aggregate on the elastic modulus, creep and creep recovery of concrete," Magazine of Concrete Research, Vol. 16, No. 48.

Dong, M. and Schmauder, S. (1995). "FE modeling of continuous fiber and particle reinforced composites by self-consistent embedded cell models," *Computational Methods in Micromechanics*, AMD-Vol. 212/-MD- Vol. 62, ASME, 81-86.

Das, B. M. (2005). "Specific gravity of soil solids." *Soil Mechanics Laboratory Manual*, Oxford University Press, New York, 9-12.

Duta, A., Cazan, C., Cosnita, M. (2011). "Fly ash in optimized composites based on recycled plastics and rubber." *World of Coal Ash (WOCA) Conference*, Denvor, CO.

Elsayed, A.A. (2006). "Investigation of one-dimensional compression and stress-strain-strength relations of synthetic lightweight aggregates composed of coal fly ash and thermo plastics," PhD dissertation, Tufts University, Medford, MA.

Elzafraney, M., Soroushian, P., and Deru, M. (2005). "Development of energy-efficient concrete buildings using recycled plastic aggregates*," Journal of Architectural Engineering*, ASCE, Vol. 11, No. 4, pp. 122-130.

Fang D. and Zhou C. (1997). "Analysis of elastoplastic deformation in metal-matrix composites with particulate reinforcements," *ACTA mechanica sinica (English series*), Vol. 13, No. 2, pp. 153-160.

Fu, S-Y, Feng X-Q, Lauke, B., and Mai, Y-W. (2008). "Effect of particle size, particle/matrix interface adhesion and particle loading on mechanical properties of particulate-polymer composites," *Composites: Part B.,* 38, pp. 933-961.

Gaudig, W., Mellert, R., Weber, U., Schmauder, S. (2003). "Self-consistent one-particle 3D unit cell model for simulation of the effect of graphite aspect ratio on Young's modulus of cast-iron." Computational Material Science, Vol. 28, pp. 654-662.

Gaudreau, A.J. (2002), "Stress-strain-strength behavior of Synthetic Lightweight Aggregates in Triaxial Compression," MS thesis, Tufts University, Medford, MA.

Glisevic, I. (2012). "NUMIX": lightweight aggregate for concrete from recycling of plastic waste, <http://danube-inco.net/object/event/11979/attach/PresentationNUMIX.ppt.> (Oct. 5, 2015).

Guleria, S. P., and Dutta, R. K. (2011). "Unconfined compressive strength of fly ash-lime-gypsum composite mixed with treated tire chips." *Journal of Materials in Civil Engineering*, Vol. 23, No. 8, pp. 1225-1263.

Hashin, Z. and Shtrikman, S. (1963). "A variational approach to the theory of the elastic behavior of multiphase materials," *J. Mech. Phys. Solids*, Vol. 11, pp. 127-140.

Hassett, D. J., Dockter, B. A., Eylands, K. E., and Pflughoeft-Hassett, D. F. (1995). "Task 5.9 - Use of coal ash in recycled plastics and composite materials." *Topical Report*, Energy & Environmental Research Center, University of North Dakota, Grand Forks, North Dakota.

Ho, S., Church, R., Klassen, K., Law, B., MacLeod, D., and Zanzotto, L. (2006). "Study of recycled polyethylene materials as asphalt modifiers." *Canada Journal of Civil Engineering*, Vol. 33, pp. 968-981.

Holmstrom, O.C., and Swan, C.W. (1999). "Geotechnical properties of innovative synthetic lightweight aggregates," *Proceedings of the 1999 International Ash Utilization Symposium*. Lexington. KY.

Kerner, E.H. (1956). "The elastic and thermo-elastic properties of composite media," *Proceedings of the Physical Society. Section B*., Vol. 69, No. 8.

Ku, H., Kota, V., and Trada, M. (2010). "Optimum percentage of fly ash reinforcement in vinyl ester composites." *Journal of Materials in Civil Engineering*, ASCE, Vol. 22, No. 1, pp. 104-107.

Kumar, B. V. K., and Prakash, P. "Use of waste plastics in cement concrete pavement." <http://www.researchgate.net/publication/229047560_USE_OF_WASTE_PLASTICS_IN_CEMENT_CONCRETE_PAVEMENT> (Oct. 5, 2015)

Li, S., Wongsto, A. (2003). "Unit cells for micromechanical analyses of particle-reinforced compoistes." Mechanics of Materials, Vol. 36, pp. 543-572.

Li, Y., White, D. J., and Peyton, R. L. (1998). "Composite material from fly ash and post-consumer PET." *Resources, Conservation and Recycling*, Vol. 24, pp. 87-93.

Ma, X. F., and Wang, Y. N. (2007). "Fly ash-reinforced thermoplastic starch composites." *Carbohydrate Polymers*, Vol. 67, pp. 32-39.

Matsunaga, T., Kim, J.K., Hardcastle, S., and Rohatgi, P.K. (2002). "Crystallinity and selected properties of fly ash particles," Material Science and Engineering A325, pp. 333-343.

Matweb (2013). <http://www.matweb.com/search/PropertySearch.aspx> (Oct, 5 2015).

Mishnaevsky, L.L. and Schmauder, S. (2001). "Continuum mesomechanical finite element modeling in materials development: a state-of-the-art view," *Appl Mech Rev*, Vol. 54, No. 1.

Naik, T. R., Kraus, R. N., Ramme, B. W., Chun, Y-M, and Kumar, R. (2006). "High-carbon fly ash in manufacturing conductive CLSM and concrete." *Journal of Materials in Civil Engineering*, ASCE, Vol. 18, No. 6, pp. 743-746.

Nasvik, J. (1991). "Plastic aggregate, colorful alternative to mineral aggregate produces striking design effects." <http://www.concreteconstruction.net/Images/Plastic%20Aggregate_tcm45-342127.pdf> (Oct. 5, 2015).

Nigam, S. K., and Akolkar, A. B. (2009). "Environmental issue in plastics waste management and remedial measures," *Focus-story*, Plasticbiz 360, <http://www.plasticbiz360.com/index.aspx?Page=article&sectname=Magazines%20-%20Focus&sectid=6&contentid=20090930200909301532168 43a26e67b2> (Oct. 5, 2015).

Packaging Today "An introduction to the history of plastics." <http://www.packagingtoday.com/introenvironment.htm> (Feb 22, 2012).

Pandermarakis, Z.G., Spathis, G., and Tsamasphyros. (2007). "Constructing a modulus map for linear elastic composites: the case of rigid reinforcements," *Polymer Composites*, pp. 593-604.

Qi, H. J., and Boyce, M. C. (2005). "Stress–strain behavior of thermoplastic polyurethanes." *Mechanics of Materials*, 37(8), pp.817-839.

Shen, Y.-L., Finot, M., Needleman, A., and Suresh, S. (1994). "Effective elastic response of two-phase composites," *Acta Metall. Mater.* Vol. 42, No. 1, pp. 77-97.

Sobhan, K., and Mashnad, M. (2000). "Fatigue durability of stabilized recycled aggregate base course containing fly ash and waste-plastic strip reinforcement." *Final Report,* Department of Civil and Geological Engineering, New Mexico State University, <http://rmrc.wisc.edu/wp-content/uploads/2012/10/P18final.pdf> (Oct. 5, 2015).

SPI (2015) "SPI Resin Identification Code – Guide to correct use." < http://www.plasticsindustry.org/AboutPlastics/content.cfm?ItemNumber=823> (Sep. 22, 2015).

Stevens, M.P. (1999). "Polymer Chemistry an Introduction." Oxford University Press, New York, NY.

Strong, A. B. (2005), "Plastics, materials and processing." 3rd edition, Brigham Yong University, Pearson Education, Inc.

Swan, C.W. (2009). "The use of Synthetic Lightweight Aggregates as a component of sustainable designs," *2009 World of Coal Ash (WOCA) Conference*, <http://www.flyash.info/2009/122-swan2009.pdf> (Oct. 5, 2015).

Swan, C.W., and Sacks, A. (2005). "Properties of Synthetic Lightweight Aggregates for use in pavement systems," *GSP 130 Advances in Pavement Engineering.*

U. S. Environmental Protection Agency (2013). "Plastics." Wastes – Resource Conservation – common wastes & Materials, <http://www.epa.gov/wastes/conserve/materials/plastics.htm> (Sep. 23, 2015).

Wansbrough, H., and Yuen, D. (2002). "Plastic recycling," New Zealand Institute of Chemistry, *XIV-Environment-E*, pp. 1-4, <http://nzic.org.nz/ChemProcesses/environment/14E.pdf> (Sep. 23, 2015).

Weingram, J. A. (2003). "Shrinkage and durability of concrete containing fly ash/mixed plastic aggregates." MS thesis, Tufts University, Medford, MA.

Wen, H, and Patton, R. (2008). "High carbon fly ash finds uses in highway construction." <http://www.dot.state.mn.us/mnroad/projects/High_Carbon_Fly_Ash/Reports/Article%20for%20Greenhighway%201-2-08.pdf > (Sep. 17, 2015).

White, D. J. (2000). "Microstructure of composite material from high-lime fly ash and RPET." *Journal of Materials in Civil Engineering*, Vol. 12, No. 1, pp. 60-65.

APPENDIX (I)

Analytical calculated elastic moduli E of SLAs made of various types of plastics.

Plastic Type	Volume Fraction (f)	H-S Upper Bound	H-S Lower Bound	Mura Expression	Counto Equation	Kerner Equation
HDPE (GPa)	0	0.80	0.80	0.80	0.80	0.80
	0.1	6.07	1.01	1.04	1.16	1.01
	0.2	11.55	1.26	1.50	1.42	1.28
	0.3	17.52	1.59	1.93	1.74	1.63
	0.4	24.16	2.02	-	2.13	2.08
	0.5	31.62	2.62	-	2.65	2.73
	0.6	40.09	3.50	-	3.42	3.69
	0.7	49.80	4.93	-	4.65	5.30
LDPE (GPa)	0	0.30	0.30	0.30	0.30	0.30
	0.1	5.68	0.38	0.40	0.44	0.38
	0.2	11.23	0.48	0.59	0.54	0.49
	0.3	17.26	0.61	0.77	0.66	0.62
	0.4	23.93	0.78	-	0.81	0.79
	0.5	31.42	1.02	-	1.01	1.04
	0.6	39.92	1.38	-	1.31	1.41
	0.7	49.66	1.97	-	1.80	2.03
PS (GPa)	0	3.00	3.00	3.00	3.00	3.00
	0.1	7.96	3.66	3.75	4.19	3.74
	0.2	13.28	4.47	5.01	5.12	4.66
	0.3	19.14	5.49	6.02	6.18	5.85
	0.4	25.68	6.81	-	7.48	7.43
	0.5	33.02	8.58	-	9.20	9.64
	0.6	41.35	11.10	-	11.60	12.96
	0.7	50.88	14.96	-	15.26	18.50
MP (GPa)	0	1.54	1.54	1.54	1.54	1.54
	0.1	6.73	1.92	1.98	2.20	1.95
	0.2	12.17	2.39	2.78	2.71	2.45
	0.3	18.11	2.98	3.47	3.29	3.10
	0.4	24.72	3.76	-	4.01	3.96
	0.5	32.15	4.82	-	4.98	5.16
	0.6	45.22	7.42	-	7.32	8.27
	0.7	50.21	8.80	-	8.56	9.99

APPENDIX (II)

(I) Summary of E (GPa) of SLAs-HCFA/PS from different methods

r/d	f	H-S Upper Bound	H-S Lower Bound	Counto Equation	Kerner Equation	PLAXIS 2D	ABAQUS 2D (R=0.9)	ABAQUS 3D Stress Control	ABAQUS 3D Strain Control
0.5	**0.083**	7.11	3.54	4.03	3.60	3.91	3.63	3.48	3.37
0.8	**0.341**	21.76	5.99	6.68	6.44	11.02	7.03	5.03	5.25
0.98	**0.627**	43.84	11.98	12.44	14.19	18.18	23.39	11.25	13.92

(II) Summary of E of SLAs-HCFA/MP computed from different methods

r/d	f	H-S Upper Bound	H-S Lower Bound	Mura Expression	Counto Equation	Kerner Equation	ABAQUS One-layer	ABAQUS Two-layer
0.3	**0.014**	1.85	1.24	1.24	1.35	1.24	1.51	1.58
0.5	**0.065**	4.26	1.51	1.55	1.78	1.56	1.38	1.76
0.65	**0.144**	8.18	1.60	1.68	1.90	1.68	1.88	2.09
0.8	**0.268**	15.11	2.07	2.57	2.43	2.23	2.55	2.89
0.98	**0.493**	30.50	3.46	-	3.86	3.94	5.19	8